The University of Hull

Switched Beam Array Antenna for 2.45 GHz RFID Localisation

being a Thesis submitted for the degree of

Doctor of Philosophy

in The University of Hull

by

DINH LOI NGUYEN
(MSc.)

November 2011

ABSTRACT

Most people are familiar with **R**adio **F**requency **Id**entification (RFID) technology as its applications are around us in many systems, such as anti-theft devices in shops, supermarkets and libraries, building access systems. The number of applications and devices has developed explosively in the past decade and has become one of the fastest growing sectors of the radio technology industry. RFID systems allow information to be attached to items such as products, animals or even people. This information may be read, and in some cases changed, by an RFID reader some distance away. RFID localisation systems are an active area of research as they add further capabilities to current RFID systems. Localisation allows the position of tagged items to be determined from the RFID communications signal. Current systems can confirm that a specific item is within the reader read range but finding the item requires a systematic search.

The primary objective of this thesis is to build a new, economical and versatile 2.45 GHz localisation system for active and passive RFID tags. Alternative systems rely upon signal strength measurements and yield large uncertainties due to the unknown orientation of the tags. The proposed system reader consists of a microstrip switched beam array antenna. The array antenna allows the estimation of the angular position of the tag. The use of two or more readers provides the tags position by triangulation. The array antenna provides other advantages such as improved read range and mitigation against interference and multipath fading.

In the process of designing the antenna array, several new, compact, slotted, circularly polarised, square patch antennas have been produced. A range of technologies have been applied to achieve miniaturisation of the microwave circuit elements require to drive the antenna array, the Butler matrix (BM). Fabricated circuits achieve significant size area reduction with similar performances compared to the conventional ones. These developments will have wide application beyond the RFID localisation system.

Finally, accuracy of the system varies with angle due to the complicated relationships between Angle of Arrival (AoA) and port output powers. The localisation algorithm along with measured power inside the standard anechoic room show that the standard deviations of the AoA estimation errors less than 1.6° for most angles in the operational range from -90 degrees to 90 degree and a standard error less than 0.6^{o} for AoA angles with 20^{o} of the perpendicular at AoA with power ratios perturbed by additive noise of standard deviation 0.5 dB.

ACKNOWLEDGEMENTS

First of all, I would like to express my sincere gratitude to my supervisors, Mr. Nick Riley and Dr. Kevin Paulson, for their constant guidance and support throughout my research. I am truly appreciated for all the time that they has dedicated for discussions on my work toward this thesis and submitted papers.

I would also like to deeply thank Mr. Steve Coopland of Electronics Workshop for circuit prototype.

I also thank the staff within the Department of Engineering for providing me services, helps and discussions.

Many thanks to all my friends particularly to Vietnamese society in Hull for the unforgettable time spent in the UK.

For my parents who brought me up with all their love and have been unconditionally supporting me to reach my every goal and ambition, thank you very much. I could not be more proud as your son.

Finally, I would like to dedicate this thesis for my grandmother who passed away in the second year. Her love and encouragement made me stronger and more focussed to finish the work.

Table of Contents

Table of Figures

List of Tables

Publications

Nguyen, D. L., Paulson, K. and **Riley, N. G.**, (2010), *A compact circularly polarized microstrip antenna for UHF RFID readers*, Proceedings of ICCVT Conference, Vietnam, December 2010.

Nguyen, D. L., Paulson, K. and **Riley, N. G.**, (2011a), *A size reduced circularly polarised square microstrip antenna for 2.45 GHz RFID applications*, IET Microwaves, Antennas and Propagation (Accepted for publication in October 2011).

CHAPTER 1. INTRODUCTION

1.1. Overview of the Thesis

Radio Frequency Identification (RFID) is a technique which uses radio waves to identify items based on data read from electronic labels (RFID tags) attached to the items. RFID systems have evolved over many years and currently operate in four bands of the radio spectrum with a wide range of available technologies. A review of some of the main aspects of RFID is presented in the following sections. Most current RFID systems do not provide information on the location of items, except, by implication, that they are within the read range of the RFID reader.

The aim of the work presented in this thesis is to develop a compact steerable-beam antenna for use in RFID systems and to use this antenna to derive location data as well as identification of items.

This chapter presents brief information on Radio Frequency Identification (RFID) particularly on RFID localisation systems. The chapter also provides a summary of the novel contributions of the research work and organisation of this thesis.

1.2. Introduction of RFID Technology

The long history of RFID is summarised in [Landt, 2005]. The technology has only developed explosively in the past decade to become one of the fastest growing sectors of the radio technology industry. The value of the entire RFID market in 2010 was $5.63 billion and is expected to increase to $5.84 billion in 2011 [IDTechEx, 2011].

RFID is an automatic identification (auto-ID) procedure that identifies an item or a person by using a radio frequency (RF) transmission [Finkenzeller, 2003]. An RFID system generally consists of a reader connected to a computer and tags (Fig. 1.1). Each of the tags has a tiny chip (integrated circuit) that has memory. If a tagged item is near the reader i.e. within the reader's interrogation zone, the item can be detected and identified by extracting the tag information via radio communications between the reader and the tag.

RFID system operating frequencies are within unlicensed spectrum, sometimes referred to as ISM (Industrial, Science and Medical) but exact frequencies vary from a country to country and can be classified into four bands: low frequency (LF), high frequency (HF), ultra high frequency (UHF) and microwave frequency [Lahiri, 2006].

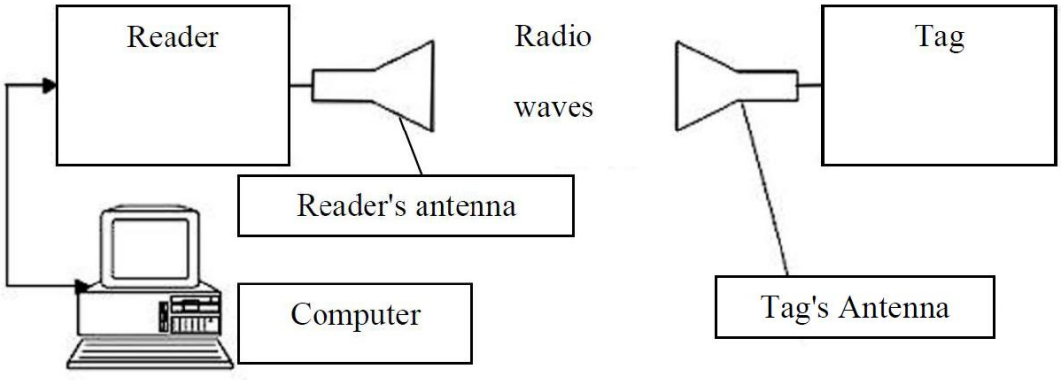

Figure 1.1. A typical RFID system

In recent years, RFID systems that work in the ultra high frequency (UHF) and microwave ranges have been the most attractive topics in the field of RFID research, due to their ability to support much larger interrogation zones, faster data rates as well as effectively reducing the dimensions of devices.

RFID system also can be categorised by tag type: active, passive and hybrid; also known as semi passive. A passive tag has no internal power source and must operate using power harvested from the reader signal. Although active systems can provide larger interrogation zones, they are often not cost effective due to the expense and limited lifetime of the power supply. Passive UHF RFID systems tend to be highly cost effective as the cost of passive RFID tags is relatively low and the tag's lifetime is much longer.

Adding localisation to existing RFID systems is a way of adding value to systems with enormous economic importance. Currently, a number of RFID localisation systems are being investigated and deployed for various applications including: container positioning, healthcare, material management, inventory management, road and mining safety [Zhou, 2008]. In this thesis, a new approach for RFID localisation using a switched beam reader is presented. The proposed system will use the tag signal, currently used only for communications, to identify tag location. This requires no modification to the tags, which are already produced in their millions. As there are many tags produced for each reader, possibly a ratio of millions to one, the economic constraint on readers is far less stringent than that on the tags. There are some UHF RFID localisation systems available on the market at the moment, such as Wi-Fi RFID systems of Aeroscout [Wi-Fi RFID] and the RFID-Radar of a South Africa company named Trolleyscan [RFID-Radar]. These systems generally use active tags (i.e. tags powered by their own battery). However the technical details of these systems are not available due to commercial confidences.

1.3. Thesis Contribution

This project develops a switched beam array antenna for RFID reader, working at ISM band of 2.45 GHz, capable of locating the position of UHF (ultra high frequency) RFID tags. The system uses separated reader antennas for transmitting and receiving in order to provide better isolation [Nikitin, 2008]. The receiving antenna is a switched beam array antenna that can switch between antenna patterns focused along different paths through the interrogation region. The tag signal collected by the receiving antenna array is used to calculate the direction to the tag so that the location can be obtained by triangularisation.

The proposed system is an economical solution for RFID localisation as it does not require additional components such as reference tags. The proposed microstrip antennas are fabricated on printed circuit boards so that they are compact and cheap. The system also overcomes the serious problem caused by tag orientation to most RFID localisation systems based on Received Signal Strength (RSS).

Switched beam antennas have many other key advantages over the traditional single near-isotropic antenna. Firstly, the antenna gain is increased so that the read range is extended. Secondly, as the array antenna has narrow main lobes, interference between tag signals is reduced, multipath delay and interference is reduced, and the collision of signals produced by multiple tags is reduced [Tseng, 2007] so increasing the successful tag identification rate [Ma, 2008]. Furthermore, the multiple antennas of the reader can also reduce fading for RFID tags [Griffin, 2007].

Other researchers and commercial ventures have produced designs for RFID readers utilising phased array antenna e.g. [Karmanka, 2008] and [Omron, 2006]. Several systems exist for active UHF RFID localisation e.g. Aeroscout and RFID-radar. However the technical details of these systems are not available due to commercial confidentiality and advertising materials seem overly optimistic and unreliable.

The system designed is the first RFID system using switched beam antenna for localisation purposes. The system has the many functional advantages listed earlier. In addition, the ability to locate tagged objects has a large number of economically important applications in the management of products and inventory in logistics and supply chains.

In addition, the process of designing compact patch antennas and compact Butler matrices for the system has lead to fundamental advances in the design and fabrication of the systems that can be widely applied in wireless communications.

These antenna designs are more compact than most published miniaturised microstrip antenna including four slits [Chen, 2001], or four bent slots [Chen, 1998b], or asymmetric patterns of circular holes [Nasimuddin, 2010] or etched on a high-permittivity substrate and surrounded by a vertical ground [Kim, 2006]. Moreover, they are simpler, easier to fabricate at the large numbers and hence with lower cost.

Miniaturisation of the Butler Matrix (BM) is achieved by replacing its components, including quadrature hybrid couplers and crossovers, with stepped impedance configuration (SIC) equivalent structures. The SIC structure is shown to be simple to design and provides effective size reduction. SICs are widely applicable and can reduce the length of any transmission line. In addition, the performance of the compact circuits is similar to the standard ones. Using SIC components the area of the reduced size branch-line coupler has been reduced by 40% compared to a conventional coupler. This technique based on microstrip technology have the advantage of simple design and fabrication at low cost as they are fabricated on a single layer substrate without any additional lumped elements or wires compared to many others published methods such as combinations of short high-impedance transmission lines, shunt lumped capacitors, [Hirota, 1990; Singh, 2001; Hettak, 2005], lumped elements [Liao, 2006; Hongerheiden, 1997], periodic open-ended stubs [Eccleston, 2003], high- low impedance resonators [Wang, 2007], high impedance lines [Mandal, 2008]. The SIC components have been integrated into a 4x4 BM similar performance to the conventional design, but with an area reduced by 40%. This is more effective miniaturisation than that achieved by the more complex eight two-step stubs method [Muhammad, 2010], working at the same frequency.

1.4. Thesis Outline

The remaining of the thesis is divided into the following chapters:

Chapter 2 introduces RFID localisation. Passive RFID systems are discussed in detail with current EU regulations and standards. Indoor localisation techniques are also introduced. This chapter also reviews antenna fundamental parameters and microstrip technology. Simulation software used in the thesis is also presented.

In the beginning parts of Chapter 3, the microstrip antenna is reviewed and the conventional square patch on FR4 substrate is designed, fabricated and measured as starting point in order to design compact antenna for portable RFID readers. Two compact antennas that are singly-fed, truncated corner, circular polarised (CP) square patch (SP) antenna are introduced. These designs are modelled, fabricated and tested.

Chapter 4 presents the advantages of the proposed system over current RFID localisation systems. It also details the design of a switched beam array fed by the BM. The conventional microstrip BM is designed, simulated, fabricated and measured. A miniaturisation technique using Stepped Impedance Configuration (SIC) is discussed and applied to design compact hybrid coupler and crossover. These component are integrated to the compact BM. This chapter also analyses the localisation system and verifies its operation using simulation and measurements.

Chapter 5 concludes this thesis with a summary of the work done and the contributions to knowledge. Recommendations on possible work to extend this research in the future are given.

CHAPTER 2. BACKGROUND AND LITERATURE REVIEW

2.1. Introduction

This chapter reviews passive UHF RFID systems and RFID localisation techniques. The fundamental characteristics of antennas are described with particular reference to the microstrip antennas used extensively in this project. The software used to calculate and simulate circuits and systems, prototypes, and measurements are described in later sections.

2.2. Passive UHF RFID System

An RFID system consists of a reader and a number of tags. The reader and tags communicate by means of radio waves. UHF RFID systems use frequencies of 433 MHz, and 868 MHz (in Europe), or 915 MHz (in USA), with 2.45 GHz and 5.8 GHz frequencies being used in microwave systems. The RFID frequency regulations in Europe and United States (US) are summarised in table 2.1. Although, publications [Finkenzeller, 2003; Lahiri, 2006] often classify the 2.45 GHz systems as microwave RFID systems. In this thesis, systems are categorised as UHF if the working frequency is in the UHF band (from 300 MHz to 3 GHz) regulated by ITU. The characteristics of 2.45 GHz systems are similar to those using other UHF bands. The operation of passive UHF RFID systems is based on backscattering communications, first described by Stockman [Stockman, 1948]. The principle of operation of a RFID system is explained via the link budget calculation in section 2.2.1.

Table 2.1. RFID regulations in Europe and the US [Lahiri, 2006 & ERC Recommendation 70-03]

Region	LF	HF	UHF band	Microwave
United States	125-134 kHz	13.56 MHz 10 Watts Effective Radiated Power (ERP)	902-928 MHz, 1 Watts ERP or 4 Watts ERP with a directional antenna with at least 50-channel hopping.	2.4000-2.4835 GHz 4 Watts ERP 5.725-5.850 GHz 4 Watts ERP
Europe	125-134 kHz	13.56 MHz	865-865.5 MHz 0.1 Watts ERP, Listen before Talk (LBT). 865.6-867.7 MHz, 2 Watts ERP, LBT 867.6-868.8 MHz, 0.5 Watts ERP, LBT	2.446-2.454 GHz 0.5 Watts Effective Isotropic Radiated Power (EIRP), unrestricted use. 4 Watts EIRP, restricted use.

2.2.1. Link Budget

A link budget calculation is required in any wireless communication system, including RFID systems. The calculation helps engineers specify the power budget for the transmitter and receiver, separated by some distance (or read range). It accounts for the sensitivity and antenna gains of the transmitter and the receiver, and the radiated power from transmitter antenna. It also considers propagation losses.

In an RFID system, the read range is specified from the link budget calculations in "downlink" and "uplink" communication i.e. the communication from the reader to the tag and from the tag to the reader respectively.

Consider an RFID system working with line-of-sight (LoS) and no polarisation loss between the reader antenna and the tag antenna, Fig. 2.1.

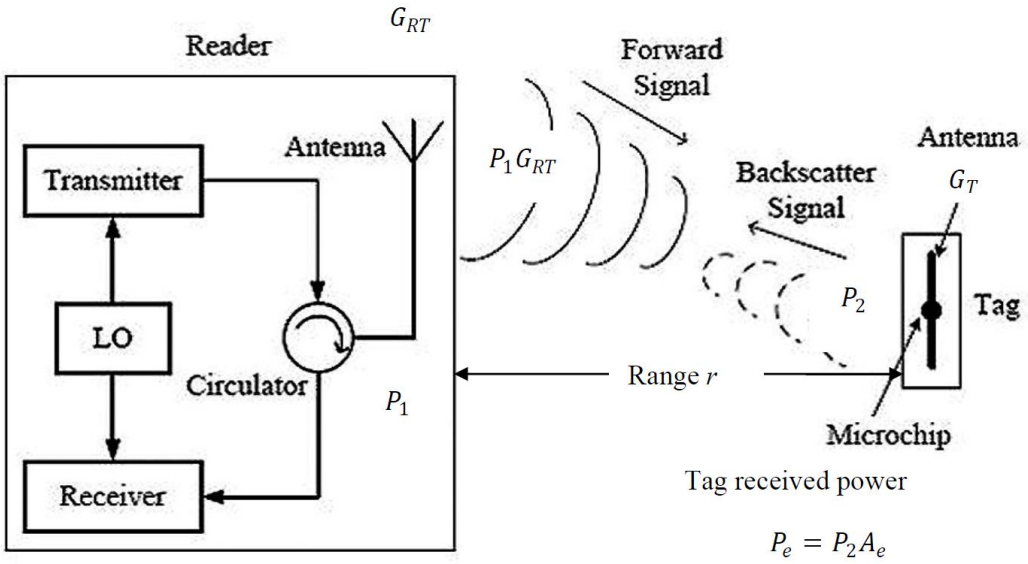

Figure 2.1. Typical passive RFID system [Fan, 2007]

The reader emits electromagnetic waves with the radiated power P_1. The reader transmitting antenna gain is G_{RT}, therefore the effective radiated power (ERP) into the surrounding space is $P_1 G_{RT}$. In the European Union (EU), the ERP is restricted to a maximum of 2W [EU commission]. Only a small part of the transmitted power reaches the tag which is proportional to the field strength $E(r)$ at distance r. The radiation intensity at the transponder P_2 is calculated by the following equation [Finkenzeller, 2010]:

$$P_2 = \frac{P_{EIRP}}{(4\pi)r^2} = \frac{P_1 G_{RT}}{(4\pi)r^2} \qquad (2.1)$$

The tag antenna has the effective aperture of A_e which is related to the tag's antenna gain by [Finkenzeller, 2010; Balanis, 2005]:

$$A_e = \frac{\lambda^2 G_T}{4\pi} \tag{2.2}$$

where G_T is the tag antenna gain and λ is the wavelength.

Therefore, the tag receives power P_e given by [Fan, 2007]:

$$P_e = P_2 A_e = P_1 \frac{G_{RT} G_T \lambda^2}{(4\pi r)^2} \tag{2.3}$$

This power is used as the energy source for the operation of the tag. The maximum distance at which the tag receives just enough power to activate is called the downlink-limited range of the RFID system:

$$P_e(r_{max}) = P_{threshold} \tag{2.4}$$

As described above, only a small proportion of the emitted power from the reader's antenna, P_1, reaches the tag antenna. A part of the irradiated power is reflected back in the direction of the reader, and this is related to the scatter aperture A_s i.e. the tag antenna radar reflectivity cross section σ of the tag antenna by [Fan, 2007]:

$$P_s = P_2 A_s = P_2 \sigma \tag{2.5}$$

The backscattered signal propagates back to the reader experiencing free space loss yielding a power at the reader of:

$$P_3 = \frac{P_S}{4\pi r^2} A_{e-reader} = P_s \frac{G_R \lambda^2}{(4\pi r)^2} \tag{2.6}$$

The radar cross section (RCS) is dependent on the relationship between the impedance of the tag chip Z_t, and the impedance of the tag antenna Z_a by [Nikintin, 2006]:

$$\sigma = G_t^2 \frac{\lambda^2}{\pi} \frac{R_a^2}{|Z_a + Z_t|^2} \tag{2.7}$$

with $Z_a = R_a + jX_a$ is the tag antenna impedance, $Z_t = R_t + jX_t$ is the tag chip impedance.

If $Z_t = 0$ (short-circuit), and the tag antenna is purely resistive i.e. $X_a = 0$ the RCS is:

$$\sigma_{sc} = G_t^2 \frac{\lambda^2}{\pi} \tag{2.8}$$

By contrast, if $Z_t = \infty$ (open-circuit), the minimum radar cross section is $\sigma_{min} = 0$. Typically for power matching, Z_t is the complex conjugate of Z_a i.e. $Z_t = Z_a^*$ and the radar cross section is:

$$\sigma = G_t^2 \frac{\lambda^2}{4\pi} \tag{2.9}$$

In the case of perfect matching between the tag chip and the antenna, the energy reflected back is equal to the energy absorbed by the tag.

Chip impedance changing is used to modulate the backscattered signal with the data from the tag.

2.2.2. UHF RFID Reader Antenna

As discussed in section 2.2.1., the tag and reader antennas are fundamental components and greatly affect the performance of any RFID system. The antenna fundamental characteristics such as radiation pattern, bandwidth, gain, and polarisation are described in section 2.4 and are key when designing any antenna including those for RFID readers.

In this project, a new reader antenna is designed to operate with existing RFID tags. The designs are based on microstrip technology, like most UHF RFID reader antennas, because they are cheap, compact, easy to fabricate and modify as well as to customise [Dobkin, 2008]. The detailed designs are given in chapters 3 and 4.

2.2.3. RFID Anti-collision

Anti-collision is a key feature of RFID systems. Anti-collision systems manage the communications between one or multiple readers and multiple tags. The algorithm ensures that only one tag is read at a time. Currently, there are two main anti-collision protocols: ALOHA and Tree [Chin, 2010]. These two algorithms can be categorised into "deterministic" and "probabilistic" [Roy, 2010]:

1. **Deterministic algorithm** (Tree): is the slow process where each bit of the tags is queried individually until identification of all the tags takes place. The algorithm requires complex hardware and memory overheads.
2. **Probabilistic algorithm** (ALOHA), is quicker as the tags transmit their identities at random intervals of time. The reader is simpler, and has lower bandwidth requirements [Chin, 2010].

2.3. RFID Localisation Techniques

At the moment there are several of RFID systems that can provide the location and identification of a tagged object e.g. Aeroscout and RFID-radar. All positioning systems, including these, use one or a combination of a few of the following techniques to locate and track an object:

- Time of Arrival (ToA).
- Time Difference of Arrival (TDoA).
- Angle of Arrival (AoA) or Direction of Arrival (DoA).
- Received signal strength (RSS).
- Pattern Recognition.

In general, a mobile device (or mobile station - MS) such as a RFID tag, is tracked by some fixed devices called base stations (BS), in this case a RFID reader.

2.3.1. Time of Arrival (ToA)

Most radar systems use the ToA technique in order to find and track a craft. Positioning systems based on ToA use the first detected peak (FDP) in a backscattered signal to determine the time of flight from the BS to the MS. Since, in air, radio waves travel close to the speed of light in free space $c \approx 3 \times 10^8$ m/s, the distance between the BS and the MS can be calculated from the time of flight. In two dimensions (2D), the position of the MS is located using tri-lateration from three or more distances from BSs to a MS.

However, this simple technique might not suitable for indoor localisation, typical for RFID applications, for several reasons. Firstly, it requires a direct path or line of sight (LoS) between the transmitter and receiver. Secondly, since the radio wave travels at speed of 300m/μs, a tiny error in time can cause serious problems with accuracy. Finally, TOA techniques require time synchronisation setting, resulting to high cost [Kharrat, 2011].

2.3.2. Time Difference of Arrival (TDoA)

The TDoA-based localisation systems are familiar due to their use in airport ranging systems. These systems are based on the time difference between received signals arriving at each BS relative to a reference BS. Therefore, they do not require knowledge of the transmission time at the MS. However the BSs need accurate time synchronisation.

The TDoA technique requires at least two time differences i.e. three BSs to locate an MS in 2D using *hyperbolic lateration*. Assuming that three BS are labelled A, B, and C; the time differences of signals received from MS X at B and C relative to reference BS A are t_{B-A} and t_{C-A} respectively (Fig. 2.2) i.e. the difference of distances of BX-AX and CX-AX are $t_{B-A}c$ and $t_{C-A}c$ metres, with c is the speed of light. Therefore, two hyperbolas can be plotted from the known time differences :

$$d_{X-B} - d_{X-A} = t_{B-A}c \tag{2.10}$$

$$d_{X-C} - d_{X-A} = t_{C-A}c \tag{2.11}$$

with $d_{X-A}, d_{X-B}\ d_{X-C}$ are the distances between X and A, B, and C, respectively.

The intersection of these hyperbolas is the MS location.

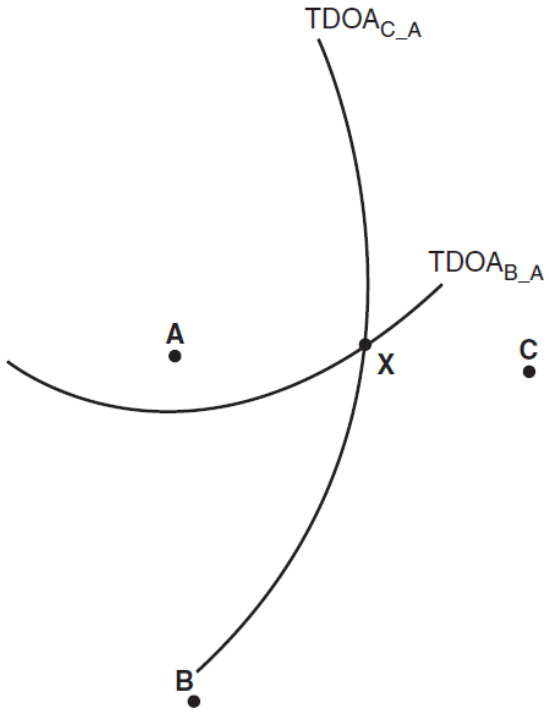

Figure 2.2. Time difference of Arrival (TDoA) [Cisco]

In the case that there are more than one intersection points between the two hyperbolas, one more BS is required to draw another hyperbola.

TDoA based systems are similar to ToA-based systems as the LoS requirement limits their application in indoor environments and they share the same disadvantages i.e. they rely upon very accurate time measurement and synchronisation.

2.3.3. Angle of Arrival (AoA) or Direction of Arrival (DoA)

Angle of arrival (AoA) or Direction of arrival (DoA), as the name implies, are localisation techniques based on the direction of propagation of an incident signal. In order to determine this, the BS must be equipped with an antenna array. From phase differences at individual elements of the array, the AoA can be calculated.

The AoA technique is used in the mobile phone industry to locate and track a mobile phone e.g. when a user makes an emergency call. The signal angles of arrival from that user to two or more base stations are used to perform triangulation to find out where the caller is. AoA is also used to locate unlicensed radio transmitters.

RFID systems often use anti-collision algorithms, therefore the AoA estimation is only required to process signals from a single tag at each time. Zhang et al. [Zhang, 2007] shows through performance analysis and simulation results that simple AoA estimation methods via structure of two antennas can be used to provide satisfactory localization performance.

2.3.4. Received Signal Strength (RSS)

RSS localisation systems measure the received signal strength at each BS. This may be derived from the wireless infrastructure since most wireless devices measure and report the RSS. In simple environments where multipath propagation does not affect the RSS and the MS has light-of-sight with the BSs, the RSS can be used to determine the distance between them. Propagation models predict that the RSS received at a distance d, RSS_d in dB, decays linearly with log-distance as follows [Alejos, 2010; Heidari, 2008]:

$$RSS_d = 10log_{10}P_r = 10log_{10}P_t - 10\alpha log_{10}d + X$$
$$+G_T(dB) + G_R(dB) - 32.4 - 20\log_{10} f \qquad (2.12)$$

where P_t, P_r are the transmitted and received power respectively, X is the shadow fading, f is the working frequency and α is the distance-power gradient i.e. the path loss exponent from the environment.

In free space where $\alpha = 2$, the propagation distance can be determined from the transmit and receive powers and triangulation can be used to locate the object given sufficient BSs. However, this cannot be used in an indoor environment since the multipath fading and shadow fading seriously affects the instantaneously RSS, which is also highly variable in both space and time.

Currently, most indoor localisation systems, including RFID systems, use a pre-determined radio map of the RSS. Pattern-recognition is used to determine the most likely position of the tracked object. This will be discussed further in the follow technique of location patterning.

2.3.5. Location Patterning (Pattern Recognition)

Location patterning is a localisation technique based on the known radio signal behaviour pattern in a specific environment. Most pattern-recognition RFID localisation systems use the received signal strength (RSS) metric to determine the location of the user. Typically a pattern-recognition system operates in two phases:

- Calibration phase,
- Operational phase.

2.3.5.1. Calibration Phase

In the calibration phase, a test mobile device is walked-around the target environment. By sampling and recording an array (or location vector) of RSS values at multiple receiving sensors (access point in the case of 802.11 WLANs) at many sample locations, the pattern is built. The number of the receiving stations that can read the mobile devices determine the size of location vector for one location [Cisco]. The calibrated RSS pattern of an environment is graphical represented by a set of grid points or notations. The greater the number of grids or notations, the more precise is the pattern.

A difficulty of determining a pattern is that the signal received at the receiving sensors varies even with the test device at a specified location. Therefore, in the calibration phase many samples of signal strength for a mobile device are recorded. The vector array element actually recorded for the pattern is determined by the technique used e.g. in the mean signal strength technique the value of an array element for a sensor is the mean signal strength of all measurements at that sensor.

The RSS depends upon many factors other than location, such as orientation of the MS antenna and the polarisation. Also, other transient objects in the environment, such as

items or the tags themselves, can affect the RSS pattern.

2.3.5.2. Operational Phase

In the operational phase, the location of a tracked device is determined by the ability to "match" the reported RSS data from a number of sensors with the pattern data measured in the calibration phase.

2.4. Antennas

Antennas are key component of any wireless systems. Antennas are devices for radiating or receiving radio waves. In RFID systems, the antennas are used to communicate between readers and tags. In this section, basic antenna parameters are discussed.

2.4.1. Fundamental Parameters of an Antenna

2.4.1.1. Resonant Frequency

The resonant frequency of an antenna is the frequency in which the antenna most efficiently transforms power between electrical oscillations in the feed and radio waves. In this thesis, the resonant frequency considered is 2.45 GHz. This is a microwave frequency within the Industrial-Scientific-Medical (ISM) bands. The ISM bands are defined by the ITU-R in 5.138, 5.150, and 5.280 of the Radio Regulations.

2.4.1.2. Bandwidth

Antenna bandwidth is the frequency range around the resonant frequency at which the efficiency of the antenna, in transmitting or receiving EM waves, is larger than a certain proportion of the resonant frequency efficiency e.g. 90%. For a transmit antenna, conservation of energy suggests that any power that is not transmitted is reflected back into the feed. A 90% efficiency is associated with a Return Loss (RL) of 10 dB. RL Bandwidth (BW) is calculated by:

$$BW = \frac{f_2 - f_1}{f_{resonant}} \times 100\% \qquad (2.13)$$

where f_1 and f_2 are the frequencies at that the antenna efficiency is the given proportion.

2.4.1.3. Impedance

In [Balanis, 2005], the antenna impedance is defined as "the impedance presented by an antenna at its terminals or the ratio of the voltage to current at a pair of terminals or the ratio of the appropriate components of the electric to magnetic fields at a point".

Any antenna has three different impedance components: radiative, resistive, and reactive. Together, these are referred to as the impedance of the antenna. Antenna impedance (Z_A) can be written:

$$Z_A = (R_r + R_L) + jX_A \qquad (2.14)$$

where R_r, R_L and X_A are radiation resistance, loss resistance and the reactance of the antenna.

Radiative resistance is proportional to radiated power. The loss resistance represents the heat dissipation of the antenna. At resonant frequency, the reactive resistance becomes zero, and the antenna is at its most efficient.

2.4.1.4. Radiation Pattern

The radiation pattern is usually a graphical representation of the radiation properties including power flux density, radiation intensity, field strength and polarization as a function of angle. Among these patterns, the power pattern which represents the spatial distribution of radiated power, is usually of most interest [Balanis, 2005]. Spherical coordinates are the most convenient and useful when describing the radiation pattern in the far-field region. It may be presented in a two-dimension (2D) or three-dimension (3D) distribution of normalised power against spherical coordinate parameters (azimuth and elevation).

There are several types of pattern: isotropic, omni-directional, and directional.

- **Isotropic pattern**

  An isotropic pattern is produced by an isotropic radiator, which radiates equally in all directions. An isotropic radiator is not physically realizable. However, it is often used as a reference for actual antennas when expressing directional properties.

- **Directional pattern**

A directional antenna transmits and receives more effectively in some specific directions than others. All practical antennas are directional.

- **Omni-directional pattern**

  An omni-directional pattern is a special case of directional patterns. This pattern is uniform in a specific plane. [Balanis, 2005]

Some fundamental parameters of antenna patterns are radiation lobe, main lobe, minor lobe (or side lobe), back lobe, half-power beamwidth and first null beamwidth.

- **Radiation lobe**

  The radiation lobe of a pattern is a peak in the radiation intensity, which is surrounded by weaker radiation intensity region. There are several types of radiation lobe: main lobe, side lobe (or minor lobe) and back lobe.

- **Main lobe**

  Main lobe is the radiation lobe containing the maximum power.

- **Minor lobe (or side lobe)**

  Any radiation lobes other than the major lobe are minor lobes or side lobes.

- **Back lobe**

  Back lobe is the radiation lobe that is in the opposite direction to the main lobe.

- **Half-power beamwidth, first-null power beamwidth**

  The angular beamwidth at the half power level, and at the first null on the either side of the main beam, are half-power beamwidth and first-null power beamwidth, respectively.

2.4.1.5. Field Regions

Three notional regions surround an antenna: reactive near field region, radiating near-field (Fresnel) region and far-field (Fraunhofer) region.

1. **Reactive near field regio**n

   The reactive near-field immediately surrounds the antenna. In this region, the reactive field is dominant. This region exists in the space around the antenna limited by the distance defined by [Balanis, 2005]:

$$R_1 = 0.62\sqrt{\frac{D^3}{\lambda}} \tag{2.15}$$

   where λ is the wavelength and D is the largest dimension of the antenna.

2. **Radiating near-field (Fresnel) region**

   The radiating near-field (Fresnel) region is the intermediate region between the reactive near-field region and the far-field region. In this region, the radiation fields are dominant and the angular field distribution is dependent on the distance from the antenna. This region is commonly assumed to exist in a region with inner boundary R_1 and the outer boundary of radius [Balanis, 2005]:

$$R_2 = \frac{2D^2}{\lambda} \tag{2.16}$$

3. **Far-field (Fraunhofer) region**

   In the called far-field (Fraunhofer) region, the field distribution is independent of the distance from the antenna. In most cases, the minimum distance from the antenna to the far-field region is R_2 defined by Equation (2.16).

2.4.1.6. Directivity

The directivity $D(\theta, \phi)$ of an antenna is a parameter that expresses the ratio of the radiation intensity in a given direction to the intensity averaged over all directions. For an isotropic antenna the directivity is unity.

When describing an antenna, its directivity often refers to maximum directivity, in the direction that the antenna radiates maximum radiation intensity.

2.4.1.7. Antenna Radiation Efficiency

In transmitting mode, an antenna is driven by a generator. The total power radiated by the antenna cannot be more than the total power provided from the generator. The radiation efficiency (e_{cd}) of the antenna is the ratio of total radiated power (P_{rad}) to the total power provided to the antenna (P_{total}).

$$e_{cd} = \frac{P_{rad}}{P_{total}} = \frac{P_{rad}}{P_{rad} + P_{in}} = \frac{R_r}{R_r + R_L} \quad (2.17)$$

2.4.1.8. Antenna Gain

The gain $G(\theta, \phi)$ of an antenna is the ratio of the radiated power density at a distant point to the total input power (P_{in}) radiated isotropically.

Gain is the product of efficiency and directivity:

$$G(\theta, \phi) = e_{cd} D(\theta, \phi) \quad (2.18)$$

When the radiation efficiency of the antenna is unity and the gain has the same value as the directivity.

2.4.1.9. Radiated Power

The radiated power of any antenna is given in terms of effective radiated power (ERP) and effective isotropic radiated power (EIRP). ERP is defined by:

$$P_{ERP} = P_{supplied}\ G_d \quad (2.19)$$

where $P_{supplied}$ is the supplied power to the antenna and G_d is the antenna gain relative to a dipole antenna.

Similarly, EIRP is the product of the supplied power and isotropic relative gain:

$$P_{EIRP} = P_{supplied}\ G_i \quad (2.20)$$

G_i is the antenna gain relative to an isotropic antenna.

The terms ERP and EIRP are very important to wireless antenna particularly in RFID because the radiated power is strictly regulated.

In RFID, the ERP and EIRP relate to the reader antennas. For the same radiated power, the reader gain is recommended as high as possible since the system power supplied is reduced resulting in lower cost, increased component life time and increased read range [Roy, 2010].

2.4.1.10. Polarisation

The polarisation of an antenna in a given direction is the polarisation of the wave radiated by the antenna in that direction. The polarisation of a radiated wave is "the property of an electromagnetic wave describing the time varying direction and relative magnitude of the electric-field vector; specifically, the figure traced as a function of time by the extremity of the vector at a fixed location in space, and the sense in which it is traced, as observed along the direction of propagation" [Balanis, 2005].

There are three special classes of polarisation: linear, circular, and elliptical.

Antenna gain can depend upon the relative alignment of the antenna to the radio wave polarisation axis. Therefore, the polarisation of the incident wave and the receiving antenna can affect the received signal due to the polarisation loss factor. If their polarisations are perpendicular to each other, the loss factor may be 100dB. Therefore, when designing an antenna the polarisation is an important aspect to be considered.

Axial Ratio (AR): is a property of an elliptically polarised field. AR is the ratio of major and minor axes of the polarisation ellipse:

$$AR = \frac{E_{max}}{E_{min}} \tag{2.21}$$

For circular polarisation, $AR = 1\ i.e.\ 0\ dB$.

In practice, elliptically polarised radiation with an AR smaller than 3 dB is considered to be circularly polarised (CP).

2.4.2. Antenna Arrays

In order to achieve a more directive antenna, and implicitly increase the gain, an antenna must have large aperture relative to the wavelength. One effective way to enlarge the dimensions of the antennas is to use multi-elements in an electrical and geometrical configuration i.e. to form an array. Often, the elements of an array are identical. The shape of the radiation pattern of an array is determined by: the geometrical configuration of the array, displacement between the elements, the excitation phase and amplitude of the individual elements and the relative pattern of the elements.

Previous work [Balanis, 2005] with the assumption of no mutual coupling, predicts the total field (in the far-zone) of an antenna array is the product of the field of a single element at reference point and the array factor (AF):

$$E(total) = [E(single\ element)] \times [AF] \tag{2.22}$$

where the AF (array factor) is dependent on the arrangement of antenna elements.

2.4.2.1. Linear Array of N Elements

In this section, some of the properties of linear array antennas are listed [Balanis, 2005]. Consider a uniformly-spaced linear array of *N* elements that are fed by uniform amplitude currents. The distance and the phase difference between two consecutive elements are d and α, respectively.

The array factor (*AF*) of this linear array is given by [Balanis, 2005]:

$$AF = 1 + e^{j\psi} + e^{j2\psi} + \cdots + e^{j(N-1)\psi} = \sum_{n=1}^{N} e^{j(n-1)\psi} \tag{2.23}$$

where $\psi = kdcos\theta + \alpha$ with $k = \frac{2\pi}{\lambda}$ is the phase constant, θ is the angle of arrival (AoA), and α is the progressive phase between two consecutive elements.

Therefore,

$$AF = \frac{1 - e^{jN\psi}}{1 - e^{j\psi}} = e^{j\left[\frac{N-1}{2}\right]\psi} \frac{sin\left(\frac{N}{2}\psi\right)}{sin\left(\frac{1}{2}\psi\right)} \tag{2.24}$$

with the reference point being the physical centre of the array, the array factor is:

$$AF = \frac{sin\left(\frac{N}{2}\psi\right)}{sin\left(\frac{1}{2}\psi\right)} \tag{2.25}$$

The nulls of the array antenna pattern due to the AF i.e. ignoring the nulls due to individual elements, can be found by setting the array factor to zero i.e. *AF* = 0.

The nulls of the array factor occur when [Balanis, 2005]:

$$\theta_{nulls} = cos^{-1}\left[\frac{\lambda}{2\pi d}(-\alpha \pm \frac{2n}{N}\pi)\right] \tag{2.26}$$

with n =1, 2, 3… and $n \neq N, 2N, 3N \ldots$

The maximum gain of the array is *N* compared with a single element antenna i.e.

$AF_{max} = N$. The maximum values occur when [Balanis, 2005]:

$$\theta_{peak} = cos^{-1}\left[\frac{\lambda}{2\pi d}(-\alpha \pm 2m\pi)\right], \text{m} = 0, 1, 2 \ldots \quad (2.27)$$

2.4.2.2. Smart Antenna

The term "smart antenna" refers to an antenna array and feed electronics which can modify the beam pattern in order to emphasise signals of interest and to minimise interfering signals [Gross, 2005].

Smart antennas can generally be classified into Switched Beam or Adaptive Array. Switched beam antennas have several predefined beam patterns. Adaptive systems allow the antenna to steer the beam to any direction of interest while simultaneously nulling interfering signals.

Smart antennas have a number of advantages over fixed antennas leading to enhanced system capacity, multipath mitigation, better signal-to-noise (SNR) ratios and improved angle of arrival (AoA) estimation.

In this thesis, switched beam antennas are studied. This type of antenna is generally fed by a radio frequency (RF) beamformer. One of the simplest and most popular beamformers is the Butler Matrix (BM), is named after its inventor [Butler, 1961]. An $N \times N$ BM is a network with N inputs and N outputs, often used to feed a uniformly spaced linear array antenna with N possible beam directions (N is often power of 2 i.e. $N = 2^i \; with \; i = 1, 2\ldots$).

The BM is the analogue equivalent of the discrete Fourier Transform and has many benefits such as:

- Simple network: BM is made up from only a few components: hybrid couplers, crossovers and phase shifters. The BM is easy to design as they are often symmetrical and easily implemented with microstrip components.

- The generated beams are high directivity and orthogonal.

However, the simple BM has some major drawbacks including:

- The BM forms beams that change with frequency i.e. the beamwidth and beam angle vary with frequency.

- The number of components grows very large when the number of antenna elements is large.

The BM is described in detail in Chapter 4.

2.5. Microstrip

Microstrip technology involves the construction of very thin layers of conductor laid upon an insulating dielectric substrate. The strips of conductive material can be glued on or, more commonly formed by printed circuit board processes such as photo-etching or milling. Microstrip circuits have many advantageous characteristics such as a low profile, compactness, light weight, mechanically robustness when mounted on rigid surfaces. They are easy to fabricate either alone or with microwave circuits, particularly monolithic microwave integrated circuits (MMICs).

All the circuits fabricated in this thesis are made up from microstrip.

2.5.1. Microstrip Antenna

The first microstrip antenna was introduced in the 1950s [Deschamp, 1953]. They have received attention since the 1970s. These antennas can be found on the surface of satellites, missiles, cars, and mobile telephones. With the advantages of the microstrip technology described above, microstrip antenna design is very flexible in terms of resonant frequency, polarisation, pattern, and impedance (Balanis, 2005). Since then, microstrip antennas have become ubiquitous in microwave radio communications systems. A CP antenna with a single microstrip-line feed is one of the simplest radiators for exciting circular polarisation.

Microstrip antennas consist of a very thin metal strip (patch) on a dielectric substrate covered by a ground plane on the other side.

The radiating frequency of the antenna is determined by the dimensions of the patch. Microstrip antennas have a broad beam that is broadside to the substrate.

The most common type of microstrip antenna is the rectangular patch as shown on Fig. 2.3. Typically the rectangular patch has the gain of about 6 to 8 dBi, and a half-power beamwidth of about 70^0 [Dobkin, 2008; Balanis, 2005]. Assuming the antenna lies in the *x*-*y* plane, the E-plane is the *x*-*z* plane, and H-plane is the *y*-*z* plane (Fig. 2.3).

There are several methods for feeding microstrip antenna, considered in the next Section. Among these, the feed method used in this project is microstrip line feed due to

the ease of fabrication and simplicity of impedance matching [Balanis, 2005].

2.5.2. Feeding and Matching to a Microstrip Antenna

There are several methods for feeding microstrip antenna such as a microstrip line, coaxial probe, aperture coupling and proximity coupling [Balanis, 2005]. Among these methods, the coaxial probe and the microstrip line are the more popular and widely used.

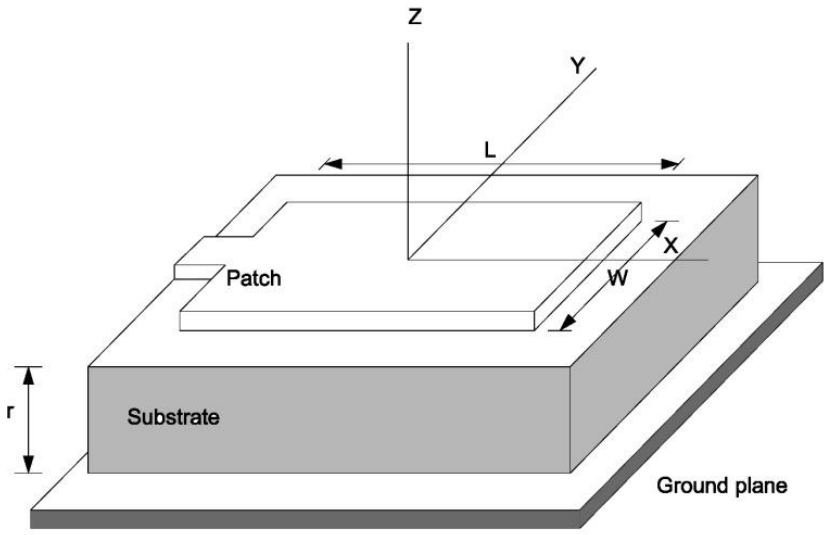

Figure 2.3. Microstrip patch antenna

Many patch antennas are driven by coaxial cable which can connect through the substrate to any point on the antenna surface. This point can be chosen to match the antenna input impedance to the characteristic impedance of the cable. To optimise power transmission to the antenna, some system is required to match the antenna to the microstrip. As the fundamental resonance typically has the largest current densities in the interior of the patch, the impedance is usually largest on the edge and decreases towards the centre of the patch. For patch antennas to be integrated into RF systems, it is more desirable for the antenna to be driven by a microstrip transmission line which joins the patch at the edge.

A standard 50-ohm transmission line terminated at the edge of a typical square patch antenna would experience a very high transmission loss due to reflection of the input signal at the antenna. In this project, most antennae are matched to 50-ohm port using a generalised transformer i.e. a short section of new transmission line is inserted between the main transmission line and the load. The dimensions of the load and new transformer transmission line are less than a wavelength and the input impedance is matched to that of the main line. The characteristic impedance Z_t and the length l of the transformer are obtained from Equations 2.28 and 2.29 given by [Pozar, 2005]:

$$Z_t = \frac{\sqrt{Z_0 R_A - R_A^2 - X_A^2}}{\sqrt{1 - \frac{R_A}{Z_0}}} \quad (2.28)$$

$$\tan(\beta l) = \frac{Z_t (Z_0 - R_A)}{Z_0 X_A} \quad (2.29)$$

where the characteristic impedance of the driving line is $Z_0 = 50\,\Omega$, the input impedance of the antenna is $Z_A = R_A + jX_A$, and β is the wavenumber: $\beta = 2\pi/\lambda$.

2.6. Software

This project uses several simulation software packages to illustrate theory and to predict the performance of circuits and systems. These include MatLab, Agilent's ADS (Advanced Design System) 2008 with its tool LineCalc and Ansys's HFSS v11.

2.6.1. ADS

Advanced Design System (ADS) is electronic design software created and developed by Agilent [ADS]. The software is very useful for RF, microwave, and high speed digital applications. ADS has been used by many companies in many application areas, but most particularly in wireless communication and networking.

In this project, ADS is used to optimise and verify the performance and size of a Butler matrix.

The LineCalc tool of ADS is used to calculate the dimensions of the microstrip transmission lines on a specific substrate from their characteristic impedance and electrical length.

2.6.2. HFSS

Electromagnetic simulation packages produce approximate solutions of Maxwell's equations. A range of numerical methods can be employed including Finite Difference Time Domain (FDTD), Method of Moments (MOM) and Finite Element Method (FEM). These techniques differ in their discretisation (or meshing) of different electromagnetic properties (MoM: surface current, FEM: electric field and FDTD: electric and magnetic field). FEM is a full-wave technique, incorporating all interactions, and with no physical approximations or assumptions. It makes FEM one of the most accurate simulation techniques. One of the most well-known FEM simulators is HFSS.

HFSS developed by Ansoft (now Ansys) subdivides objects or regions into 3D elements, usually tetrahedra [HFSS]. One of the key advantages of the HFSS is that its

graphical interface is friendly to users, simplifying the handling of complex structures. The simulator employs adaptive meshing to calculate parameters including S Parameters, resonant frequency, and fields. Some performance parameters of the HFSS FEM package include [HFSS help documents]:

- **Number of Passes**: In HFSS, the number of passes is the number of mesh refinement cycles that HFSS performs. The number of passes is directly related to the number of created tetrahedral elements. This value has an upper limit preventing the refinement algorithm from diverging and the calculations from taking too long. The number of passes should be set as large as possible, however due to the limit of the computer resource, this parameter is set to 20 for most antenna and circuit simulations, and 10 for larger systems.

- **Convergence criteria**: The simulator refines the mesh until changes in the parameters of interest become sufficiently small. The convergence criterion used in this project is known as Maximum Delta S.

- **Delta S**: is the change of the S-parameters between two consecutive passes. The Maximum Delta S is the maximum difference of S-matrix magnitudes between two consecutive passes: $\mathrm{Max}\left(\left|S_{ij}^{N}\right| - \left|S_{ij}^{N-1}\right|\right)$, where adaptive mesh refinement takes place between stages *N-1* and *N*. During the design, the Maximum Delta Magnitude S is often set to be as small as $1e^{-4}$ i.e. 0.01% so that in most cases the simulator stops when it has finished the specified Number of Passes.

- **Radiation boundary**: Generally, an absorbing region (radiation boundary) is required when simulating waves radiated into space, particularly when evaluating antenna designs, as the FEM technique does not include a radiation condition. The waves are absorbed at the boundary so that reflected waves do not interact with the antenna. The radiation boundary can have any shape and the distance to the radiating source is, in most cases, greater than a quarter wavelength unless it is in a direction with a small amount of radiated energy. In this project the absorbing region is referred to the Air Box i.e. the Air Box is assigned the Radiation boundary. An Air box is defined by three lengths in *X*, *Y* and *Z* axes as $d_X \times d_Y \times d_Z$ (if not specified these lengths are in millimetres).

HFSS is used thorough this project for antenna designs circuit design and system analysis.

2.7. Prototype Production

All circuits and antennas were fabricated by LPKF's circuit board plotter ProtoMat S62 [LPKF], located in the Electronics Workshops of the Engineering Department. This machine provides 3-D operation with fine resolution (resolution precision as fine as 0.25 μm) and a fast speed. The working area is limited to 229 mm × 305 mm, and so this is also the area limitation for all the circuits in this project. A summary of the specifications of the plotter ProtoMat S62 can be found in Appendix 1.

The machine only supports a limited number of file formats, including Gerber. To obtain the Gerber file, the circuit models in HFSS are exported into GDSII file format. These GDSII files are then imported to ADS software. ADS software exports the circuit layout to the Gerber files.

2.7.1. Prototyping Board

All circuits are made up from copper, double-sided FR4 (abbreviation for Flame Resistant). FR4 is a very common prototyping board. The major advantages of this board include its low cost, high strength to weight ratio, ease of circuit fabrication and versatility in different environments.

The prototyping boards used throughout this project are Farnell's photo-resist copper cladboard.

The specifications of the board are listed in Appendix 2.

The specified board thickness is 1.60 mm. In practice, the measured values are between 1.59 mm and 1.60 mm, depending on individual substrate. The specified dielectric constant (or relative permittivity) and dielectric loss tangent at 1 MHz are 5.0 and 0.02, respectively. The measured relative permittivity of the board at the UHF RFID frequency of 2.45 GHz is $\varepsilon_r = 4.1$. The boards are used in all circuits and antennas. Board characteristics are not mentioned later in circuit design sections.

2.8. Measurements

Circuit and antenna measurements were taken within the Electronics Laboratory in the Department of Engineering, The University of Hull.

The S-parameters of all circuits were measured using an Agilent E8358A Network Analyzer. Depending on the number of ports (more than 2 ports), the required number of 50-Ω terminators were used for measurement.

Antenna measurements were taken in the screened room using absorbing sheets where necessary.

2.9. Summary

To summarise, Chapter 2 reviewed the fundamental background theory used in this project. In early sections, passive UHF RFID systems and the current localisation techniques are studied. Later sections introduced the microstrip antennas properties used to design all the antennas in this project. The use of switched beam array antennas proposed for RFID localisation was also discussed. Simulation software, including Agilent ADS and Ansoft HFSS, were introduced and their properties and parameters were discussed. Finally, the physical production of prototype microwave circuits was introduced and the materials and production processes described.

CHAPTER 3. MICROSTRIP RFID READER ANTENNA

3.1. Introduction

The reader antenna is one of the most vital components in an RFID system. Most UHF and microwave RFID reader antennas are patch or microstrip antennas because they are cheap, simple to fabricate, easy to modify and customise and adapt to a range of environments. Patch antennas are also one of the most effective radiators for exciting circular polarisation, which is often required in reader antenna designs in order to read tags in arbitrary orientation.

Compact CPMAs are often found in handheld or portable readers because the antenna is cheap, and the RFID reader may not require high gain and wide circular polarisation (i.e. 3-dB AR) bandwidth and RL bandwidth [Dobkin, 2008].

In section 3.2, general techniques used to analyse microstrip antenna are discussed. Section 3.3 describes the design process of a conventional square patch (SP) antenna. Initial parameters are derived from theory. These are refined by numerical analysis. Antennas are fabricated and parameters are compared with measurements. In section 3.3, a conventional corner truncated CP SP is designed, simulated and tested. Two new compact designs of microstrip antennas with slots and slits, fed by microstrip line are discussed in section 3.4.

3.2. Analysis Techniques for Rectangular Microstrip Patch

3.2.1. Transmission Line Model

The transmission line model is the simplest analytical description of a rectangular microstrip patch. It considers the patch to be two parallel radiating slots, each of width W and height (thickness) h, separated by a distance L (Fig. 3.1). However, it is the least accurate model.

In the transmission line model, a patch antenna is modelled as a section of transmission line. The characteristic impedance, Z_0, and the propagation constant, β, depend upon the patch dimensions and substrate parameters. A patch of dimension $L \times W$ is described by four edges. These four edges are classified as radiating or non-radiating edges depending on the field variation along their length i.e. the feed location.

In Fig. 3.1, the edges along the y axis are non-radiating as they almost cancel their radiating power. The edges along z-axis are radiating, and the field along their length is almost uniform.

As in the figure, the fields at the edges of the patch undergo fringing i.e. the field exists outside the dielectric thus causing a change in the effective dielectric constant. The fringing effect depends upon the dimensions of the patch and the height of the substrate. For the principal *E*-plane (*xy*-plane), fringing is a function of the ratio of the length of the patch *L* to the height *h* of the substrate (*L*/*h*) and the dielectric constant ε_r of the substrate. Normally, due to the fact that the substrate thickness is much smaller than the patch dimensions, the fringing effect is small. However, it must be taken into account because it influences the resonant frequency of the antenna.

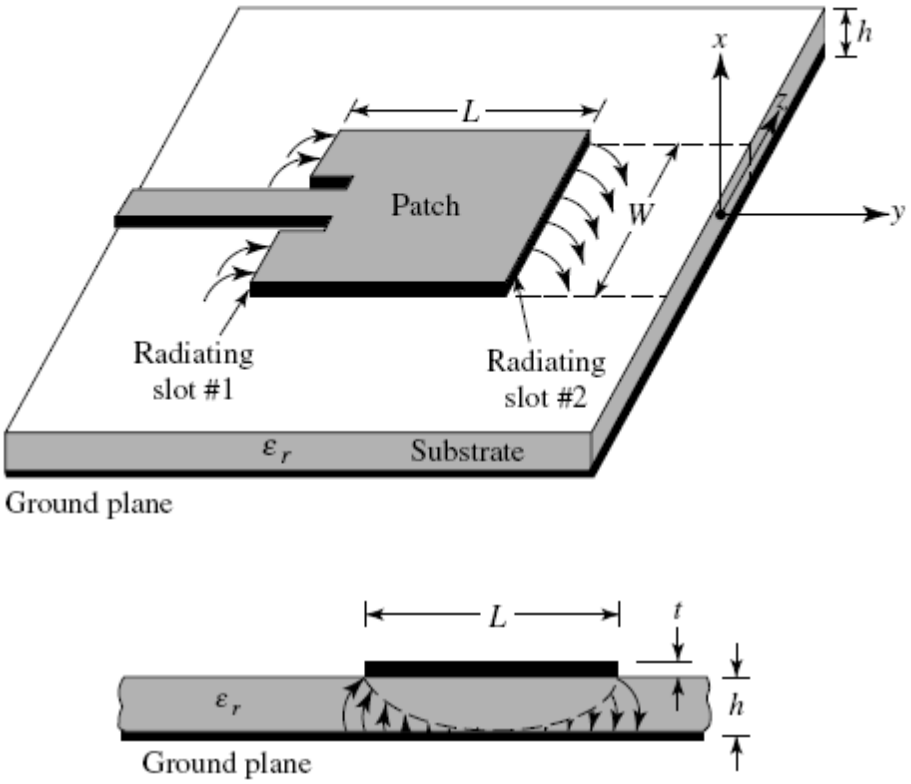

Figure 3.1. Rectangular microstrip antenna (Top view and side view)

(Diagram is taken from [Balanis, 2005])

Typically, most of the electric field lines concentrate in the substrate and parts of some lines exist in the air. Fringing effects, therefore, electrically extend the patch's physical dimensions. Since some of the waves travel in the substrate and in the air, an effective dielectric constant is introduced to take into account of fringing effects, so that the wave propagation in the line remains the same.

The initial values (at low frequencies) of the effective dielectric constant are given by [Balanis, 2005]:

$$\varepsilon_{eff} = \frac{\varepsilon_r + 1}{2} + \frac{\varepsilon_r - 1}{2} \frac{1}{\sqrt{1 + 12\frac{h}{W}}} \tag{3.1}$$

The fringing effects make the patch electrically larger than it physical dimensions. As shown on Fig. 3.2, the principal *E*-plane (*xy*-plane) is extended by $2\Delta L$. The extended length (ΔL) is calculated by the following formula:

$$\Delta L = 0.412 \times h \frac{\varepsilon_{eff} + 0.3}{\varepsilon_{eff} - 0.258} \frac{\frac{W}{h} + 0.264}{\frac{W}{h} + 0.8} \tag{3.2}$$

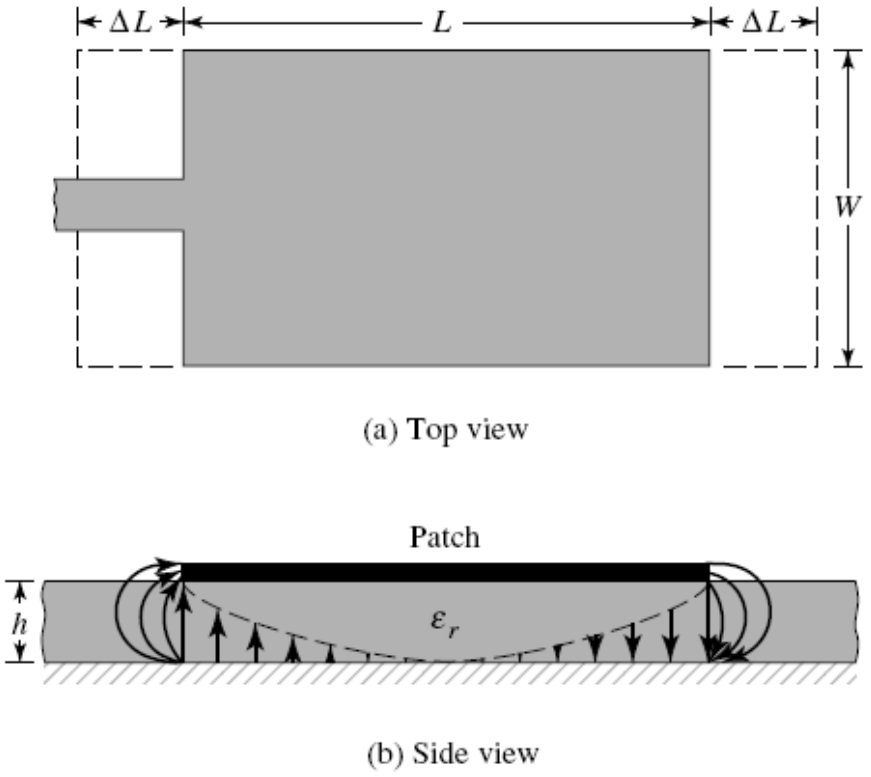

Figure 3.2. Physical and effective length of microstrip antenna

(Diagram is taken from [Balanis, 2005])

The resonant frequency is:

$$f = \frac{c}{2(L + \Delta L)\sqrt{\varepsilon_{eff}}} \tag{3.3}$$

with c is the speed of light.

The two radiating edges are characterised by a load admittance of:

$$Y_S = G_S + jB_S$$

The conductance of radiating slots, without taking into account mutual effects between the slots, can be calculated with the assumption of $h < 0.1\lambda_0$ by using [Milligan, 2005]:

$$G = \frac{W}{120\lambda_0}\left[1 - \frac{(kh)^2}{24}\right] \tag{3.4}$$

where $k = \frac{2\pi}{\lambda_0}$ is the free-space propagation constant.

The resonant input impedance is real and equal to:

$$Z_{in} = R_{in} = \frac{1}{2G} \tag{3.5}$$

3.2.2. Cavity Model

Microstrip antennas are narrow-band antenna and can be considered as lossy cavities [Garg, 2001]. In a cavity model, the patch dimensions are extended to account for the fringing effects. The region between the extended patch and ground plane can be assumed to be a resonant cavity surrounded by a magnetic wall.

Fig. 3.3 shows the charge distribution on the upper and lower surfaces of the patch, as well as on the surface of the ground plane. The movement of these charges due to attractive and repulsive mechanisms create corresponding current densities. The attraction between opposite charges on the bottom surface of the patch and the ground plane, keeps the charge concentrated on the bottom of the patch. The repulsive mechanism between like charges on the bottom surface of the patch tends to push some charge from the bottom of the patch, around its edges, to its top surface.

Since, for most practical microstrip antenna, the thickness of the substrate is much smaller than the patch dimensions, the attractive mechanism dominates. Most of the charge concentration and current flow remains underneath the patch. The current flows around the edges of the patch to its top surface can be neglected. This allows the four side walls to be modelled as perfect magnetic conducting surfaces.

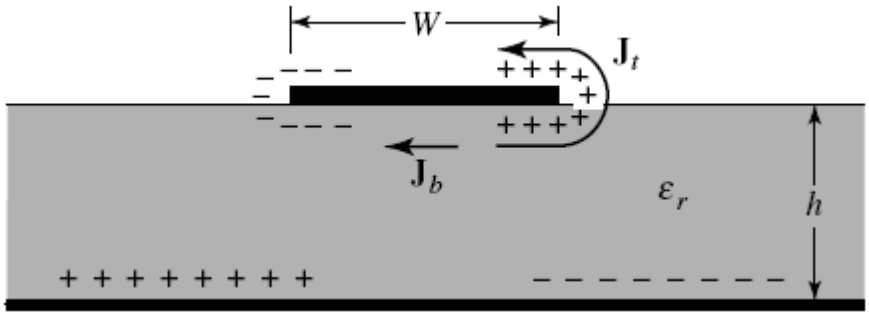

Figure 3.3. Cavity model of rectangular microstrip antenna

(Diagram is taken from [Huang, 2008])

In the multimode cavity model, the total electric field in the cavity can be expressed as the sum of the fields associated with each sinusoidal mode [Huang, 2008]:

$$E_z(x,y) = \sum_m \sum_n C_{mn} \cdot \cos\left(\frac{m\pi}{L}x\right) \cdot \cos\left(\frac{n\pi}{W}y\right) \tag{3.6}$$

where C_{mn} is a constant that depends on the feed location.

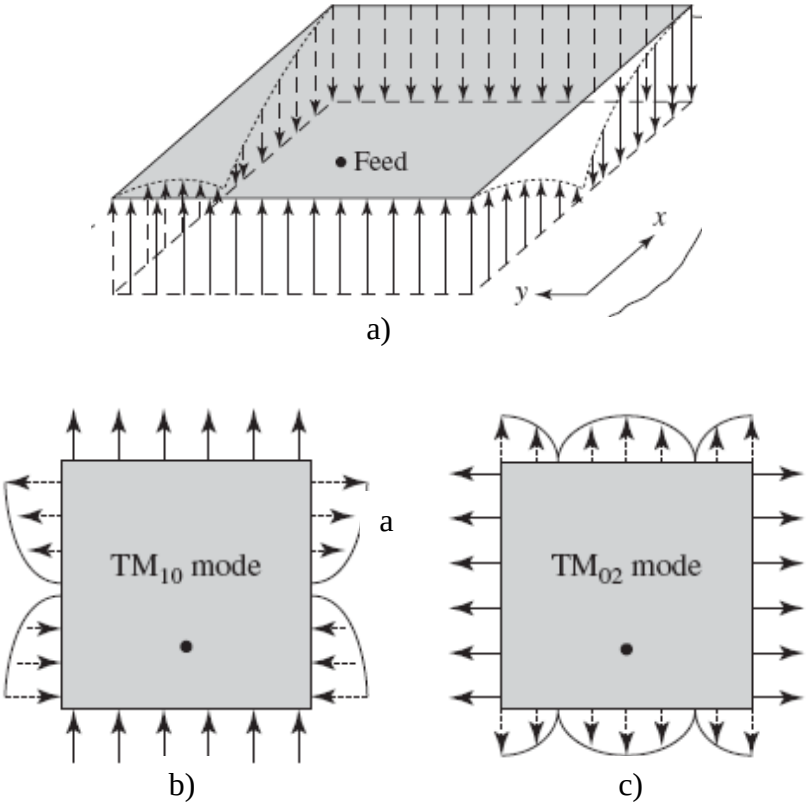

Figure 3.4. Different mode of rectangular microstrip antenna

(Diagram is taken from [Huang, 2008])

As described above, due to the very thin substrate, the fields are assumed to be aligned in the *z*-direction and uniform in this direction. If the length of the patch L is approximately half the effective wavelength, the most dominant mode is the TM_{10} mode and the field variation is shown in Fig. 3.4.

These figures indicate that there is a line that passes through the centre of patch with almost no field variation. Shorting pins or additional feed probes can be placed along this central line without disturbing the performance of the patch.

From the Fig. 3.4.a, the left- and right-edge fringing fields do not contribute much to far fields due to their oscillatory behaviour and, hence, cancel each other in the far field. The top- and bottom-edge fringing fields are the primary contributors to the far-field radiation from a patch. This is also equivalent to the two slots in the transmission line model.

The TM_{02} mode, as illustrated in the Fig. 3.4.c, contributes to the cross-polarisation radiation. In this mode, the left and right edges contribute to the far-field radiation but with lower magnitude than the mode TM_{10}. The top- and bottom-edge fringing fields contribute to the co-polarisation radiation in both the *E*- and *H*-planes, while the left- and right-edge fringing fields yield the cross-polarisation radiation only in the *H*-plane pattern, as illustrated in Fig. 3.5.

Therefore, from knowledge of the total field at the edges of the patch from all modes, the total far-field radiation patterns can be found by integrating the equivalent edge magnetic currents. The input impedance can be determined from the total radiated power and the input power.

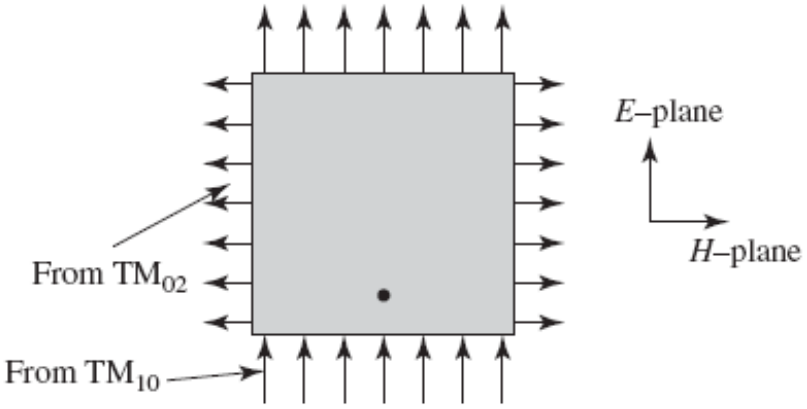

Figure 3.5. *E* and *H*- plane pattern of rectangular microstrip antenna

(Diagram is taken from [Huang, 2008])

The cavity model technique determines the mode structure underneath the patch based on the assumption of no field variation in *z*-direction. It is not very accurate, especially when the substrate is relatively thick [Huang, 2008].

3.3. Square Patch Antenna on FR4 Substrate

In this subsection, a square patch antenna is designed on standard FR4 substrate, to work at 2.45GHz. The antenna is also fabricated and tested. It is fed by a microstrip line with a quarter-wavelength transformer matching network.

The substrate has dielectric constant $\varepsilon_r = 4.1$ and dielectric loss tangent of 0.20 and thickness of $h = 1.6\ mm$ (1/16 inch).

3.3.1. Design Procedures

1. Find an approximate patch size *a* ($a = L = W$) using the following steps:
   1.1. First the width is assumed to be a half-wavelength:
   $$W = \frac{c}{2f\sqrt{\varepsilon_r}} \approx 30.24\ mm$$
   1.2. Calculate effective dielectric constant using equation (3.1):
   $$\varepsilon_{eff} = \frac{\varepsilon_r + 1}{2} + \frac{\varepsilon_r - 1}{2}\frac{1}{\sqrt{1 + 12\frac{h}{W}}} = 3.76$$
   1.3. The effective length extension due to fringing effects is calculated from equation (3.2)
   $$\Delta L = 0.412 \times h\frac{\varepsilon_{eff} + 0.3}{\varepsilon_{eff} - 0.258}\frac{\frac{W}{h} + 0.264}{\frac{W}{h} + 0.8} \cong 0.74\ mm$$
   1.4. The actual length is
   $$L = \frac{c}{2f\sqrt{\varepsilon_{eff}}} - 2\Delta L = 28.76\ mm$$
2. Estimate impedance at the edge of patch using equations (3.4) and (3.5):
   $$R_{edge} = \frac{1}{2G}$$
   Where G is the admittance of a radiating slot, typically calculated by using:
   $$G = \frac{\pi W}{\eta\lambda_0}\left[1 - \frac{(kh)^2}{24}\right]$$

These values are rough as the ground plane is assumed infinite, and so these parameters need to be refined by more detailed simulation.

3.3.2. Simulation

The patch dimensions (obtained in section 3.3.1) and the ground plane size of 70 mm × 60 mm, were used as input parameters to HFSS simulation software. The simulated resonant frequency is slightly different from the design frequency of 2.45 GHz.

The model of the square patch on FR4 substrate with a quarter wavelength transformer (QWT) is shown in Fig. 3.6.

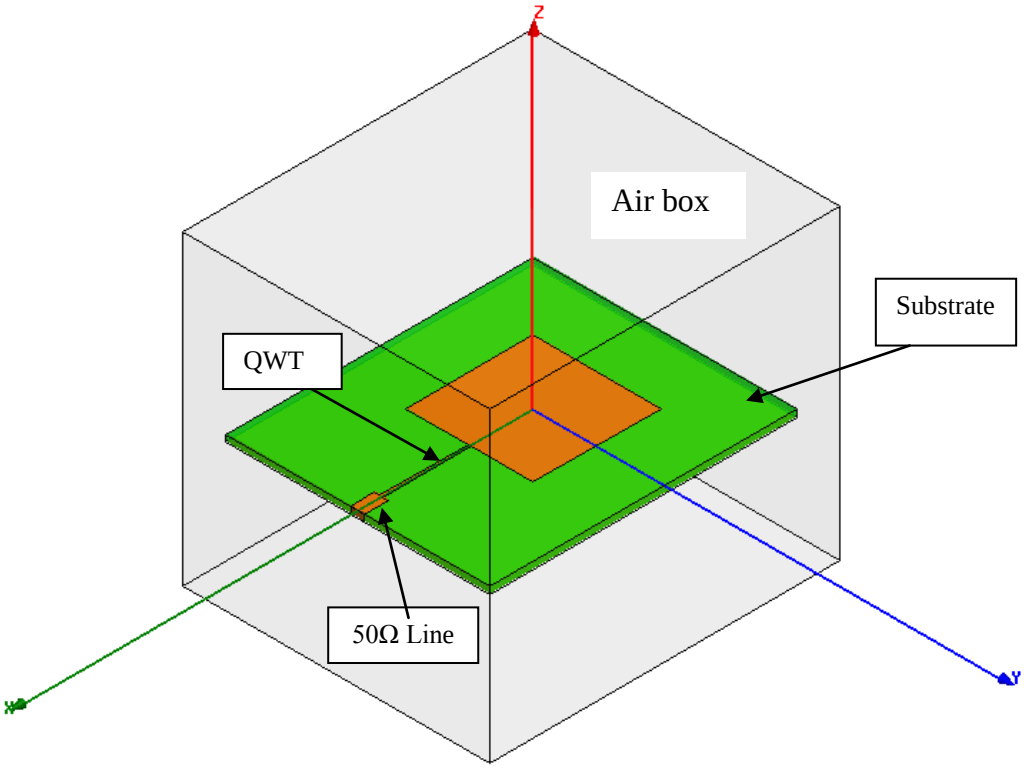

Figure 3.6. HFSS Model of the square patch on FR4

The air box size is 80 mm × 70 mm × 70 mm (in *x*-, *y*-, *z*- axis directions). The results were obtained after 20 passes, and the region was divided to 19802 tetrahedras.

A number of parameter variations were simulated to determine that the size of the patch is 29.10 mm to achieve the desired resonant frequency of 2.45 GHz. The patch is fed by a transmission line with quarter wavelength transformer for matching.

The resistance at the patch's edge can be calculated using equations (3.4) and (3.5). HFSS yields a better estimate of the resistance at the resonant frequency 2.45 GHz of 184.86 Ω. The quarter wavelength matching technique is used to match the patch with a 50-ohm line. The characteristic impedance of the QWT is:

$$Z_{qwt} = \sqrt{Z_0 R_{edge}} \tag{3.6}$$

where $Z_0 = 50\Omega$ and R_{edge} is the impedance at the edge of patch.

Hence, the characteristic impedance of the QWT is 96.14 Ω. The width and length of the transformer obtained using the ADS LineCalc application are 0.85 mm and 17.96 mm, respectively. The width of 50-ohm line is 3.23 mm.

The dimensions of the transformer were optimised by HFSS in order to achieve the largest return loss (RL) at 2.45 GHz. The optimised dimensions are 0.70 mm and 20 mm. The simulated RL and the 3-D radiation pattern are shown in Fig. 3.7 and 3.8 respectively. The simulated return loss at 2.45 GHz is greater than 30 dB.

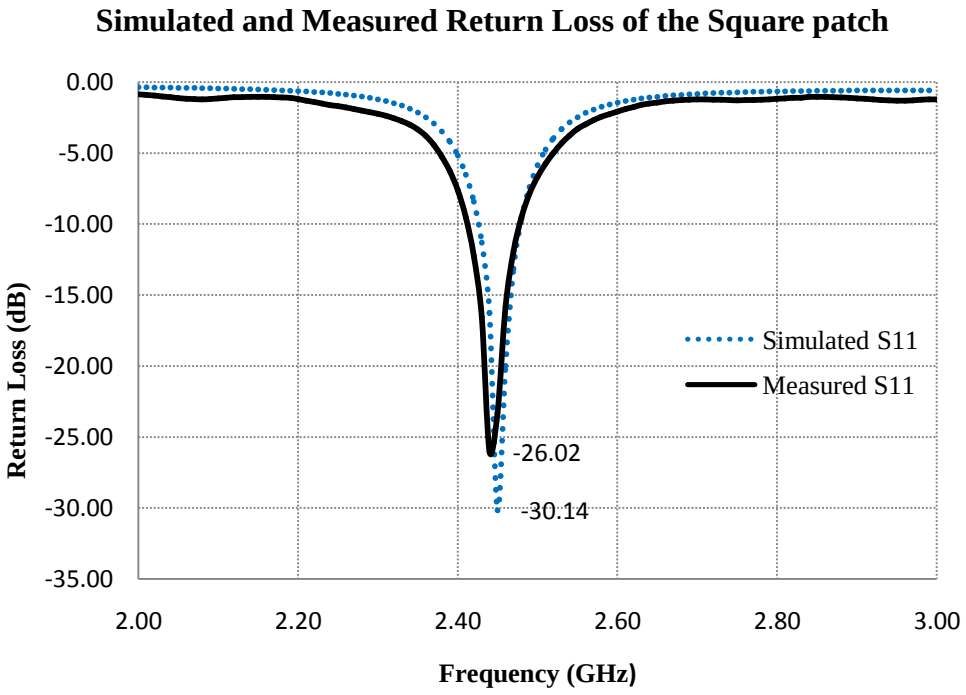

Figure 3.7. Simulated and Measured Return Loss of the Square Patch

The simulated radiation patterns show a directivity of 5.87 dBi and the gain of 2.12 dBi along the bore-sight direction. The radiation patterns of gain and directivity have a very similar shape. This is due to the loss on the substrate.

3.3.3. Fabricated Antenna and Measurements

The fabricated patch antenna (dimensions described in section 3.3.2) is shown in Fig. 3.9.

The measured antenna performance is consistent with the results of simulation in that differences are within simulation and fabrication errors. The measured RL (Fig. 3.7) shows the resonant frequency of 2.44 GHz where the RL is 26.02 dB. The simulated resonant frequency is 2.45 GHz where the RL is 34.14 dB. Measured radiation data show that the directivity is 5.80 dBi direction and the simulated one is 5.87 dBi in broadside.

The differences from the simulation results are due to limitations in the uniformity and estimation of the relative permittivity of the substrate and simulation errors due to the limited volume of simulation, the boundary conditions and number of finite elements.

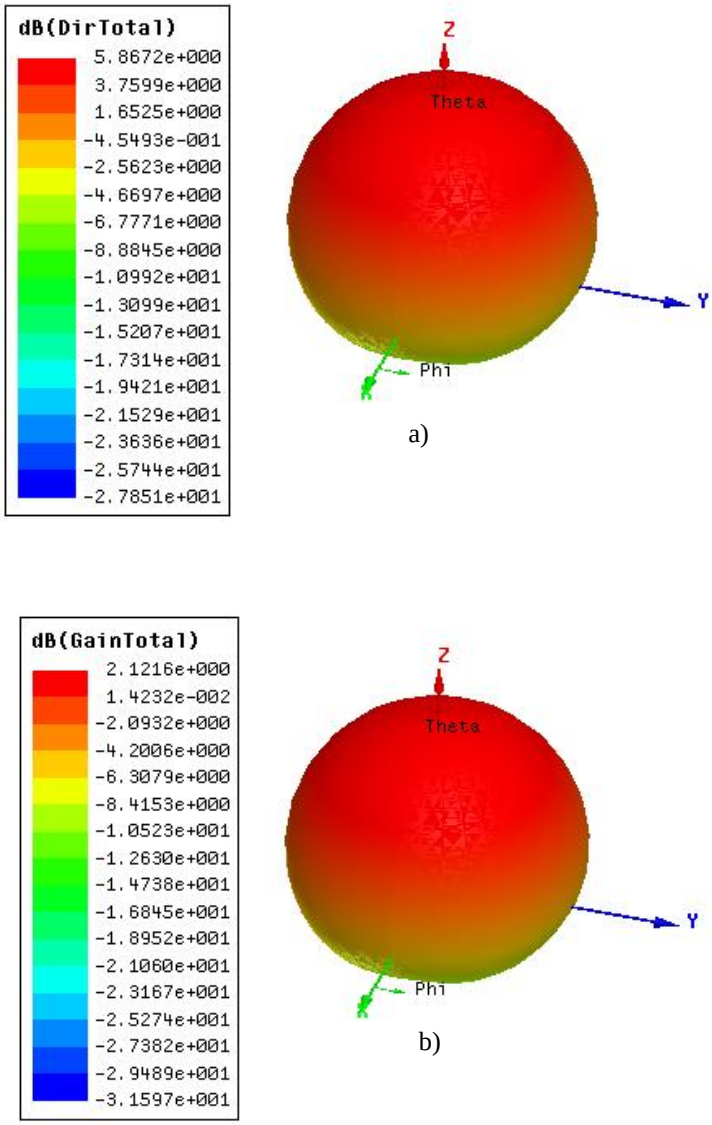

Figure 3.8. Simulated radiation pattern of the patch: a) Directivity; b) Gain

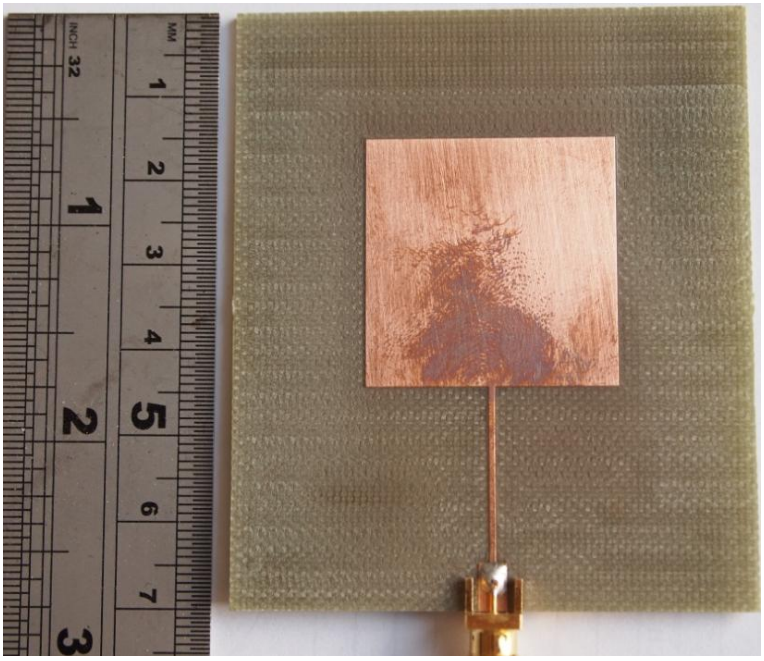

Figure 3.9. Fabricated Square Patch Antenna

3.4. Conventional Circularly Polarised (CP) antenna for RFID Systems

Generally, the tag's antennas are very small compared to a wavelength. Most are dipole antennas which excite linear polarisation. In practice, the tags can be laid in arbitrary orientation. Therefore, most RFID systems equip the reader with a circularly polarised antenna in order to avoid strong polarisation losses.

In this section, circularly polarised patch antennas are designed, fabricated and tested.

3.4.1. Circular Polarised Patch Antenna

Circular polarised patch antennas are normally categorised into two types based on the feed design: dual-fed CP antenna and single fed [Haneisi, 1989].

3.4.1.1. Dual-fed CP Patch Antenna

The fundamental configurations of a dual-fed CP patch antenna are shown in Fig. 3.10. The patches are fed by an external polariser that excites two modes of equal amplitude and 90° out of phase. This type of antenna can be classified using the shape of an external polariser: offset-feeding (Fig. 3.10.a) and 3-dB hybrid (Fig. 3.10.b).

3.4.1.2. Single-fed CP Patch Antenna

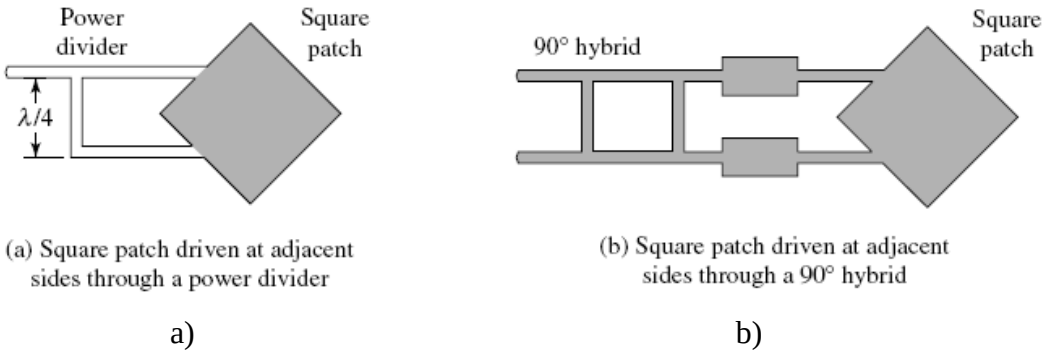

(a) Square patch driven at adjacent sides through a power divider

(b) Square patch driven at adjacent sides through a 90° hybrid

a) b)

Figure 3.10. Example of Dual-fed CP Circular Patch: a) Off-set feeding; b) 3-dB hybrid

(Diagram is taken from [Huang, 1994])

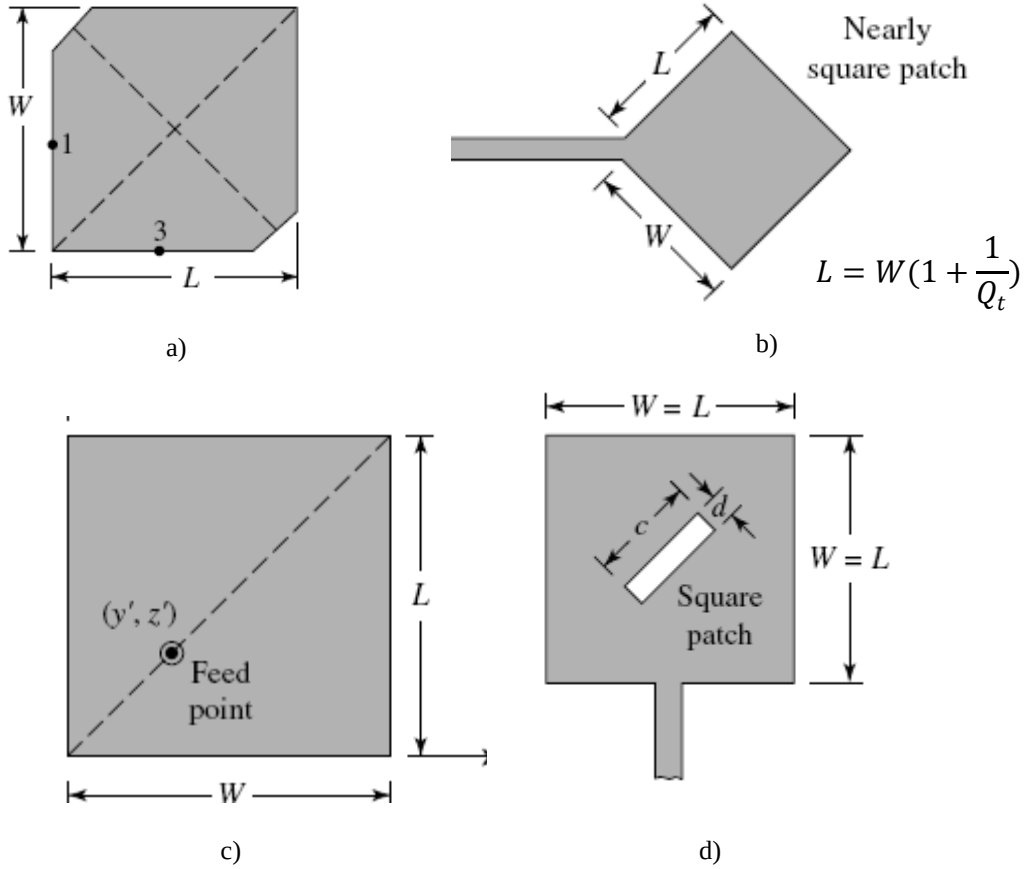

a) b)

c) d)

Figure 3.11. Some types of Single-fed CP patch antenna (Diagram is taken from [Balanis, 2005])

a) corner truncated patch, b) nearly square patch feed by transmission line,

c) nearly square patch feed by coaxial line, d) thin slot square patch

A single-fed CP antenna is one of the simplest radiators for exciting circular polarisation. Typical configurations of this type of antenna are shown in Fig. 3.11. Single-fed antenna can excite circular polarisation as the generated mode can be separated into two orthogonal modes by the effect of a perturbation segment such as a

slot or truncated segments (Fig. 3.11). Consequently, by setting the perturbation segment on the edge of the patch, the generated mode is separated into two orthogonal modes. For specific perturbation segments, both modes are excited in equal amplitude and 90° out of phase at the centre frequency. Therefore, the antenna can excite circular polarisation with single feed.

3.4.2. Conventional Truncated Corner CP Square Patch (SP) UHF RFID Reader Antenna

Compared to the dual-fed, the single-fed CP patch antenna is simpler and more compact as it does not need the external polariser. For this reason, it is more suitable for RFID applications.

Many designs of single-feed CP SP antennas have been reported and a summary is available in [Garg, 2001]. These typically include one or more perturbation segments in order to detune the degenerate modes present in a symmetrical patch. One of the most popular designs is the corner truncated square patch (SP), introduced in 1983 by Sharma and Gupta [Sharma, 1983].

In this section, a conventional truncated corner CP SP antenna is designed.

The truncated corner square patch (as shown on Fig. 3.11.a) can excite left-handed circular polarisation (LHCP) or right-handed circular polarisation (RHCP) depending on the feed position (Fig. 3.12). The condition for circular polarisation is:

$$\frac{\Delta S}{S} = \frac{1}{2Q} \tag{3.7}$$

Where $S, \Delta S$ are the areas of unperturbed square patch and the perturbation ($S = a^2$), c is the truncated size ($\Delta S = c^2$) and Q is the quality factor, that represents for the antenna losses [Balanis, 2005] of the square patch length a.

The unloaded Q is calculated by [Huang, 2008]:

$$Q = \frac{c\sqrt{\varepsilon_{eff}}}{4 \times f \times h} \tag{3.8}$$

The resonant frequencies of the new modes are [Garg, 2001]:

$$f_1 = f_0\left(1 - 2\frac{\Delta S}{S}\right) \tag{3.9}$$

$$f_2 = f_0 \tag{3.10}$$

where f_0 is the resonant frequency of the unperturbed square patch. The circular

polarisation frequency f_{cp} occurs at the mean of these two frequencies.

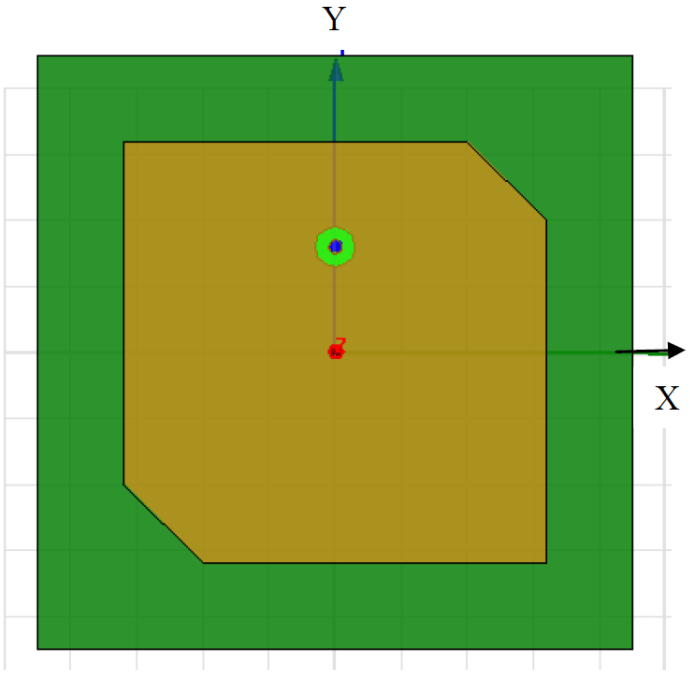

Figure 3.12. Corner truncated CP SP antenna excites RHCP (Feed point on the y-axis)

The design procedures for a right-hand circular polarisation (RHCP) corner truncated patch antenna for UHF RFID reader are described in the following section. The antenna is designed to operate at 2.45 GHz and will be fabricated on FR4 board.

3.4.2.1. Design Procedures

1. Apply the design procedures for a conventional square patch (section 3.2.1) to calculate the square patch size of 30.09 mm.
2. Apply the condition for circular polarisation (Equation 3.7) to find out the truncated corner size *c*:

   The calculated quality factor Q is : $Q = \frac{c\sqrt{\varepsilon_{eff}}}{4 \times f \times h} = 37.01$

   So that

   $$\frac{c}{a} = \sqrt{\frac{\Delta S}{S}} = \sqrt{\frac{1}{2Q}} \cong 0.116$$

   Therefore, the truncated size is $c \cong 0.116 \times 30.09 \cong 3.49\ mm$

3.4.2.2. Simulations

The ground plane of the Antenna FR4 substrate has dimensions of 100.00 mm × 70.00 mm, (Length × Width).

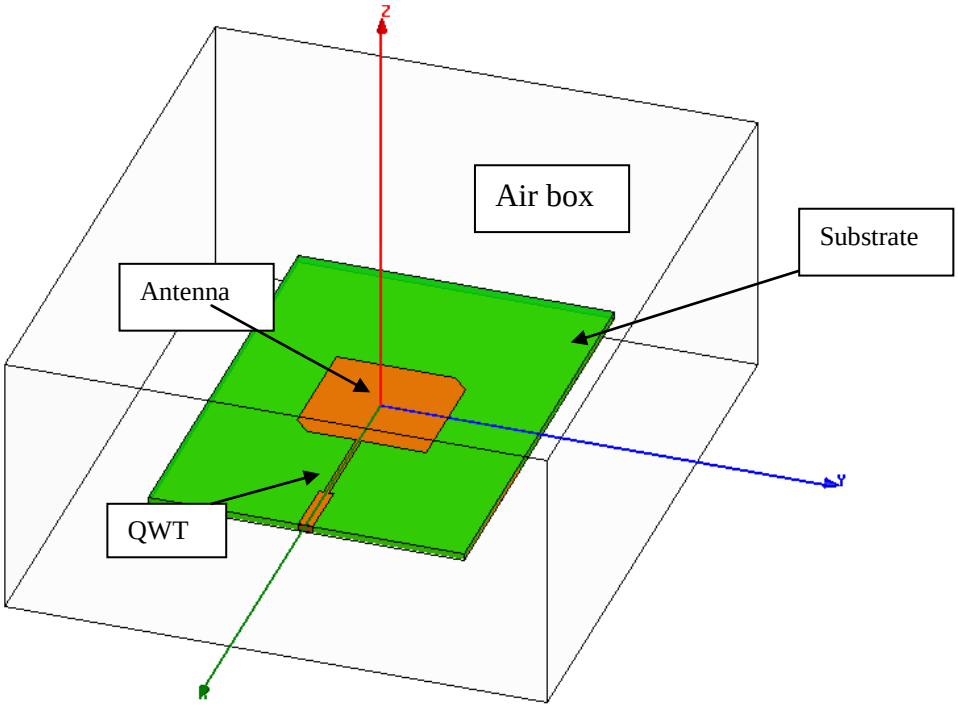

Figure 3.13. HFSS model of the conventional, truncated square patch fed by a microstrip line

Firstly, the antenna without a feed network is simulated. A series of patch dimensions (a, c) are simulated with parameters scattered around the parameters obtained in section 3.4.2.1. The simulated response of the stand alone patch are not precisely those of a fed antenna, but they provide a good approximation.

The CP patch size and truncated corner size are 29.7 mm and 3.5 mm, respectively. The edge resistance at the CP patch is about 105.64 Ω. Therefore, the patch is matched with a QWT with a characteristic impedance of 72.68 Ω, calculated by Equation (3.6). The QWT length and width are 17.63 mm and 1.63 mm, respectively.

These values are used as an initial approximation for the CP patch in a HFSS model (Fig. 3.13).

The Air Box used has dimensions 140 mm × 120 mm × 60 mm. These values were refined to impose the resonant frequency of 2.45 GHz. At this frequency the axial ratio (AR) is smaller than 1 dB. The antenna size and corner size are 29.6 mm and 3.4 mm, respectively. The QWT dimensions are 21.5 mm and 1.2 mm.

The results were obtained after 20 passes. The region was divided to 30907 tetrahedras, and the Max Magnitude Delta S is 0.0034 or 0.34%.

Fig. 3.14 shows that the resonant frequency is 2.45 GHz and the RL is 29.23 dB. The

10-dB RL bandwidth is about 100 MHz or 4.08%.

The simulated AR results show that minimum AR is 0.28 dB at the design frequency. The 3-dB bandwidth of AR is about 30 MHz or 1.22%.

The beamwidths for circular polarisation ($AR < 3\ dB$) in *xz* plane ($\phi = 0°$ plane) and *yz* plane ($\phi = 90°$ plane) are $100°$ and $240°$, respectively.

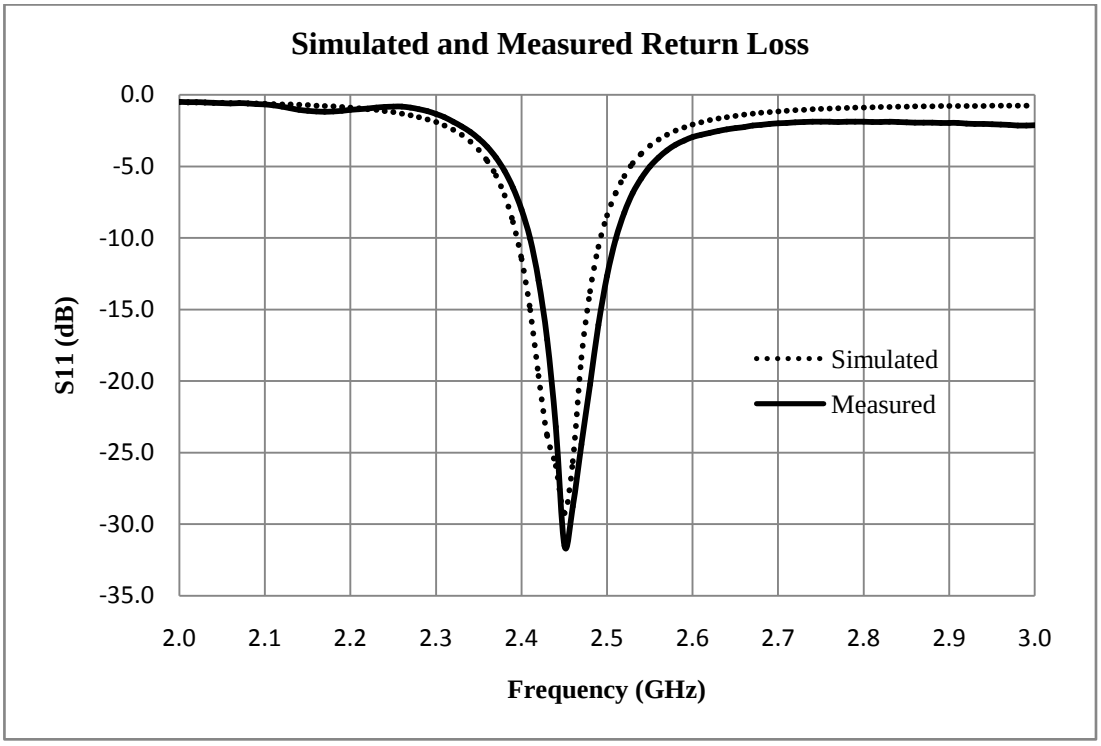

Figure 3.14. Simulated and Measured RL of the conventional corner truncated CP SP antenna

3.4.2.3. Fabrication and Measured Results

The fabricated standard corner truncated CP SP antenna (dimensions can be found in section 3.4.2.2) is shown in Fig. 3.15.

The measured and simulated data agree remarkably well. Measured return loss data (Fig. 3.14) show the resonant frequency of 2.45 GHz where the return loss is 31.50 dB.

Measured minimum AR at the design frequency 2.45 GHz is 0.58 dB.

Figure 3.15. The fabricated conventional corner truncated CP SP antenna

A summary of the performance of the conventional corner truncated CP SP antenna at 2.45 GHz is shown in Table 3.1.

Table 3.1. Performance of the conventional corner truncated CP SP antenna at 2.45 GHz

Frequency 2.45 GHz	**Return Loss** (dB)	**10-dB RL Bandwidth**	**Gain** (dBi)	**Axial Ratio** (dB)	**3-dB AR Bandwidth**
Simulated	29.23	4%	7.31	0.28	1.22%
Measured	31.50	4%	7.0	0.58	1.02%

3.5. Compact Microstrip CP Antennas for Portable RFID Reader

In this section, two compact designs of corner truncated, CP, square patch (SP) antenna, suitable for a portable RFID reader are discussed in details. The design, simulation, fabrication and testing of the antennas are discussed.

As described above, the single-fed microstrip antenna is preferred for use as a RFID reader antenna, over dual-fed, because it is simpler and more compact as it does not need an external feeding network.

In recent decades, due to the requirement of compactness in wireless systems, research on miniaturisation of microstrip antennas has been particularly active. There are many techniques to miniaturise microstrip antenna, summarised in [Wong, 2002], such as four slits [Chen, 2001], or four bent slots [Chen, 1998b], or asymmetric patterns of circular

holes [Nasimuddin, 2010] or etched on a high-permittivity substrate and surrounded by a vertical ground [Kim, 2006]. One of the most popular techniques is to insert slots or slits into the patch antenna, and these have been reviewed in [Nasimuddin, 2011]. The slots/slits force greater meandering in the fundamental-mode current paths and so the patch size can be reduced while maintaining the resonant frequency

The antenna designed in this section is a singly-fed, truncated corner, CP SP antenna that is simpler, easier to fabricate at the large numbers and hence with lower cost than other published designs.

3.5.1. Compact Antenna Design 1

A compact design of corner truncated CP SP antenna can be achieved using four pairs of slits, however this antenna cannot be fed by the inset-fed technique [Wong, 2000]. In this section, the design is reconsidered with an optimised microstrip feed structure. The size of the proposed antenna can be reduced by about 51% compared to a conventional corner truncated CP SP by inserting four pairs of slits.

The proposed compact CP antenna is designed and simulated. Measured results are described in detail for the fabricated antenna, compared with simulated results and an optimised design is also simulated.

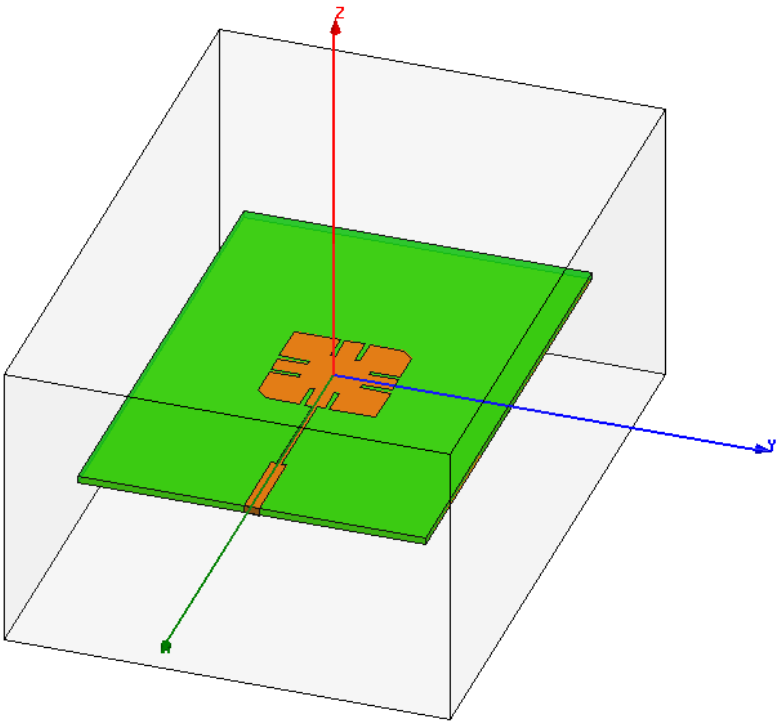

Figure 3.16. Compact slotted/slit corner truncated CP SP antenna

3.5.1.1. Design Procedures and Simulations

The antenna configuration is shown on Fig. 3.16. The patch is defined by the five dimensions *a, c, l, m,* and *n* whose effect on performance is investigated (see Fig. 3.17).

The first step when designing the antenna is to estimate the antenna patch size *a* and the corner truncated size *c* to achieve sufficient antenna performances for most 2.45 GHz RFID systems. The objectives of the design are a resonant frequency of 2.45 GHz with RL greater than 20 dB, bandwidth and the AR at 2.45 GHz is lower than 1 dB.

The slit positions and dimensions are fixed. Each slit is 6 mm long and 0.4 mm wide ($l = 6\ mm,\ m = 3.2\ mm,\ n = 4\ mm$). The two slits in a pair are separated by the 3.2 mm width of the 50-Ω transmission line.

The substrate dimensions are 110 mm × 70 mm × 1.59 mm (Length x Width x Thickness).

HFSS models for different values of patch size and truncated corner size (a, c) were simulated. After a number of simulations, antenna parameters were found that achieved antenna's RL greater than 30 dB and AR less than 1 dB, at working frequency 2.45 GHz ($RL_{2.45\ GHz} > 30dB;\ AR_{2.45\ GHz} < 1dB$). The patch size and truncated corner size are $a = 24.35\ mm$ and $c = 2.3\ mm$, respectively.

The antenna is also matched to a 50-ohm port by using a generalised transformer. Similar procedures to calculate the transformer dimensions described in section 3.4.2.2 were used. The transformer width and length are 0.95 mm and 21.5 mm, respectively (Figure 3.17).

The slots increase the length of the current streamlines associated with the fundamental mode of excitation. Consequently the fundamental frequency is lower than for a similar antenna without slots. Hence, for the same resonant frequency, the slotted antenna can be smaller than the conventional design. The dimensions of the slits determine the size reduction. For this design, the side length a is approximately 17.5% smaller than an antenna without slits.

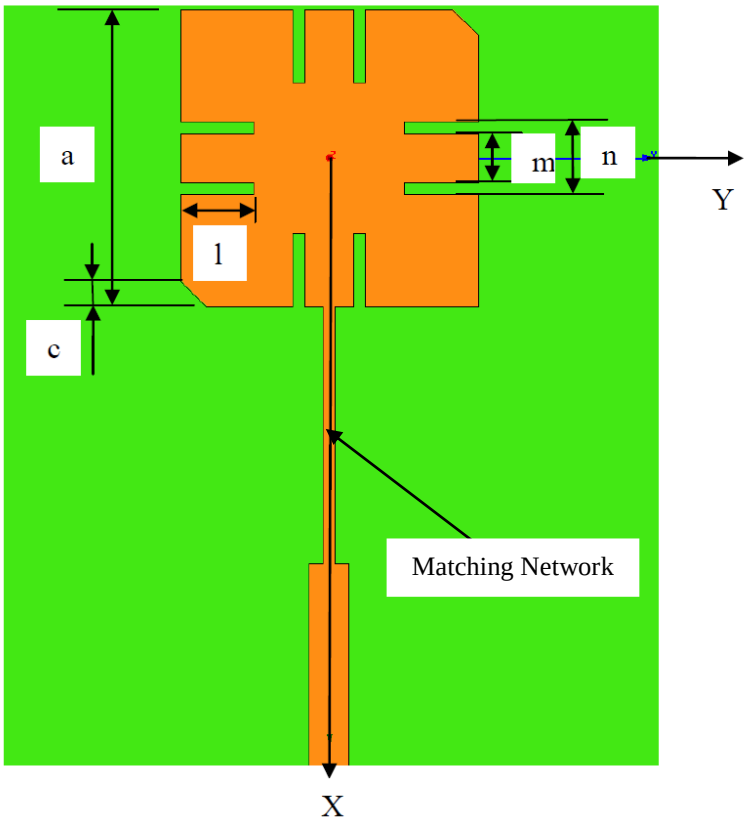

Figure 3.17. Antenna design 1 configuration

The antenna is fed by microstrip line along the X axis so that it radiates a right-hand CP signal. When the feed line lies on the Y–axis, a left hand circular polarization will be produced.

3.5.1.2. Simulated and Measured Results

The antenna model with dimensions described above was sent to the Engineering Workshop for fabrication. The antenna was fabricated by a milling process using double-sided copper FR4 substrate, so that the ground plane covers the opposite side of substrate (Fig. 3.18). The antenna was simulated with 20 HFSS passes.

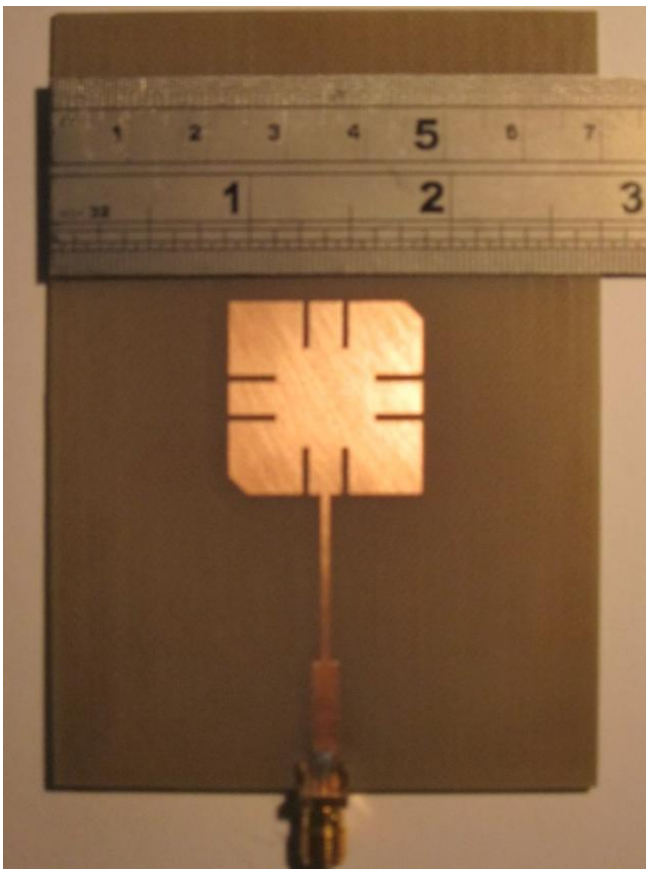

Figure 3.18. Fabricated antenna

Figure 3.19 shows the simulated Reflection Coefficient (S_{11}) of the antenna model and the measured results for the fabricated antenna.

The simulation predicted a fundamental resonant frequency of 2.45 GHz (where the Return Loss is about 40.11 dB). The measured results match the simulated results within the errors expected given the granularity of the simulation and precision of the fabrication technique. The measured resonant frequency is 2.45 GHz with a Return Loss of 34.20 dB. The bandwidth for the RL of 10 dB is about 80 MHz or 3.26%.

Figure 3.20 shows the Axial Ratio (AR) in the broadside direction for the proposed antenna derived from the simulation and measured on the fabricated antenna.

The circular polarisation bandwidth of the simulated antenna, determined from 3 dB AR, is about 20 MHz i.e. about 0.8%. The measured results agree well with simulation results.

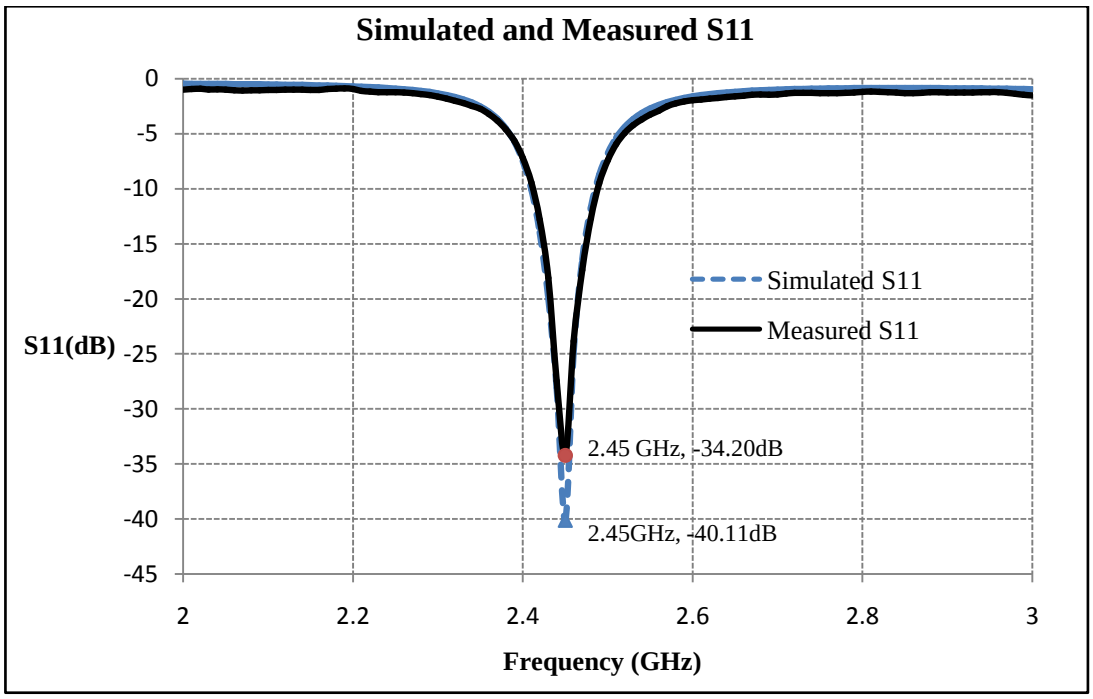

Figure 3.19. Simulated and measured return loss of designed antenna

The beamwidths of circular polarisation ($AR < 3\ dB$) of about 100° in *xz* plane (or $\phi = 0°$ plane) and 140° in *yz* plane (or $\phi = 90°$ plane) are both simulated and verified by measurement.

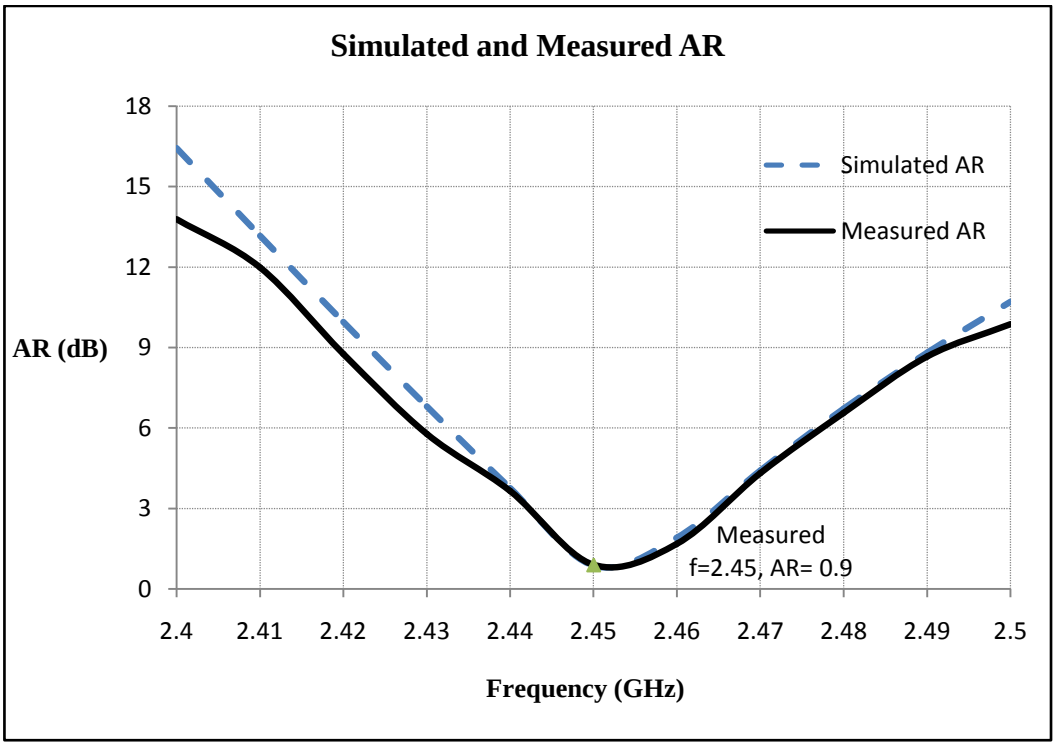

Figure 3.20. Axial ratio (AR) of the designed antenna in broadside direction

This antenna's radiation pattern was measured and normalised (Figure 3.21). The half-power beamwidth is 78°. The maximum directivity along the broadside direction obtained from the measured data is 6.9 dB at 2.45 GHz.

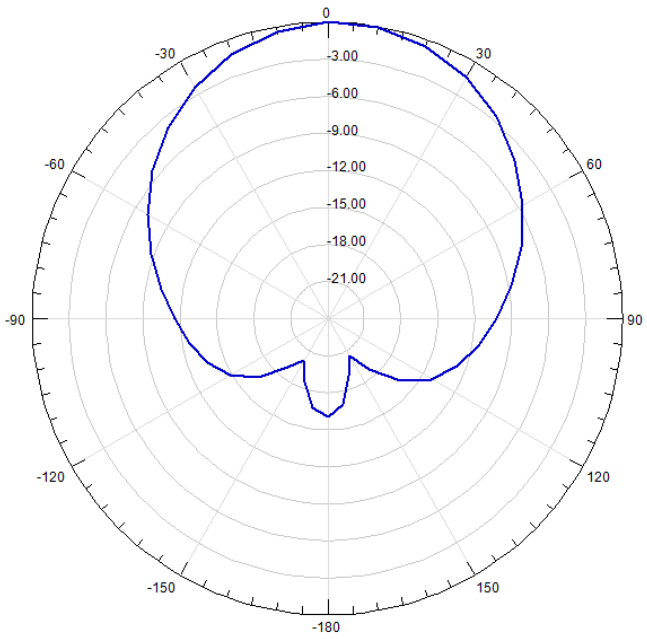

Figure 3.21. Normalised radiation pattern of the fabricated antenna on E-plane (*xz* plane)

3.5.1.3. Size Optimisation

In this section, further investigation of the effect of patch design on the performance of three, corner truncated CP SP antennas with edge feeding, have been simulated and fabricated and a further optimised design simulated. Antenna A is the conventional design without slots. Antenna B is the fabricated one with dimensions shown in section 3.5.1.2. Antenna C has the same patch length as the antenna B with the slots length maximised to 8.8 mm (the slot length is limited by the patch size). Antenna D is optimised for a minimum patch size at a frequency of 2.45 GHz. Table 3.2 lists the dimensions defining each antenna i.e. the edge length (*a*) the truncated corner length (*c*) and the slot length (*l*). The resonant frequency, AR and RL, measured from each antenna, are also listed.

Comparing antennas A and B; the proposed antenna is smaller i.e. the patch edge length has been reduced by approximately 17.5% and the area has reduced by 32%. From the same antenna patch size, the longer the slot the lower the working frequency, Antenna C with the longer 8.8 mm slots, has a lower resonant frequency due to greater meandering forced onto the current streamlines. The centre frequency of antenna C occurs at 1.96 GHz that is lowered by about 20% in frequency compared to that of the antenna B.

Table 3.2. Dimensions and measured parameters of four antennas A, B, C and D

Antennas	**Length of Slots** (*l*) mm	**Patch Size** (*a*) mm	**Truncated Corner Size** (*c*) mm	**Resonant Frequency** GHz	**Axial Ratio** (AR) dB	**Return Loss** (RL) dB
A: Standard	-----	29.50	3.30	2.45	0.58	27.08
B: Proposed	6.00	24.35	2.30	2.45	0.90	34.20
C: Longer slits	8.80	24.35	2.50	1.96	0.99	25.43
D: Optimised design	6.97	20.20	1.73	2.45	0.99	27.51

A series of slot lengths (*l*), patch sizes (*a*), corner truncated sizes (*c*) with appropriate matching networks were simulated to optimise the antenna working at the same resonant frequency of 2.45 GHz. The optimised design, antenna D (with parameter as shown in table 3.2), has reduced the patch length by 31.5% equivalent to reduce the patch area by 51.1% compared to standard design A.

3.5.2. Compact Antenna Design 2

In this section, a more compact antenna design utilising a set of slots is introduced. This design is more compact than most current slotted or slitted CP patch design including the square ring method (size reduction of 19% [Chen, 1998a]), square ring and a slit (size reduction of 19% [Chen, 1998c]), slits (size reduction of 36% [Chen, 2001], or 55% [Wong, 2000]) and asymmetric circular slots with and without slits (size reduction of about 10% and 22% [Nasimuddin, 2010]).

This compact CP antenna was designed, simulated, fabricated and tested in similar procedures to the compact antenna 1.

3.5.2.1. Design Procedures and Simulation Model

This section describes a novel compact antenna with the addition of slits and slots. The antenna was initially designed using heuristics and then the design was modelled with HFSS. The modelling allowed the geometry of the designs to be adjusted to ensure the same resonant frequency and to optimise other figures of merit such as AR and RL bandwidths.

This antenna is fabricated on the same size and material board as the antenna design 1 (section 3.5.1).

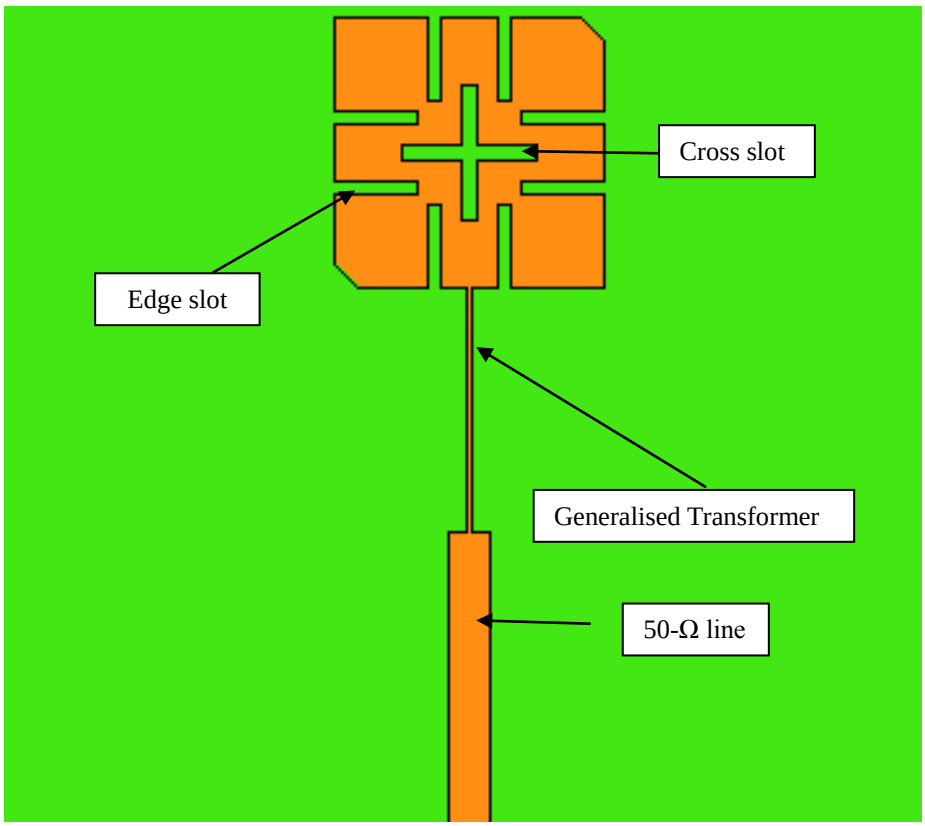

Figure 3.22. Compact CP SP utilised set of slots

The proposed design of compact, corner truncated, CP, SP antenna using four identical pairs of slits and a cross slot at the centre is shown in Fig. 3.22. The patch is defined by a set of dimensions of a, c, x_1, y_1, y_2, w and x_2 (Fig. 3.23). The effect on performance, of varying these parameters, has been investigated by simulation.

In the first step of designing this antenna, the values of *c* and *a* were refined to impose the resonant frequency of 2.45 GHz and radiate CP waves.

The slit and slot dimensions were chosen. Each slit is 6 mm long and 1 mm wide, and the two slits in a pair are separated by 4.0 mm ($x_1 = 6.0$ mm, $y_1 = 6.0$ mm, $y_2 = 4.0$ mm). The cross slot has width of $w = 1.0$ mm and length of $x_2 = 10.0$ mm.

The proposed design, optimised for a resonant frequency of 2.45 GHz, has a patch size of $a = 19.60\ mm$ and the truncated corners' length of $c = 1.70\ mm$.

A generalised transformer matching network was used to match the antenna to a 50-ohm port. The transformer dimensions were obtained by similar procedures as those described in section 3.4.2.2. The transformer width and length are 0.7 mm and 17.9 mm, respectively.

The antenna excites right hand CP radiation as the feeding on the X-axis.

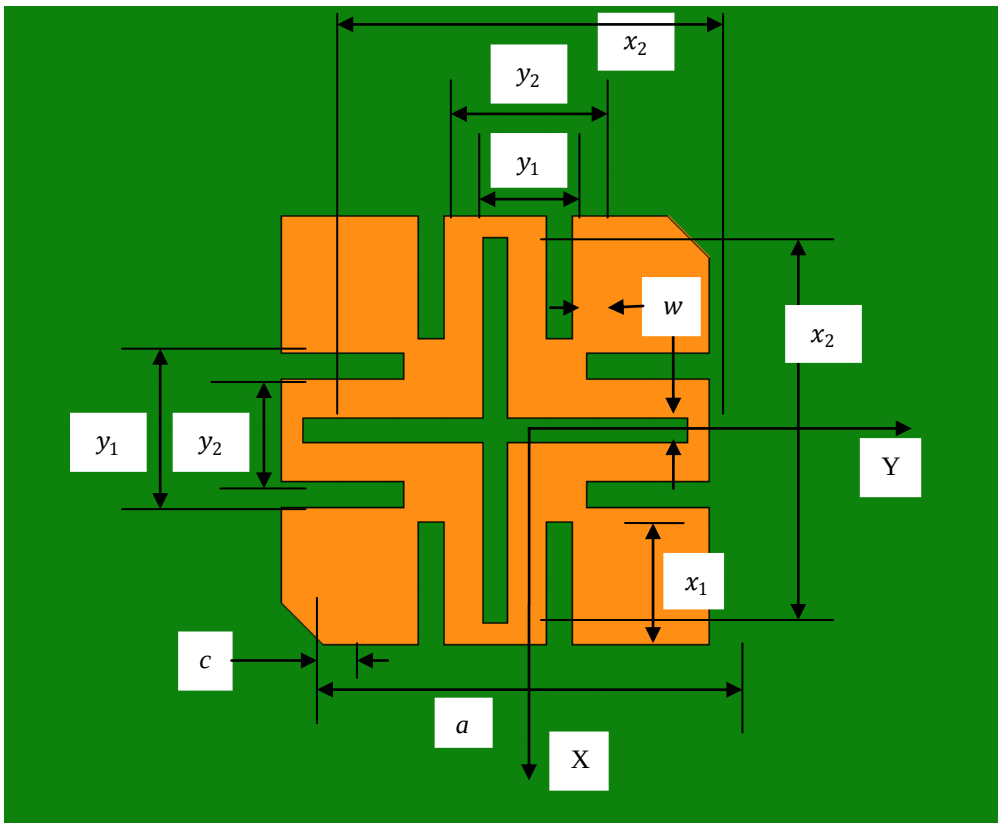

Figure 3.23. Proposed antenna configuration

3.5.2.2. Simulated and Measured Results

The fabricated antenna (Fig. 3.24) was tested in the shielded room and the measured results are compared with the simulated predictions.

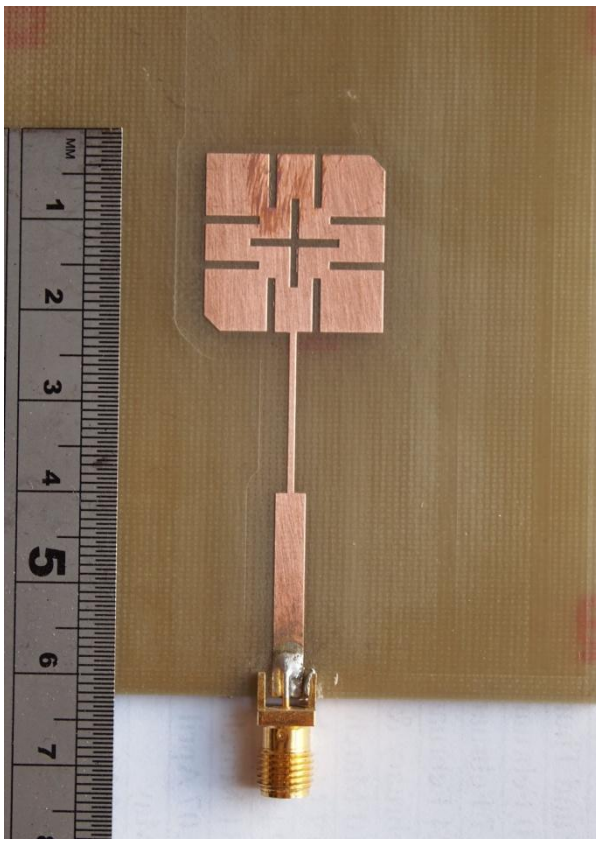

Figure 3.24. Fabricated compact antenna 2

As shown on Fig. 3.25, the simulation predicted a fundamental resonant frequency of 2.455 GHz (where the RL is 27.51dB). The bandwidth for a RL 10 dB lower i.e. VSWR = 1.93, is about 60 MHz or 2.45% of the design resonant frequency. These figures agree well with the measured characteristics. Fig. 3.25 also shows the Reflection Coefficient (S_{11}) measured by the Network Analyzer over the frequency range 2 GHz to 3 GHz. The measured resonant frequency is 2.470 GHz with a Return Loss of 26.28 dB. The bandwidth for a reflection coefficient of -10 dB is about 70 MHz or 2.85%. As mentioned in previous sections, the differences between measured and simulated results are caused by a range of aspects such as the limitations in the uniformity, the error of the estimation of the relative dielectric constant of the substrate and simulation errors due to the limited volume of simulation, the boundary conditions and number of finite elements.

The current distribution on the patch surface (Fig. 3.26) shows that the lowest current densities are located at the patch corners and the strongest currents (in red) are around the end of the slot and slits. Therefore, the surface current path is effectively lengthened by the slot and slits resulting in lower resonance frequency.

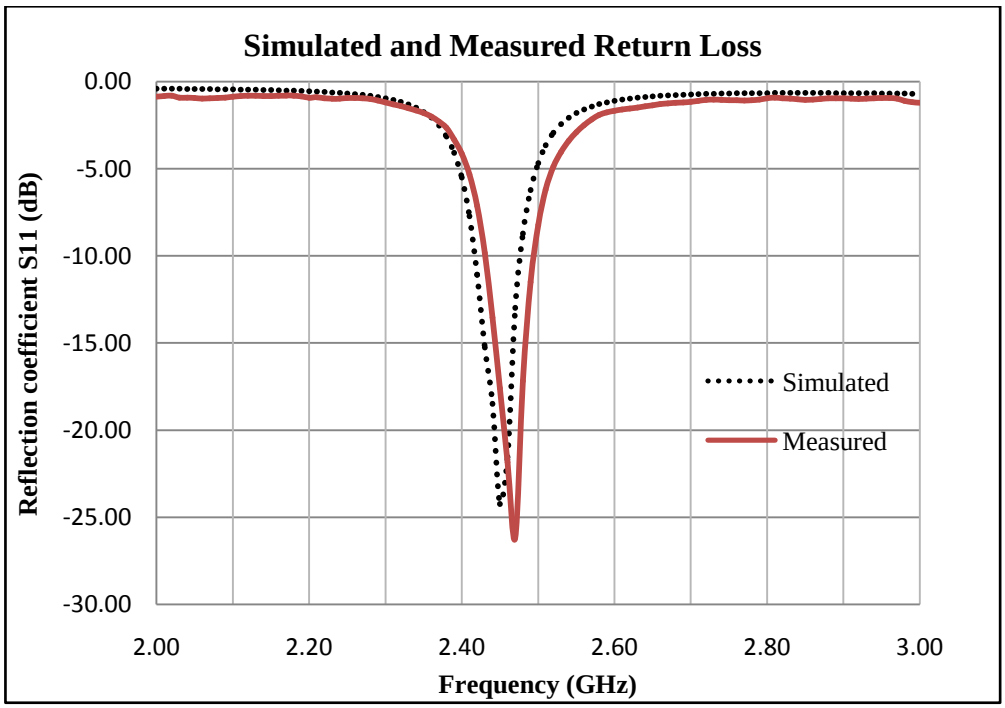

Figure 3.25. Simulated and Measured RL of the antenna 2

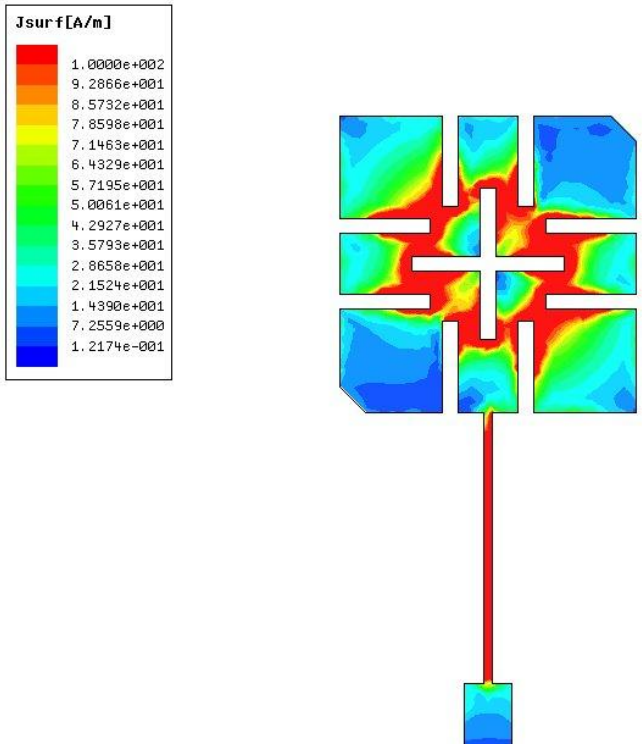

Figure 3.26. Simulated patch surface current magnitude distribution (J_{surf}) of phase 0 at 2.45 GHz

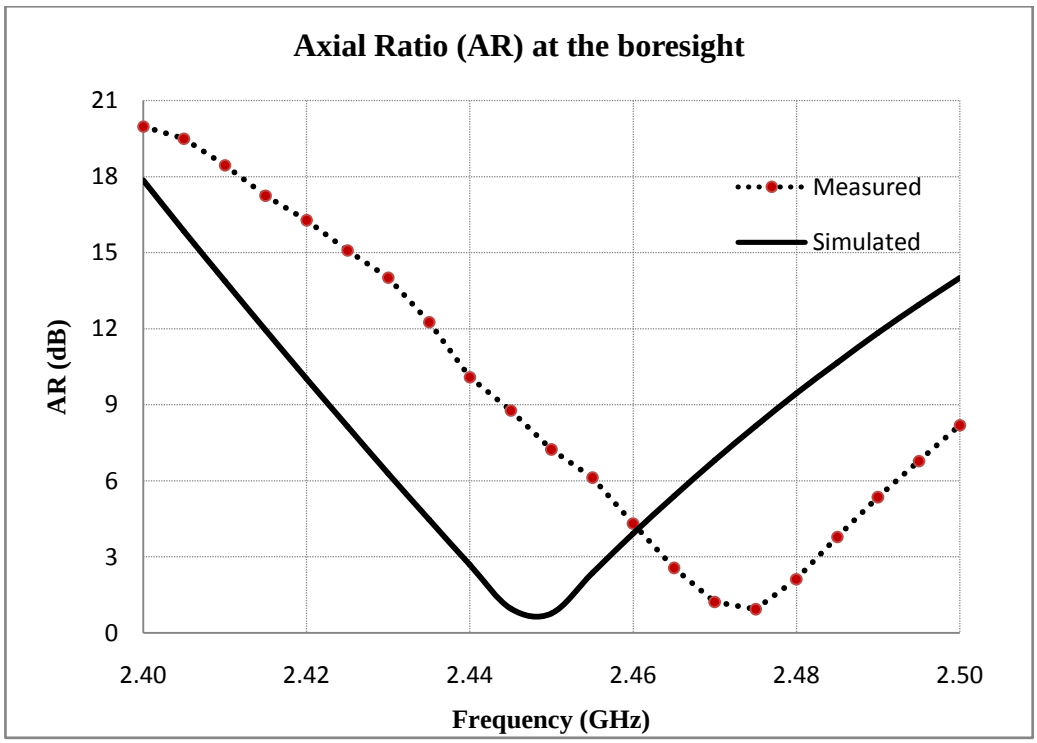

Figure 3.27. Axial ratio (AR) of the compact antenna 2 at the bore-sight

The quality of the CP field radiated, AR, was measured using a linearly polarised horn antenna that was rotated in the plane normal to the direction of the incident field in the RF shielded room. Fig. 3.27 shows the simulated and the measured AR along the bore-sight. The CP bandwidth of the simulated antenna, determined from 3 dB AR, is about 20 MHz i.e. about 0.8% of the designed centre frequency of 2.45 GHz. The simulation also shows that at 2.45 GHz the AR along the bore-sight is minimal i.e. $AR_{min} = 0.77\ dB$.

The beamwidths for circular polarisation ($AR < 3\ dB$) in *xz* plane ($\phi = 0°$ plane) and in *yz* plane ($\phi = 90°$ plane) are verified by measurement to be approximately $70°$, which agrees well with simulation.

The antenna radiation pattern was measured. The normalised pattern is illustrated in Fig. 3.28. The measured half-power beamwidths in *xz* and *yz* plane are 80° and 90°, respectively. The maximum directivity in *yz* plane, as calculated from the measured data, is 6.59 dB at broadside direction, and in *xz* plane is 6.73 dB at direction of $\theta = 10°$.

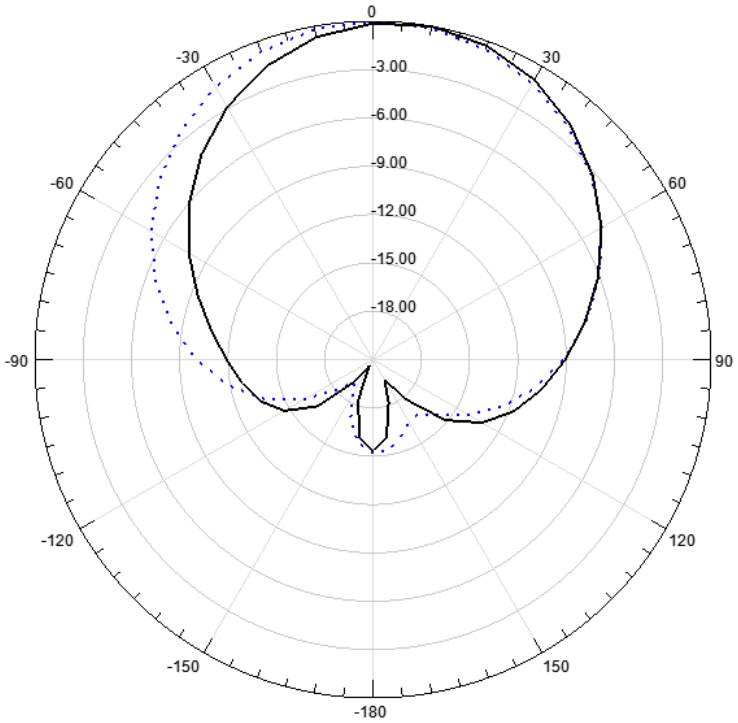

Figure 3.28. Measured radiation patterns at the bore-sight direction.

(XZ plane Solid Black, YZ plane Dot Blue)

3.5.2.3. Size Optimisation

In this section, the dimensions of the slits and slot are optimised to minimise the size of the patch. For the antenna design 2, the patch edge length a is approximately a third smaller than the conventional corner truncated CP, SP with patch size of 29.50 mm.

The patch size length a is minimised by modifying the length of cross slot x_2, and length of the slits x_1, and the corner truncation size c to maintain circular polarisation. First of all, the proposed antenna was modified by maximising the length of slots and slits. Simulation results show that the modified antenna works at a frequency of 2.05 GHz i.e. 83.7% of the designed frequency. It implies that the size of an antenna resonant at 2.45 GHz would be about 16.5 mm. A series of models of corner truncated, CP, SP antennas with edge feeds have been simulated. A brute-force search of the (x_1, x_2, c) parameter space was performed to identify antennas (with appropriate matching networks) that met a range of constraints on resonant frequency, AR and RL, with patch sizes centred on 16.5 mm and varied in steps of 0.1 mm. Refined brute-force searches were performed in the parameter space regions identified as containing optimal solutions. The parameters of antenna N (See Table 3.3) were identified to yield a minimum area antenna with a resonant frequency of 2.45 GHz.

The optimised antenna has size length of $a = 16.80$ mm. This antenna and its matched feed have been fabricated and are illustrated in Fig. 3.29.

Antenna A is the standard design without slots (section 3.4). Antenna M and N are antenna design 2 and its optimised design for minimum patch size at a frequency of 2.45 GHz. Table 3.3 lists the dimensions defining each antenna i.e. the edge length (a), the truncated corner length (c), the slits length (x_1) and the cross slot length (x_2). Measured values of resonant frequency, AR and RL are also listed in Table 3.3, for each antenna.

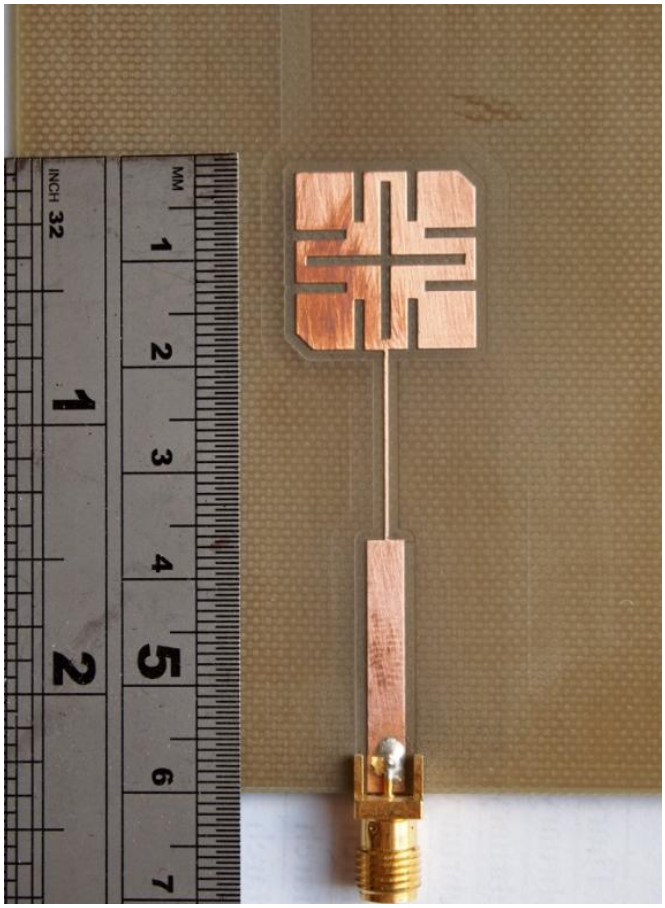

Figure 3.29. Optimised Antenna N

Comparing antennas A and M; the proposed antenna is smaller i.e. the patch edge length has been reduced by approximately 33.56% and the area has reduced by 55.85%. The optimised antenna N (See Fig. 3.29) with the longer cross-slot of 15 mm has the smallest patch size length due to greatest meandering forced onto the current streamlines. The optimised design, antenna N (with parameters shown in table 1), achieves a reduction of 43.05% in patch length or 67.56% in area compared to conventional design A.

Optimised antenna C has similar radiation pattern to antenna B. Their gains are smaller than the conventional one. This has been verified by measured gains of these antennas (6.6 dBi compared to 7.0 dBi).

However, due to the high reactive impedance at the edge, the microstrip feeding technique using generalised matching may not be suitable. As the characteristic impedance of the line becomes very large, the resulting transformer line is very thin and may not conduct enough power to the antenna.

Table 3.3. Dimensions and measured parameters of three antennas A, M, and N

	Antennas	**A: Conventional**	**M: Proposed**	**N: Optimised**
Dimensions	Patch size (a), mm	29.50	19.60	16.80
	Length of Slits (x_1), mm	-----	6.00	4.80
	Cross slot Length (x_2), mm	-----	10.00	15.00
	Truncation Size (c), mm	3.30	1.70	1.62
Measured Values	Resonant Frequency, GHz	2.45	2.47	2.47
	Axial Ratio (AR), dB	0.58	0.93	0.99
	Return Loss	27.08	26.28	25.44
	Bandwidth of 10-dB RL	4.08%	2.85%	2.65%
	Gain, dBi	7.0	6.73	6.6

3.5.2.4. Proposal of a More Compact Design

As the current streamlines are forced into more complex meanders, the antennas become smaller but the input impedance, at the edge, increases. The antenna illustrated in Fig. 3.30 can be generalised into a snowflake design with a large number of slots and slits. The design yields an antenna with an area only 20% that of the standard CP, SP with no slots or slits. However, the input impedance at the edge has an extremely large reactive component ($Z_{edge} = 360.70 - j346.92\ \Omega$) so the generalised matching technique is not suitable. Other matching techniques could be used, such as single or double stub matching. However, the success of matching becomes critically dependent upon the exact geometry and electrical properties of the stubs.

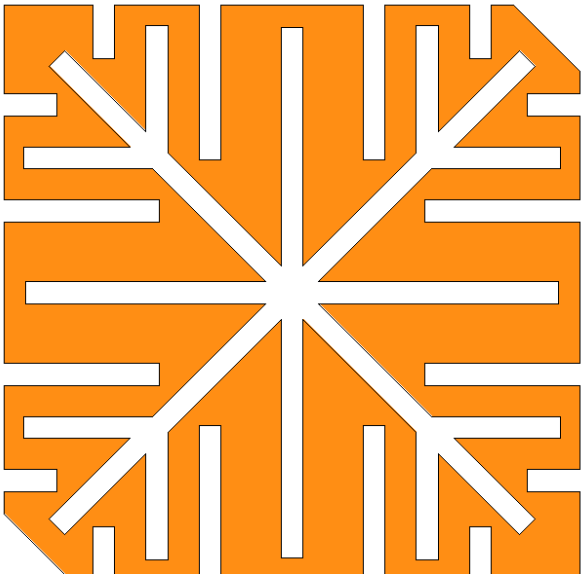

Figure 3.30. An improved design

3.6. Summary

In this chapter, the design process for a RFID reader antenna has been systematically outlined. Firstly, the microstrip analysis techniques are studied. The techniques are then used to estimate the dimensions of the designed antennas. The conventional microstrip SP antenna was designed. Optimised design procedures using HFSS were discussed in details. The simple SP model is then used as the platform to design the corner truncated CP SP; one of the most common in RFID reader antenna.

In the remaining parts of this chapter, several new compact, CP, microstrip antennas for UHF RFID reader are presented. Simulated and measured results show that the proposed antenna yields adequate performance at the target frequency 2.45 GHz. These antennas yield significant miniaturisation compared to a standard corner truncated CP SP antenna operating at the same frequency, and compared to other published solutions. The proposed compact designs have significant advantages, including simple structure, low fabrication cost, and good performance across the narrow target bandwidth. The antenna can be used as an array element in a switched beam array described in the following chapter.

To conclude, these antennas are highly recommended for portable UHF RFID readers. The trade-off between size reduction and matching design is taken into account for design specifications.

CHAPTER 4. SWITCHED BEAM ARRAY ANTENNA FOR 2.45 GHZ RFID LOCALISATION SYSTEMS

4.1. Introduction

This chapter presents a hardware solution for a RFID localisation system working within ISM band of 2.45 GHz. The reader uses a switched beam antenna to determine the azimuth of an RFID tag. The reader array antenna is fed via a 4 × 4 Butler Matrix (BM). The proposed system is evaluated by simulation and results are compared to data measured on a fabricated system.

Chapter 4 includes several sections including:

- Section 4.2: A review of the current achievements in RFID localisation and the advantages of the proposed system;
- Section 4.3: Design the feed network, a 4 × 4 BM (4 inputs, 4 outputs) and of the array antenna. The theoretical and simulated performances of the BM are described and then compared to measured data;
- Section 4.4: Introduces a size reduced BM utilising a Stepped Impedance Configuration (SIC);
- Section 4.5: The performance of the switched beam array antenna.
- Section 4.6: Analysis of localisation abilities.
- Section 4.7: Summary.

4.2. RFID Localisation Systems

The primary purpose of RFID systems is to identify tagged objects. Most of the systems deployed in practice only provide pre-written information from the tags that are within its read range. In the last decade, localisation RFID has been a very active research topic both in academia and industry.

Many methods have been reported for RFID localisation such as Surface Acoustic Wave (SAW) based systems [Arumungam, 2007; Bechteler, 2003], active RFID systems [Ni, 2004; Oktem, 2008; Wang, 2007; Bekkali, 2007; Huang 2006; Bouet, 2008; Zhao, 2007; Jin, 2006 and Han 2007], reader array structures [Zhang, 2007], reference passive tags [Bhatia, 2009], mobile readers [Kim, 2009] and phase difference techniques [Nikitin, 2010; Hekimian-Willinams, 2010].

Recently, the use of phased arrays of antennas to estimate Direction of Arrival (DoA) has been considered and theoretical analysis of potential performance has been

published [Abedin, 2009; Tongliang, 2010; Angerer, 2010]. Using these techniques, a single reader could provide the direction to a tag.

This chapter introduces a new RFID localisation technique based on ratios of powers from the outputs of the beam-switching circuit. The design of a reader array antenna and its feed network, the Butler Matrix (BM), will be described in later sections.

The proposed array antenna and feed network are designed using microstrip technology. The reader antenna is compact, light weight, robust, easy to fabricate and integrate with other components. Therefore, it can be widely deployed for many RFID applications.

The system is primarily designed for passive RFID systems which are typically simpler and more economical than most RFID localisation approaches based on active tags and/or utilising reference tags. The proposed reader antenna can also be used in active RFID systems for localisation purposes if a greater read range is required.

A single switched beam reader can provide information of azimuth Angle of Arrival (AoA) of the tag. This information can be used with other techniques such as range estimation based on phase delay to provide 2D tag location. 2D tag location also can be obtained by triangularisation with multiple switched beam antennas. This technique has significant advantages over systems utilising the Received Signal Strength (RSS) as the orientation of the tag or mismatched losses in the systems do not affect the localisation result.

The use of array antenna in RFID readers has other key benefits such as range extension and interference mitigation.

4.3. Conventional Butler Matrix (BM)

In this section, BM, one of the most popular microwave circuit beamformers, is studied in detail. Then, a 4 × 4 BM used to feed a switched beam antenna is designed, simulated and tested.

A BM is an analogue microwave circuit consisting of a set of quadrature couplers, crossovers and phase shifters, that can produce several simultaneous fixed beams [Gross, 2005].

An $N \times N$ BM (N inputs, N outputs) is often used to feed a switched beam array antenna that has N possible beam patterns, where N is generally a power of 2 i.e. $N = 2^i \; with \; i = 1,2\ldots$ The structure of an array antenna fed by an 8 × 8 BM and its beam

patterns are shown in Fig. 4.1.

When a BM is connected to an array antenna, it will provide the same power to each antenna element and constant phase differences between consecutive elements of $\varphi_i = \pi i/N$ where, $i = \pm(1, 3, 5, .., N-1)$ depending on which port is fed.

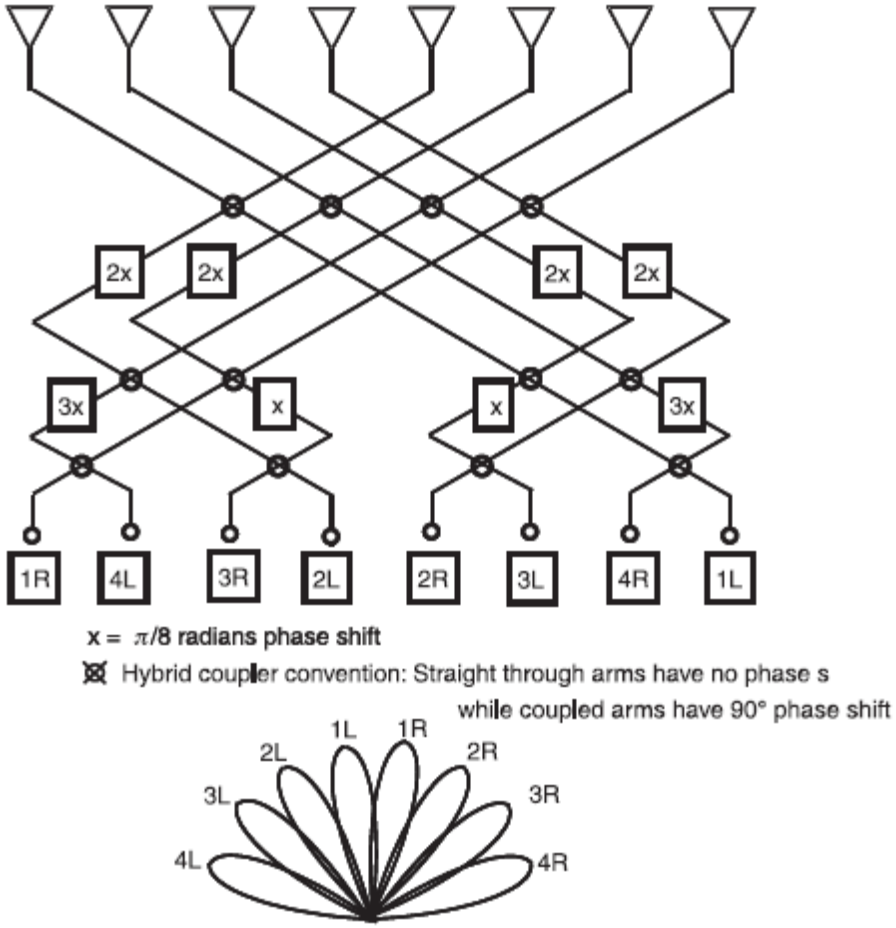

Figure 4.1. The structure and beam patterns of an array fed by 8 × 8 BM (Diagram is taken from [Mailloux, 2005])

If the BM feeds a linear array of N elements, the array factor can be expressed as [Gross, 2005]:

$$AF(\theta) = \frac{\sin(N\pi\frac{d}{\lambda}sin\theta - \frac{i\pi}{2})}{N\pi\frac{d}{\lambda}sin\theta - \frac{i\pi}{2}} = \frac{\sin\left[N\pi\frac{d}{\lambda}(sin\theta - sin\theta_i)\right]}{N\pi\frac{d}{\lambda}(sin\theta - sin\theta_i)} \qquad (4.1)$$

where θ_i is the angle of the i^{th} beam measured from the broadside, and d is the distance between two consecutive elements. The beam position is then given by [Milligan, 2005]:

$$sin\theta_i = \frac{i\lambda}{2Nd} \text{ with } i = \pm(1,3,5,..,N-1) \tag{4.2}$$

and d is the distance between two consecutive elements of the array.

Matlab software has been used to calculate parameters related to a BM.

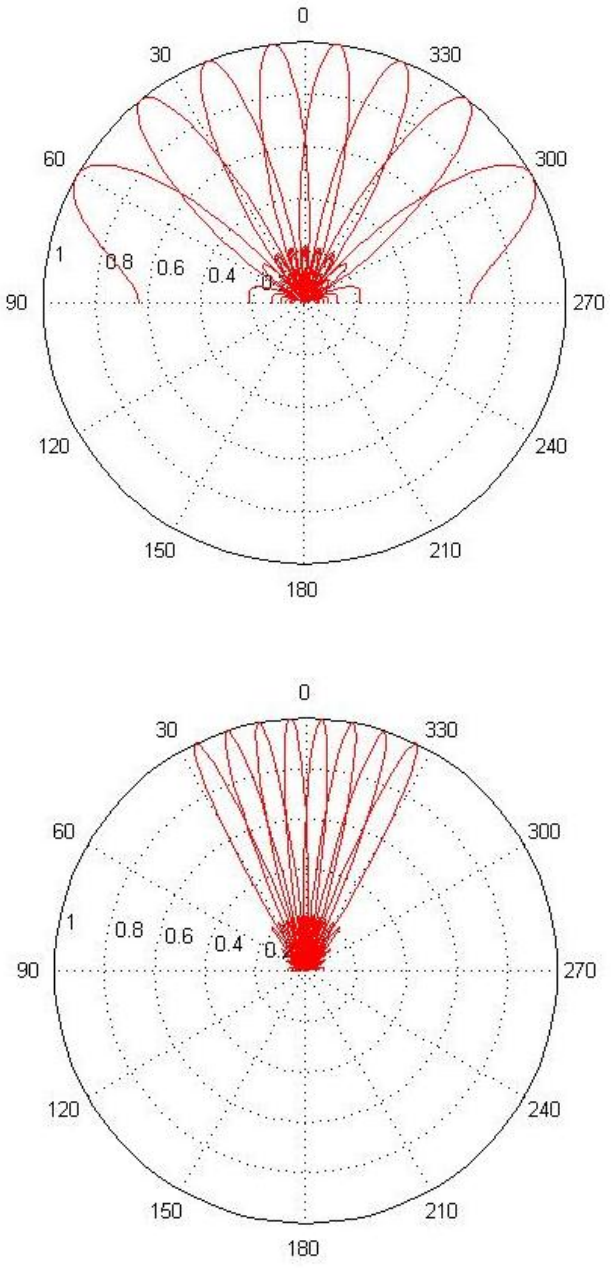

Figure 4.2. 8 × 8 Butler matrix array factor a) $d = \lambda/2$ (top); b) $d = \lambda$ (bottom)

The further apart the elements, the narrower the beamwidth and the closer the beams are grouped (Fig. 4.2). However, the adjacent beam crossover level does not change and is:

$$F_{xov} = \frac{1}{Nsin(\pi/2N)} \tag{4.3}$$

Beam coverage from the centre of the first beam to the centre of the last beam is given by:

$$\theta_{coverage} = 2sin^{-1}\left(\frac{(N-1)\lambda}{2Nd}\right) \tag{4.4}$$

A 4 × 4 BM consists of four quadrature hybrid couplers, two crossovers, and two 45° phase shifters (Fig. 4.3). The components of the BM are described in detail in the following subsections.

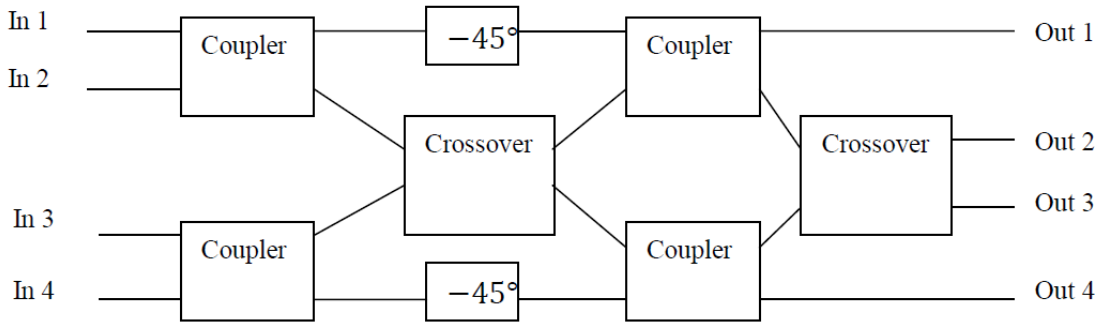

Figure 4.3. Typical 4 × 4 Butler Matrix [Tseng, 2008; Muhammad, 2010]

4.3.1. Quadrature Hybrid Coupler

A quadrature hybrid coupler, also known as a branch-line hybrid, is one of a range of quadrature couplers, along with Lange couplers and overlay couplers. A quadrature hybrid coupler is a 3-dB directional coupler in which the input is split into two outputs that are equal in magnitude and quadrature in phase i.e. with a 90° phase difference [Pozar, 2005]. This coupler is often made of microstrip transmission lines as illustrated in Fig. 4.4, with port 1 is the input port, port 4 is the isolated port and ports 2 and 3 are output ports.

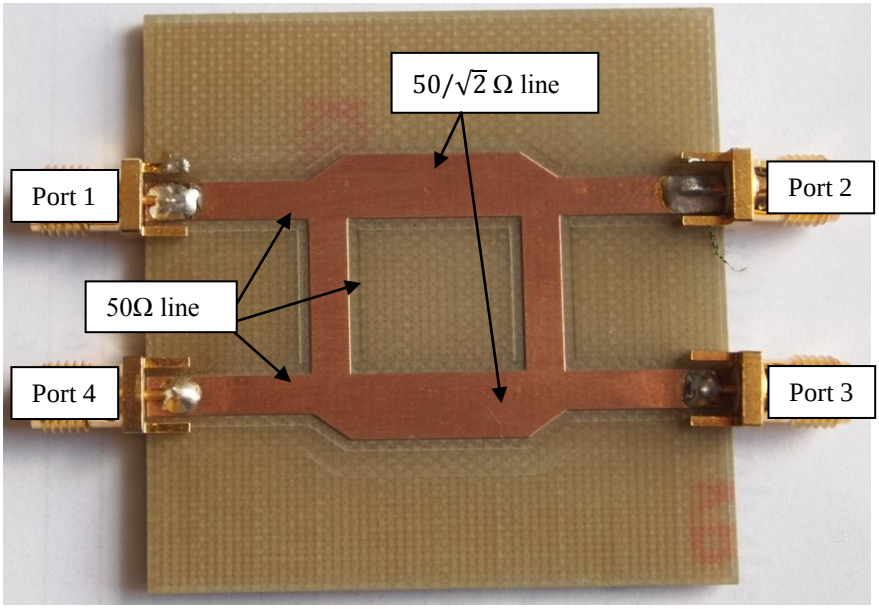

Figure 4.4. Geometry of a microstrip quadrature hybrid coupler

Ideally, power entering port 1 is equally divided to port 2 and port 3 with a 90° phase difference between them, and no power is coupled to port 4. The Scattering matrix ([S] matrix) is given by [Pozar, 2005]:

$$[S] = \frac{-1}{\sqrt{2}}\begin{bmatrix} 0 & j & 1 & 0 \\ j & 0 & 0 & 1 \\ 1 & 0 & 0 & j \\ 0 & 1 & j & 0 \end{bmatrix} \tag{4.5}$$

As can be seen in Fig. 4.4, the quadrature hybrid coupler is symmetric so that any port can be used as input port.

4.3.1.1. Simulated Performance

An ideal quadrature hybrid coupler, operating at 2.45 GHz, has been modelled with ideal components in ADS (Fig. 4.5).

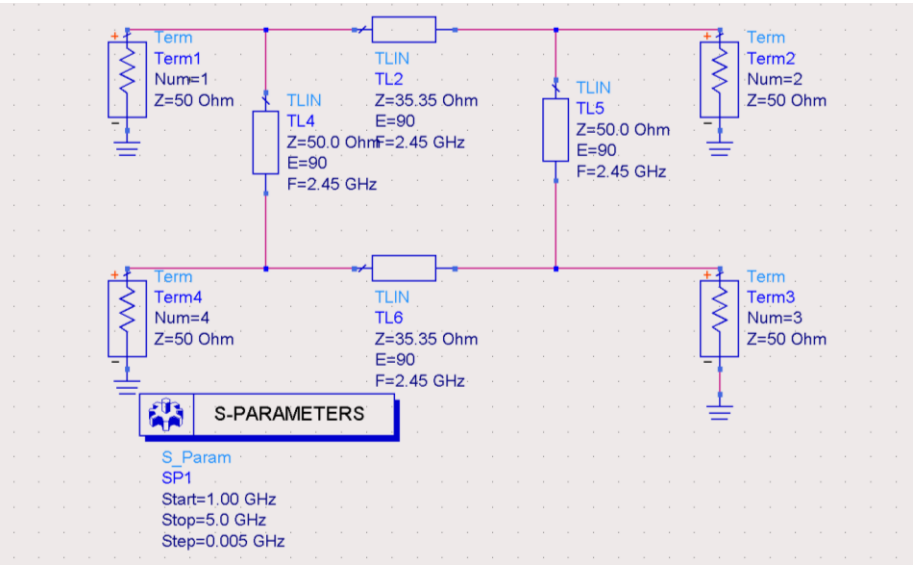

Figure 4.5. ADS model of an ideal quadrature hybrid coupler

Simulated results for the coupler are shown in Fig. 4.6 and the circuit performance at the working frequency of 2.45 GHz is summarised in table 4.1.

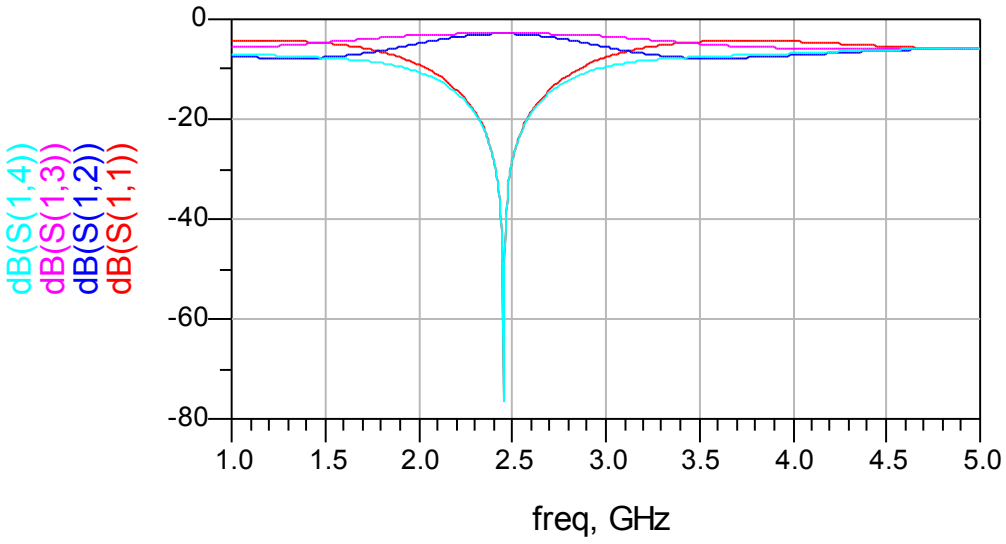

Fig 4.6. ADS simulated S-parameters of the ideal quadrature hybrid coupler

Table 4.1. Simulated results of ideal coupler

Frequency	**Return Loss**	**Transmission coefficients**				**Isolation**
2.45 GHz	S_{11}	S_{21}		S_{31}		S_{41}
	<-70 dB	Magnitude	Phase	Magnitude	Phase	<-70 dB
		-3.0 dB	-90°	-3.0 dB	−180°	

Simulated results also confirm that at the working frequency, the outputs are equal to half the input in power and 90° different in phase. The power reflected at port 1 and transmitted to port 4 are both numerically equivalent to zero, indicated by a value less than -70 dB by the simulation.

4.3.1.2. HFSS Simulation

As discussed previously, the conventional microstrip branch-line coupler is made from four quarter-wavelength transmission lines of 50-Ω and 35.35-Ω (Fig. 4.4).

The coupler was laid on FR4 board with thickness of 1.6 mm. LineCalc software was used to extract the dimensions of these two arms as follows:

- 50-Ω arm: Width is 3.23 mm and length is 17.14 mm
- 35.35-Ω arm: Width is 5.48 mm and length is 16.71 mm.

Initially, the dimensions above were used to create a HFSS model. Simulated results show that the working frequency is lower than 2.45 GHz.

A range of sets of lengths for these two arms were simulated to determine the geometry that yields the desired electrical characteristics. The lengths of the coupler 50-Ω and 35.35-Ω arms, determined by simulation, are 18.75 mm and 18.50 mm respectively. The actual lengths are larger than a quarter-wavelength due to the discontinuity at the junction [Pozar, 2005]. The simulated performance of the optimised coupler, obtained by HFSS, is shown in Fig. 4.7 and the circuit parameters at the design frequency of 2.45 GHz are summarised in Table 4.2.

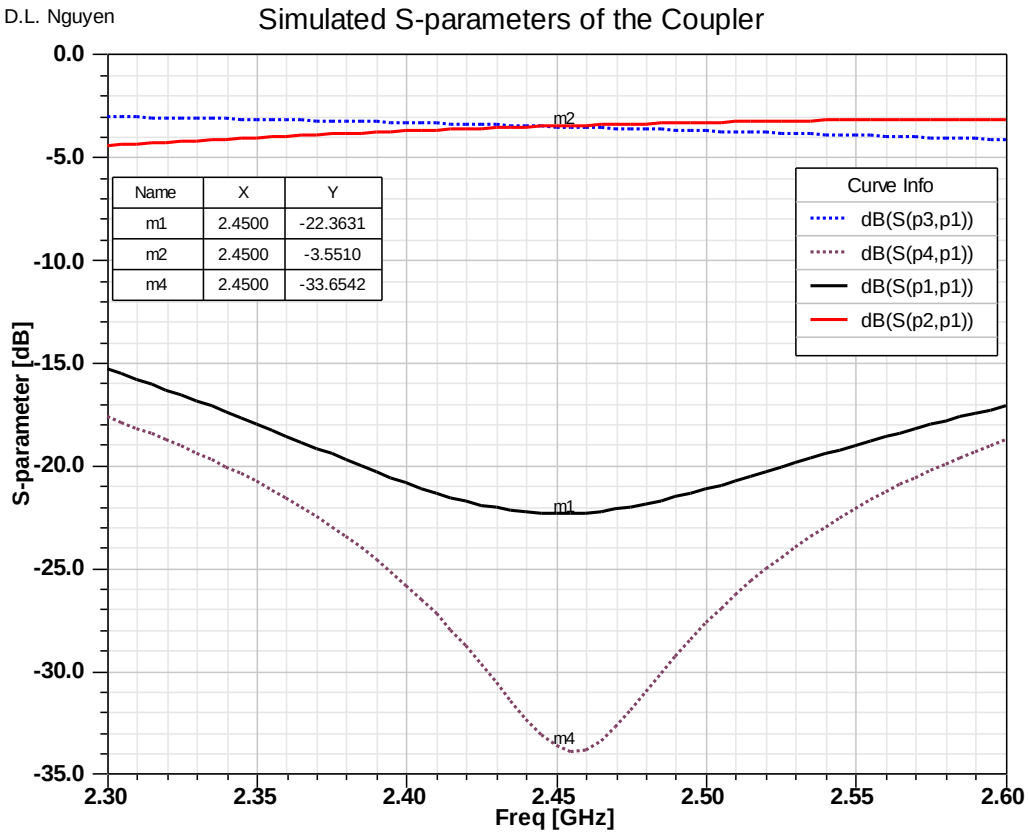

Figure 4.7. Simulated S-parameters of the standard quadrature hybrid coupler

Table 4.2. HFSS Simulated S-parameters of the coupler at 2.45 GHz

S_{11}	S_{21}	S_{31}	S_{41}	$Phase(S_{21}) - Phase(S_{31})$
-22.36 dB	-3.55 dB	−3.58 dB	−33.65 dB	88.63°

4.3.2. Crossover

A crossover, or cross-coupler, is a 0 dB coupler used to cross two transmission lines with minimal coupling between them. The circuit can be implemented by cascading two quadrature hybrid couplers with modifications to the line widths, [Wight,1976], as shown in Fig. 4.8. The circuit elements c_1, c_2 are quarter wavelength 50-Ω transmission lines that has width of w_{50}. The [S] matrix of the crossover is given by [Neron, 2005]:

$$[S] = \begin{bmatrix} 0 & 0 & j & 0 \\ 0 & 0 & 0 & j \\ j & 0 & 0 & 0 \\ 0 & j & 0 & 0 \end{bmatrix} \qquad (4.6)$$

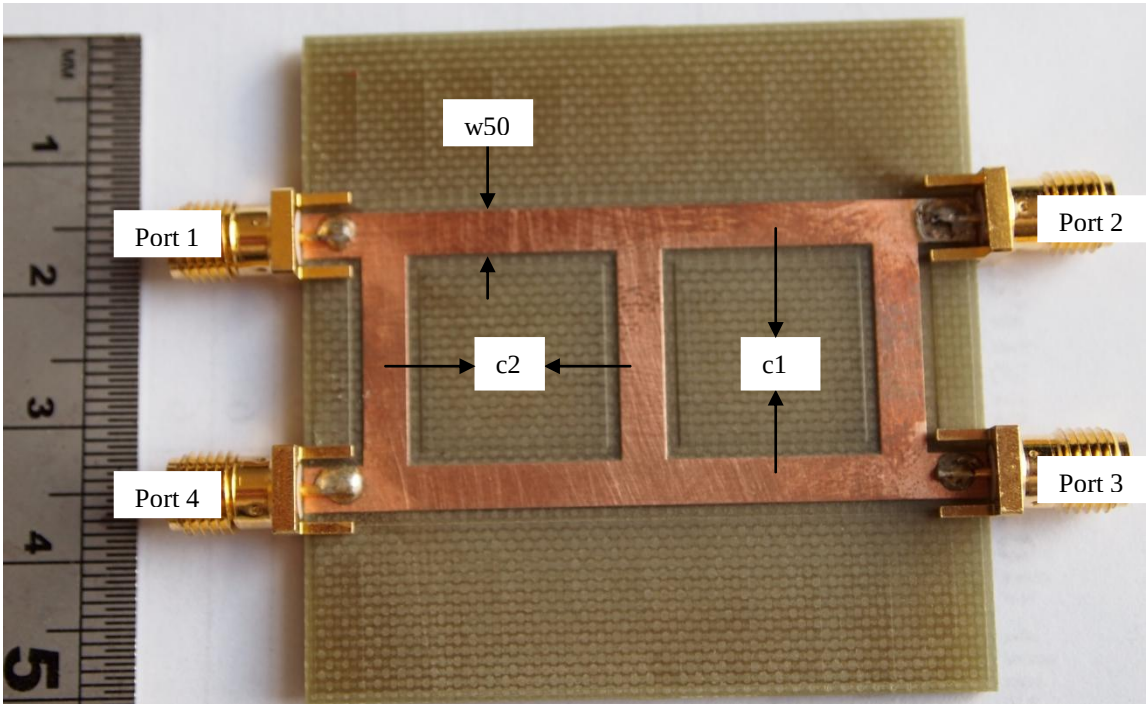

Figure 4.8. Geometry of the crossover

4.3.2.1. Simulated Performance

The operation of an ideal crossover is illustrated using ADS (Fig. 4.9). Simulated results (Fig. 4.10 and 4.11) show that, at the design frequency of 2.45 GHz, the transmission coefficient from port 1 to port 3 is 0 dB ($S_{31} = 0\ dB$) i.e. all the power fed to port 1 will arrive at port 3 and no power will reach to port 2 or port 4 ($S_{21}, S_{41} < 100\ dB$).

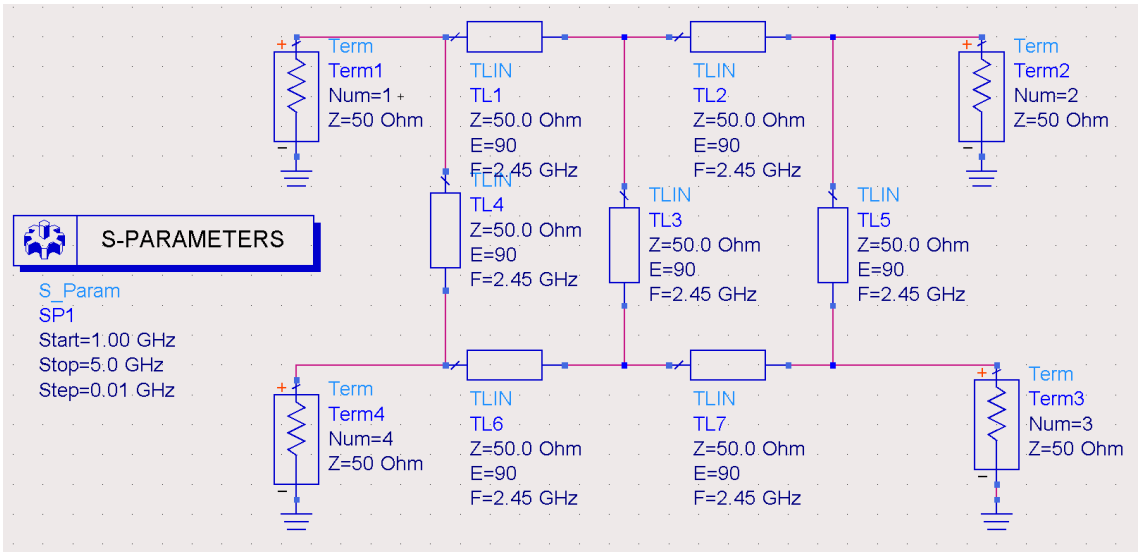

Figure 4.9. ADS model of the ideal crossover

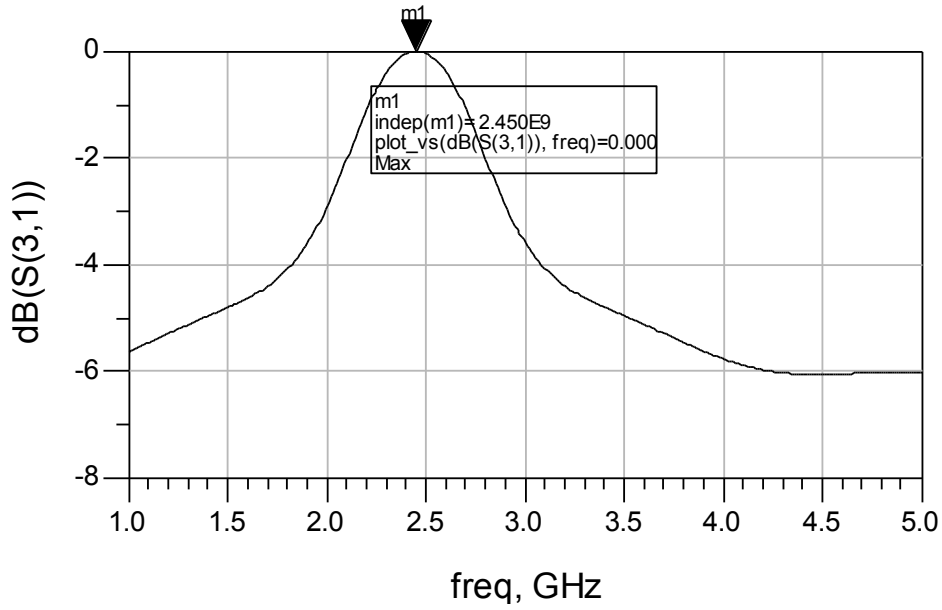

Figure 4.10. Simulated transmission coefficient S_{31}

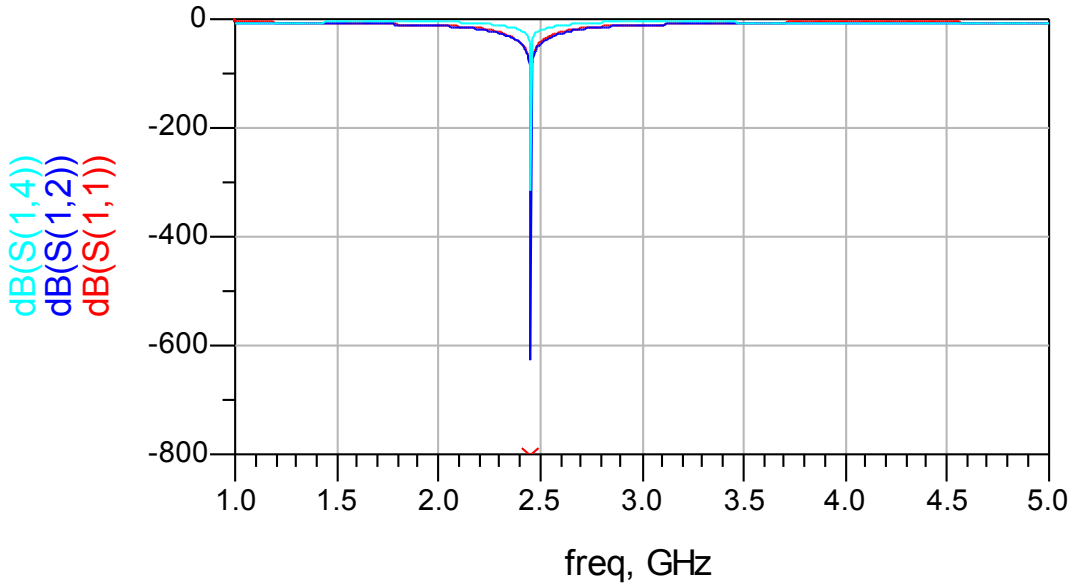

Figure 4.11. Simulated Reflection coefficient (S_{11}) and Isolations (S_{S12}; S_{14})

4.3.2.2. HFSS Simulation

The crossover consists of a number of quarter-wavelength transmission lines with characteristic impedances of 50-Ω (Fig. 4.12). The dimensions of the quarter-wavelength section obtained by LineCalc (in section 4.3.1.2) were used as the initial approximation.

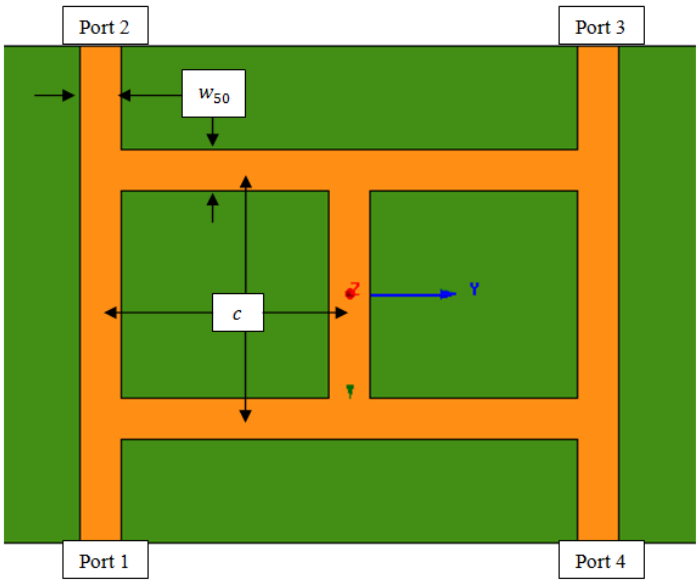

Figure 4.12. HFSS model of the crossover

As with the coupler design, simulated results show that the working frequency is lower than 2.45 GHz. This is because of the discontinuity effects. The actual length of the crossover arms is $c = 20$ mm. The simulated performance of the crossover tuned to operate at the design frequency, obtained by HFSS, is shown in Fig. 4.13.

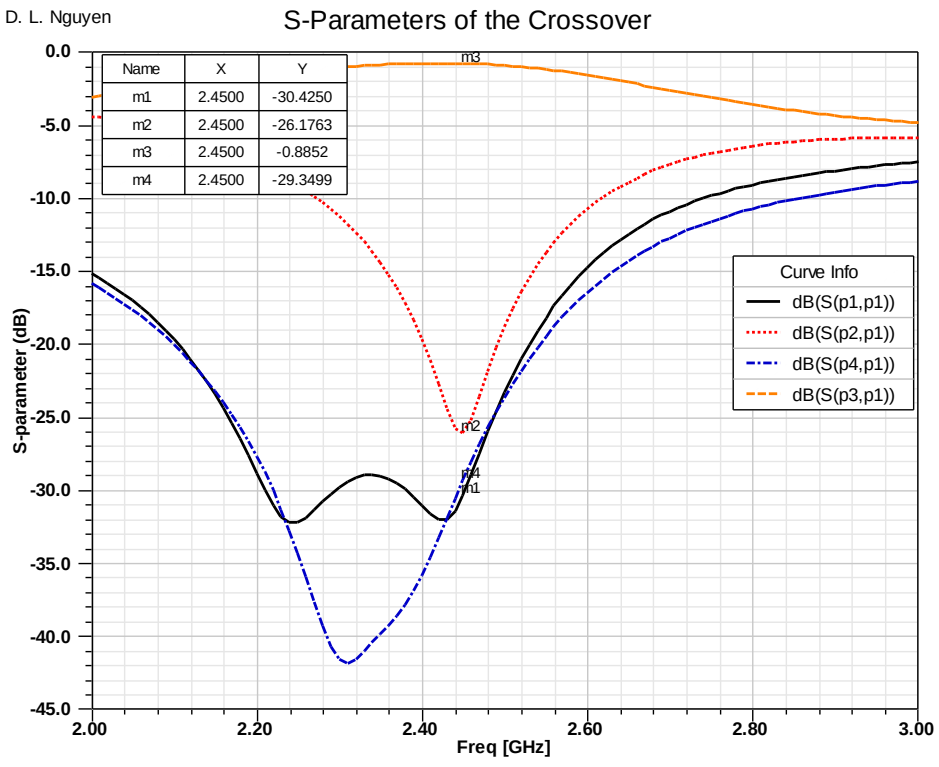

Figure 4.13. Simulated S-parameters of the conventional crossover

In Fig. 4.13, the four markers m_1, m_2, m_3 and m_4 are the values of $S_{11}; S_{21}; S_{31}; S_{41}$ at the design frequency of 2.45 GHz (Table 4.3). These values show that, at this frequency, most of the power fed to port 1 arrives at port 3 (82%), almost no power arrives at port 1 and port 4 (about 0.1%). A small amount of power is dissipated during transmission on the lossy substrate.

Table 4.3. HFSS Simulated performance of the crossover

Frequency	S_{11} (dB)	S_{21} (dB)	S_{31} (dB)	S_{41} (dB)
2.45 GHz	-30.43	-26.18	−0.89	−29.35

4.3.3. Phase Shifters (PSs)

A BM contains several phase shifters. Phase shifters are required to compensate for the phase rotation introduced by the crossovers. The simplest phase shifter is a microstrip transmission line.

Consider a transmission line length *l*. The phase shift is related to the free space wavelength λ_0 and is given by [Pozar, 2005]:

$$\phi = \frac{2\pi\sqrt{\varepsilon_e}}{\lambda_0} l \tag{4.7}$$

The effective dielectric constant ε_e of the substrate given by [Balanis, 2005]:

$$\varepsilon_e = \frac{\varepsilon_r + 1}{2} + \frac{\varepsilon_r - 1}{2} \frac{1}{\sqrt{1 + \frac{12h}{W}}} \tag{4.8}$$

where h and ε_r are the thickness and dielectric constant (or relative permittivity) of the substrate and W is the width of the transmission line.

4.3.4. Simulation and Prototype of the 4 × 4 BM

Consider the 4 × 4 BM (see Fig. 4.3). The input signals at ports 1 to 4 are I_1, I_2, I_3 and I_4, and the output signals at ports 5 to 8 are O_1, O_2, O_3 and O_4.

The corresponding outputs at the hybrid couplers are Q_1, Q_2, Q_3 and Q_4.

$$Q_1 = \frac{1}{\sqrt{2}}(I_1\angle -90° + I_2\angle -180°)$$

$$Q_2 = \frac{1}{\sqrt{2}}(I_1\angle -180° + I_2\angle -90°)$$

$$Q_3 = \frac{1}{\sqrt{2}}(I_3\angle -90° + I_4\angle -180°)$$

$$Q_4 = \frac{1}{\sqrt{2}}(I_3\angle -180° + I_4\angle -90°)$$

Phase of Q1 is delayed by 45° and Q3 are inputs of the coupler to produce outputs at port 5 and 7 (O_1 *and* O_3) of:

$$O_1 = \frac{1}{2}(I_1\angle -225° + I_2\angle -315° + I_3\angle -270° + I_4\angle 0°)$$

$$O_3 = \frac{1}{2}(I_1\angle -315° + I_2\angle -45° + I_3\angle -180° + I_4\angle -270°)$$

Similarly, we have:

$$O_2 = \frac{1}{2}(I_1\angle -270° + I_2\angle -180° + I_3\angle -45° + I_4\angle -315°)$$

$$O_4 = \frac{1}{2}(I_1\angle 0° + I_2\angle -270° + I_3\angle -315° + I_4\angle -225°)$$

$$\begin{bmatrix} O_1 \\ O_2 \\ O_3 \\ O_4 \end{bmatrix} = \frac{1}{2}\begin{bmatrix} e^{-j5\pi/4} & e^{-j7\pi/4} & e^{-j3\pi/2} & e^{-j0\pi} \\ e^{-j3\pi/2} & e^{-j\pi} & e^{-j\pi/4} & e^{-j7\pi/4} \\ e^{-j7\pi/4} & e^{-j\pi/4} & e^{-j\pi} & e^{-j3\pi/2} \\ e^{-j0\pi} & e^{-j3\pi/2} & e^{-j7\pi/4} & e^{-j5\pi/4} \end{bmatrix}\begin{bmatrix} I_1 \\ I_2 \\ I_3 \\ I_4 \end{bmatrix}$$

The phase progressions are $[45° \quad -135° \quad 135° \quad -45°]$

If an uniform linear array of four antenna elements is fed by the 4 × 4 BM, the array main beam direction is determined by which port is fed and the distance between two consecutive elements *d* (Table 4.4).

Table 4.4. Phase progressions and main beam directions of switch beam array fed by a 4 × 4 BM

Fed Port	Progression phase	Main beam direction
Port 1	45°	$sin^{-1}\frac{\lambda}{8d}$
Port 2	−135°	$-sin^{-1}\frac{3\lambda}{8d}$
Port 3	135°	$sin^{-1}\frac{3\lambda}{8d}$
Port 4	−45°	$-sin^{-1}\frac{\lambda}{8d}$

4.3.4.1. 4 × 4 BM Simulation

A 4 × 4 BM consists of four couplers, four phase shifters and two crossovers. The arrangement is shown in Fig. 4.14.

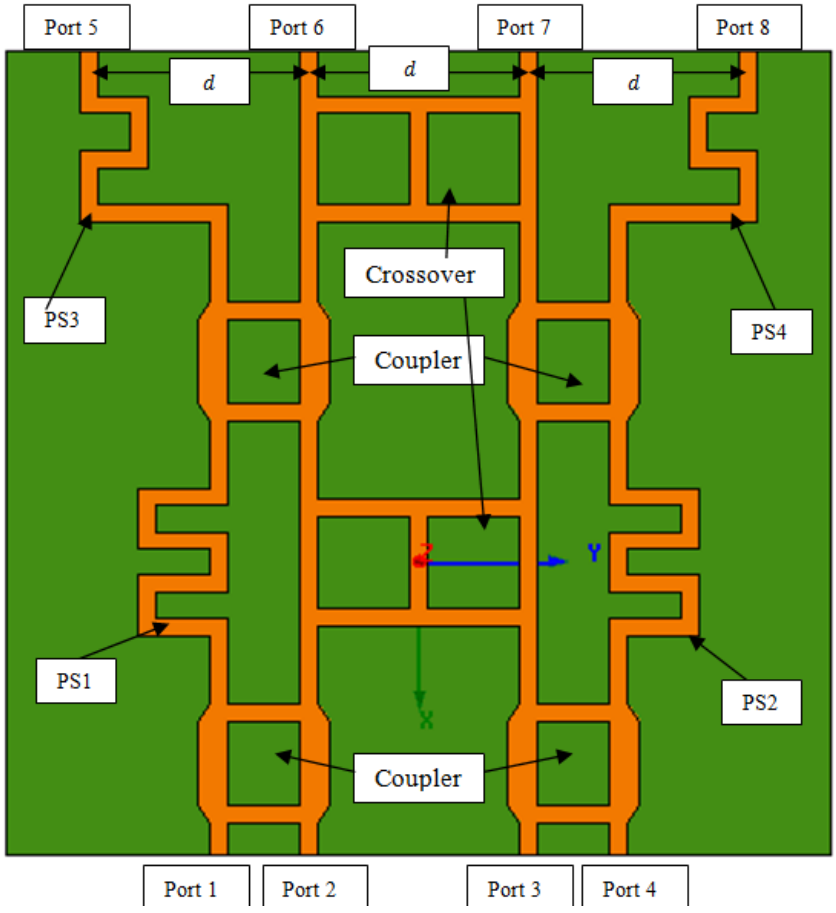

Figure 4.14. Layout of the 4 × 4 BM

The dimensions of the coupler and the crossover are described in section 4.3.2.2 and 4.3.1.2.

The first four ports (Ports 1, 2, 3 and 4) are input ports, and the remaining ports are

outputs. Consider an array fed by the BM, with consecutive antenna elements separated by d. In this project, d is chosen to be 40 mm.

The BM has four PSs (see Fig. 4.14). PS_2 and PS_4 are mirror images of the PS_1 and PS_3.

1. PS_1

The PS is a 50-Ω meander line with width of $w_{50} = 3.23$ mm on the FR4 board. PS_1 is defined by a set of three lengths (s_0, s_1, s_2) (Fig 4.15.a).

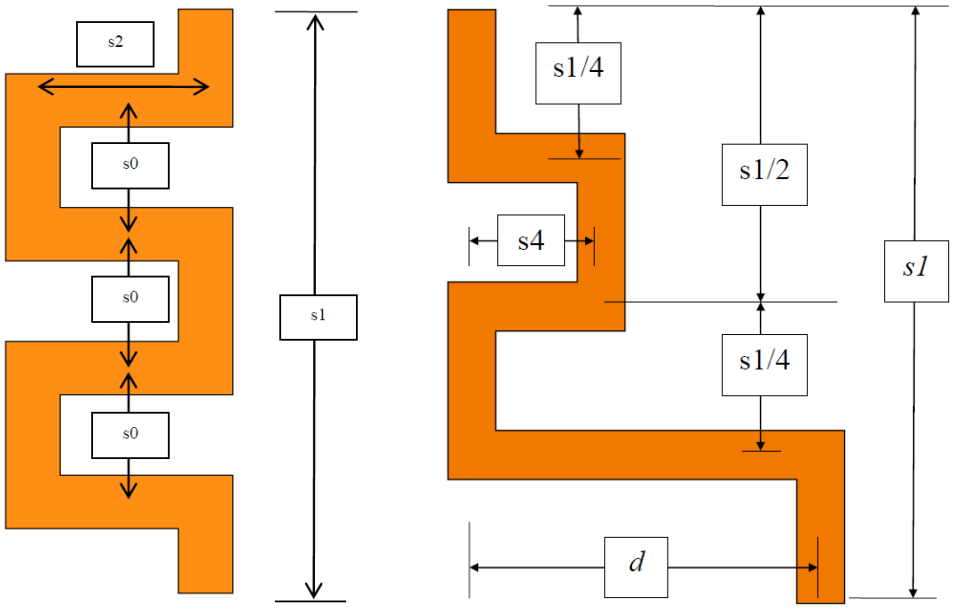

a) b)

Figure 4.15. Phase shifters a) PS 1; b) PS 3

The length $s_1 = 40mm$ equals to the length of the crossover and length s_0 was chosen to be fixed at 8 mm. The length of s_2 was modified to achieve a phase delay of 45° compare to the crossover output. The required length, determined by HFSS simulation, is $s_2 = 12.9mm$.

2. PS_3

Similar to PS_1, PS_3 is defined by a set of three lengths (d, s_1, s_4) (Fig 4.15.b). Values of d and s_1 are chosen to be 40 mm, variations of s_4 are simulated. The value of $s_4 = 8.9$ mm yields the same phase delay as the crossover.

The performance of the BM can be characterised by the response to inputs at ports 1 and

2, due to the mirror symmetry of the circuit i.e. reversing the numbering of the inputs and outputs has no effect. The performance of the whole BM is determined by the interactions between the building blocks i.e. the quadrature couplers, the crossovers and the phase delays. The performance of the 4 × 4 BM, predicted by HFSS simulation, is illustrated in Fig. 4.16, 4.17 and 4.18.

The reflection coefficients at the input ports ($S_{11}, S_{22}, S_{33}, S_{44}$) are lower than the -20 dB at 2.45 GHz considered sufficient for most wireless applications. The transmission coefficients ($S_{ij}\ with\ i \neq j$) range from -7.70 dB to -9.53 dB showing that when one input is fed the output power is almost equally divided between the four output ports.

When a 2.45 GHz tone is input into port 1, the phase differences between consecutive output ports are $43.36°, 47.74°$ and $46.47°$ (Table 4.5). The simulated results show that the phase progression error is within $2.74°$ of the theoretical target phase progression of $45°$.

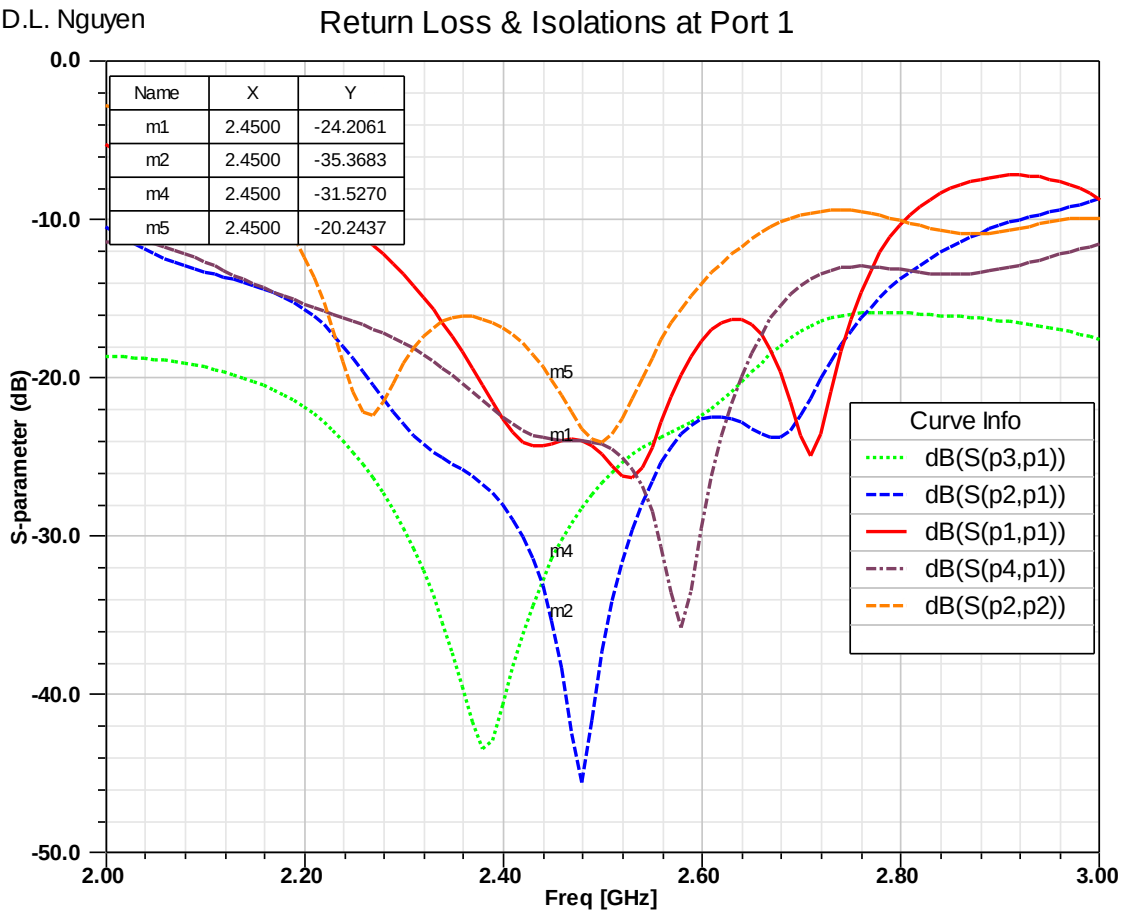

Figure 4.16. Simulated return losses and isolations between port 1 and other ports

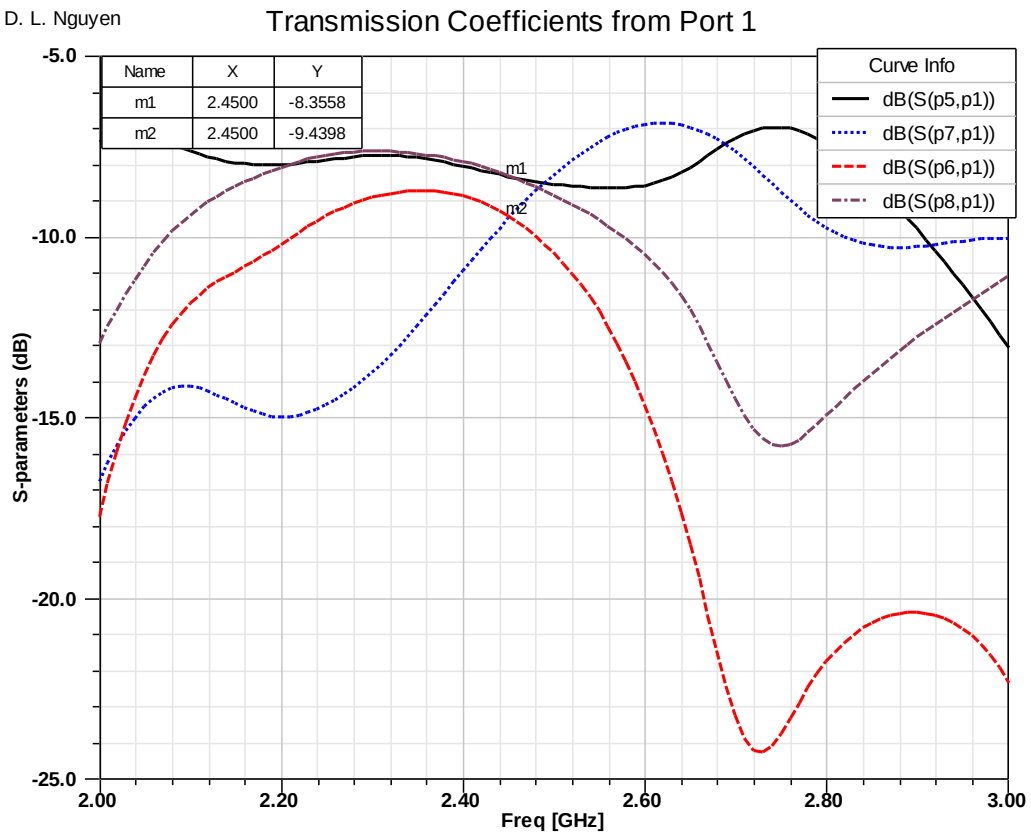

Figure 4.17. Simulated Transmission coefficients from port 1

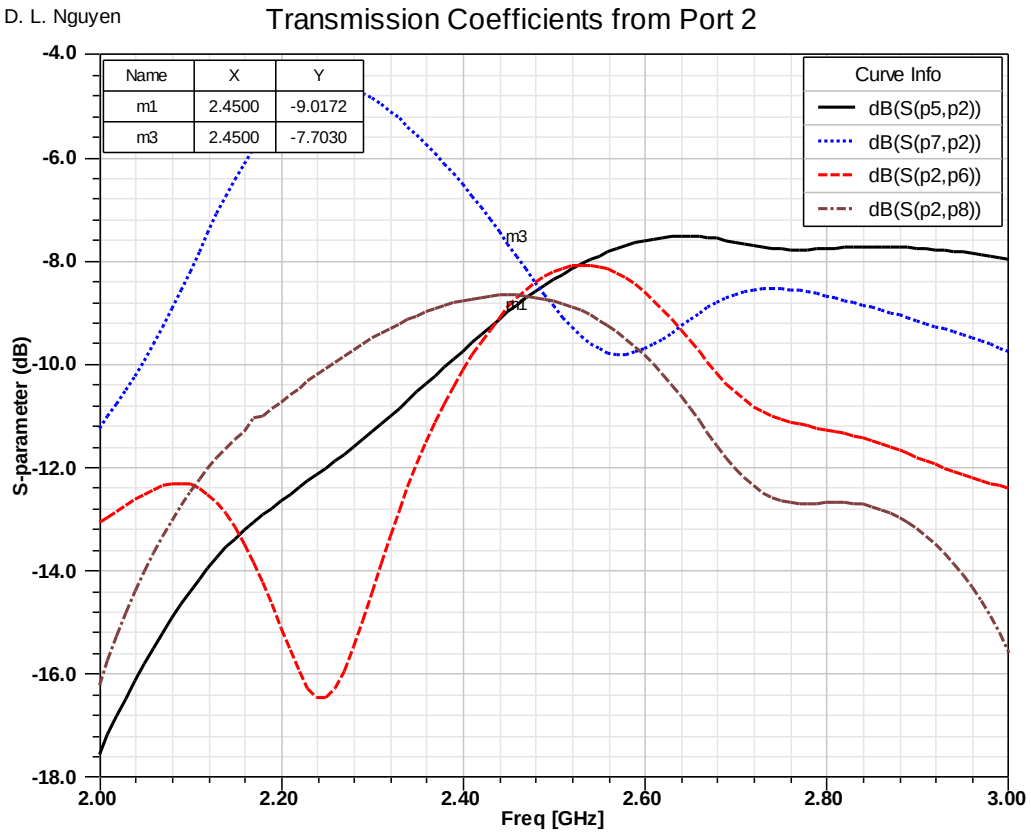

Figure 4.18. Simulated transmission coefficients from port 2

4.3.4.2. Prototype and Measured Results

The fabricated BM is shown in Fig. 4.19. The performance of the BM was measured by using the Agilent Network Analyzer and plotted using Microsoft's Excel. Measured results are well-agreed with simulated predictions.

Simulated and measured return losses at port 1 (in black) and port 2 (in red) are shown in Fig. 4.20. The S-parameters showing the circuit's characteristics at the working frequency of 2.45 GHz are summarised in Table 4.5. Ideal 4 × 4 BM have no return loss at any ports ($S_{ii} = -\infty \; with \; i = 1..4$), no isolation between input ports ($S_{ij} = -\infty \; with \; i,j = 1..4; i \neq j$) and the power is equally divided into the four output ports ($S_{ij} = -6 \; dB \; with \; j = 1..4; i = 5..8$). Progression phases between outputs are dependent on which port is fed e.g. when port 1 is fed the phase progression is 45 degrees.

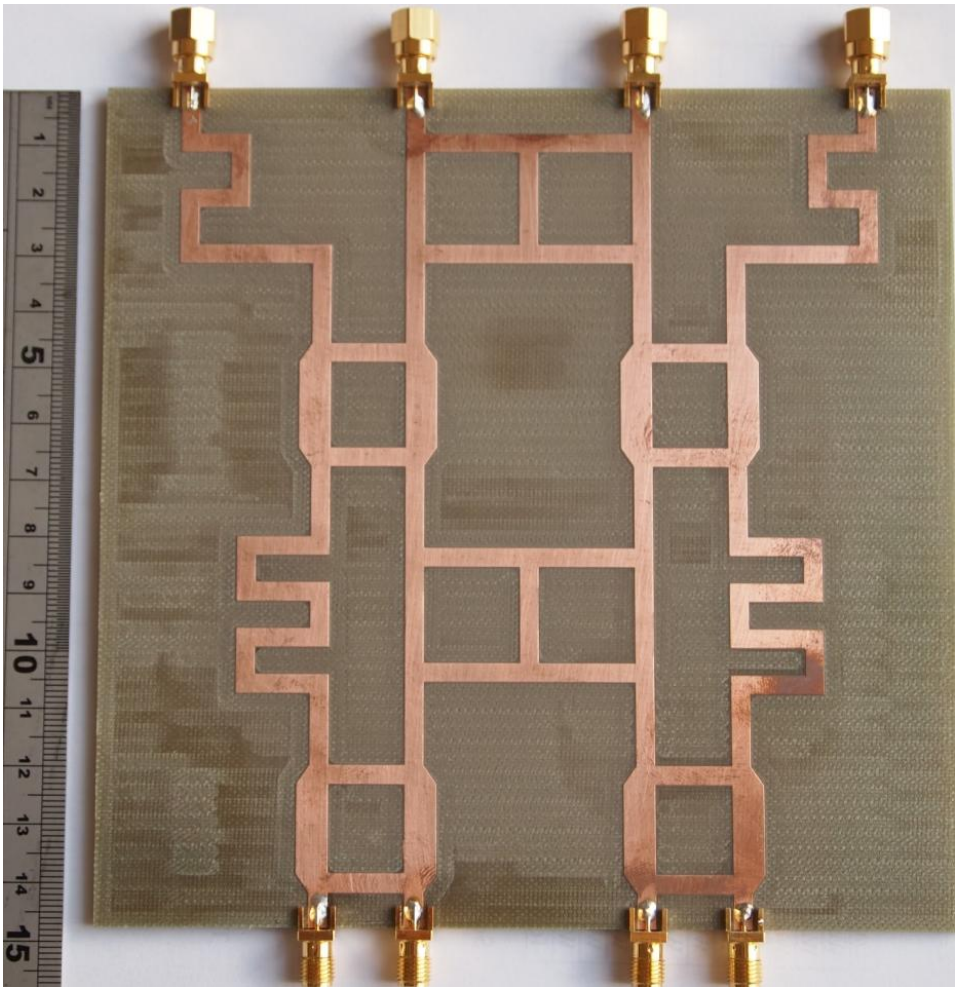

Figure 4.19. Microstrip 4 × 4 BM

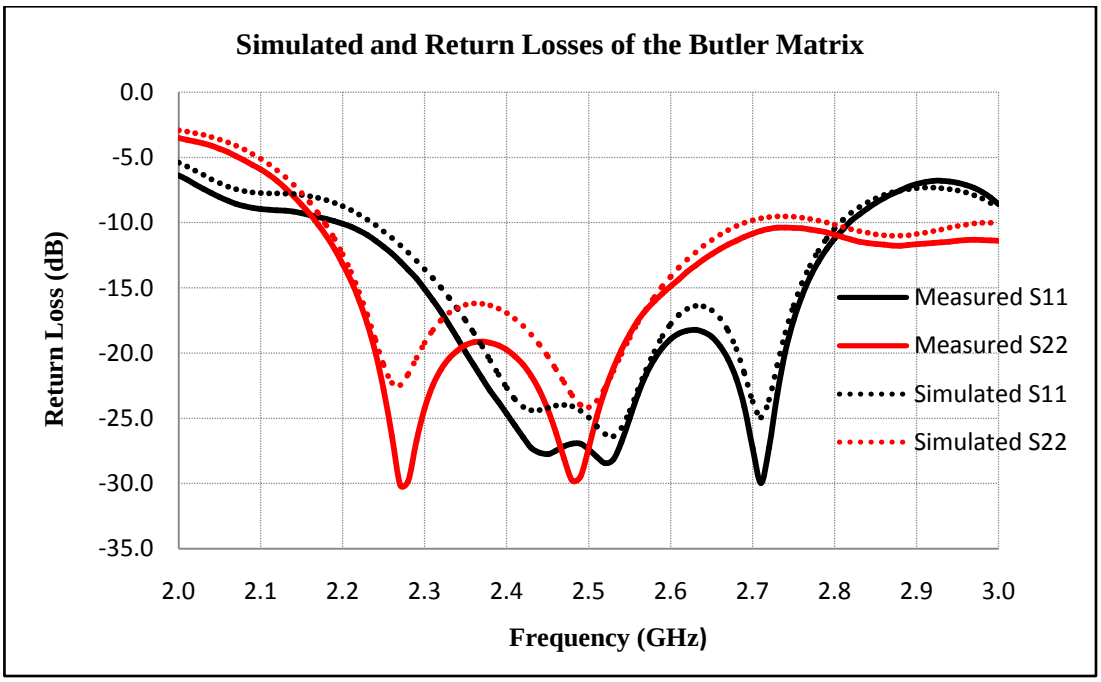

Figure 4.20. Simulated and Measured Return Losses of the 4 × 4 BM

Table 4.5. S-parameters of the 4 × 4 BM

Frequency (2.45 GHz)	Theoretical	Simulated	Measured
S_{11}	-∞	-24.21 dB	-27.75 dB
S_{21}	-∞	-35.37 dB	-40.56 dB
S_{31}	-∞	-31.53 dB	-32.33 dB
S_{41}	-∞	-23.99 dB	-26.01 dB
S_{22}	-∞	-20.24 dB	-24.33 dB
S_{51}	-6.00 dB	-8.36 dB	-8.78 dB
S_{61}	-6.00 dB	-9.44 dB	-9.34 dB
S_{71}	-6.00 dB	-9.53 dB	-9.58 dB
S_{81}	-6.00 dB	-8.33 dB	-8.60 dB
S_{52}	-6.00 dB	-9.02 dB	-8.96 dB
S_{62}	-6.00 dB	-8.93 dB	-9.10 dB
S_{72}	-6.00 dB	-7.70 dB	-7.98 dB
S_{82}	-6.00 dB	-8.69 dB	-9.02 dB
$Ang(S_{61} - S_{51})$ (degrees)	45	43.36	46.90
$Ang(S_{71} - S_{61})$ (degrees)	45	47.74	47.45
$Ang(S_{81} - S_{71})$ (degrees)	45	46.47	48.12
$Ang(S_{62} - S_{52})$ (degrees)	-135	-132.59	-130.13
$Ang(S_{72} - S_{62})$ (degrees)	-135	-146.23	-146.23
$Ang(S_{82} - S_{72})$ (degrees)	-135	-124.44	-124.27

4.4. Compact Stepped Impedance Configuration (SIC) Microstrip BM

In this section, a compact 4 × 4 BM utilising SIC elements is analysed, designed and tested. As described in the previous section, a 4 × 4 BM consists of hybrid couplers and crossovers. Miniaturisation is achieved in these circuits by using SIC equivalent structures. SIC structures are shown to be easy to design and provide effective size reduction. They are widely applicable and can reduce the length of any transmission lines. In addition, the performance of the compact circuits is similar to the standard ones. Using SIC components, the area of the branch-line coupler has been reduced by 40% compared to a conventional coupler. This is more effective miniaturisation than that achieved by the more complex eight two-step stubs method, [Muhammad, 2010], working at the same frequency. This technique is even more effective in size reduction at lower frequencies. Similarly, applying SIC technology to a standard crossover similarly reduces the area by almost 40%, with only minor changes in performance. The SIC components have been integrated into a 4x4 BM with performance similar to the conventional design and also yielding an area reduction of 40%.

4.4.1. Equivalent SIC Structure of a Transmission Line (TL)

A two-port network may be defined by its ABCD matrix, given by [Pozar, 2005]:

$$\begin{bmatrix} V_{in} \\ I_{in} \end{bmatrix} = \begin{bmatrix} A & B \\ C & D \end{bmatrix} \begin{bmatrix} V_{out} \\ I_{out} \end{bmatrix} \tag{4.9}$$

where V_{in}, V_{out}, I_{in} and I_{out} are input, output voltages and currents at the ports of the network.

Consider a TL with characteristic impedance Z_0 and electrical length θ. The ABCD matrix of this TL is [Pozar, 2005]:

$$\begin{bmatrix} A & B \\ C & D \end{bmatrix} = \begin{bmatrix} cos\theta & jZ_0 sin\theta \\ j\dfrac{1}{Z_0} sin\theta & cos\theta \end{bmatrix} \tag{4.10}$$

It can be replaced by an equivalent SIC transmission line as shown in Fig. 4.21. The ABCD matrix of the equivalent SIC TL may be calculated by multiplication of the matrix for each section:

$$\begin{bmatrix} A & B \\ C & D \end{bmatrix} = \begin{bmatrix} cos\theta_1 & jZ_1 sin\theta_1 \\ j\dfrac{1}{Z_1} sin\theta_1 & cos\theta_1 \end{bmatrix} \begin{bmatrix} cos\theta_2 & jZ_2 sin\theta_2 \\ j\dfrac{1}{Z_2} sin\theta_2 & cos\theta_2 \end{bmatrix} \begin{bmatrix} cos\theta_3 & jZ_3 sin\theta_3 \\ j\dfrac{1}{Z_3} sin\theta_3 & cos\theta_3 \end{bmatrix}$$

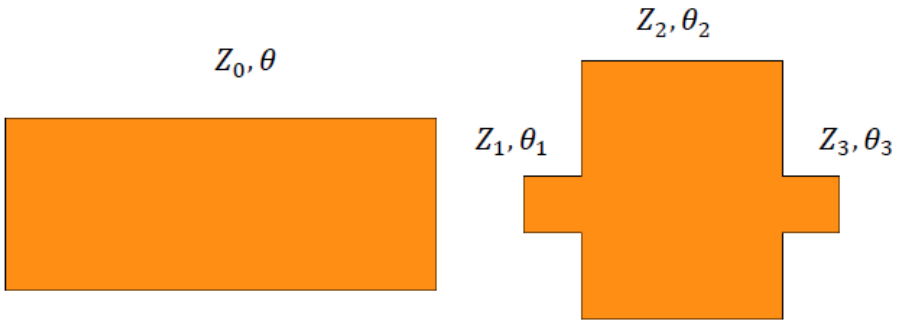

Figure 4.21. Equivalent stepped impedance configuration of a transmission line

For simplicity, the third section is often chosen to be the same as the first section i.e. $Z_1 = Z_3 \; and \; \theta_1 = \theta_3$.

Therefore:

$$A = D = cos\theta = cos\theta_2(cos^2\theta_1 - sin^2\theta_1) - sin\theta_1 cos\theta_1 sin\theta_2 \left(\frac{Z_1}{Z_2} + \frac{Z_2}{Z_1}\right) \tag{4.11}$$

$$B = jZ_0 sin\theta = j\left[2Z_1 sin\theta_1 cos\theta_1 cos\theta_2 - \frac{Z_1^2}{Z_2} sin^2\theta_1 sin\theta_2 + Z_2 cos^2\theta_1 sin\theta_2\right] \tag{4.12}$$

$$C = j\frac{1}{Z_0} sin\theta = j\left[2\frac{1}{Z_1} sin\theta_1 cos\theta_1 cos\theta_2 - \frac{Z_2}{Z_1^2} sin^2\theta_1 sin\theta_2 + \frac{1}{Z_2} cos^2\theta_1 sin\theta_2\right] \tag{4.13}$$

If

$$M = \frac{Z_1}{Z_0}; K = \frac{Z_1}{Z_2} \; (K > M > 1)$$

Equations (4.11), (4.12) and (4.13) become:

$$Kcos\theta_2(cos^2\theta_1 - sin^2\theta_1) - sin\theta_1 cos\theta_1 sin\theta_2(1 + K^2) = cos\theta \tag{4.14}$$

$$2Ksin\theta_1 cos\theta_1 cos\theta_2 + sin\theta_2(cos^2\theta_1 - K^2 sin^2\theta_1) = \frac{K}{M} sin\theta \tag{4.15}$$

$$2Ksin\theta_1 cos\theta_1 cos\theta_2 + sin\theta_2(K^2 cos^2\theta_1 - sin^2\theta_1) = \frac{1}{Z_0} sin\theta \tag{4.16}$$

From (4.14):

$$sin\theta_2 = Kcos\theta_2 \frac{cos^2\theta_1 - sin^2\theta_1}{(1+K^2)sin\theta_1 cos\theta_1} - \frac{cos\theta}{(1+K^2)sin\theta_1 cos\theta_1} \quad (4.17)$$

Substituting (4.17) into (4.15) to obtain:

$$cos\theta_2 = \frac{cos\theta(1 - K^2 tan^2\theta_1) + \frac{1}{M} sin\theta(1+K^2)tan\theta_1}{1 + K^2 tan^2\theta_1} \quad (4.18)$$

Now using (4.17) and (4.18) to achieve:

$$tan^2\theta_1(K^2M^2 - 1) + 2tan\theta_1[Mcot\theta(K^2 - 1)] - (K^2 - M^2) = 0 \quad (4.19)$$

Given the characteristic impedances of the TLs, the value of θ_1 may be found by solving the quadratic (4.19) and then substituted into (4.18) to determine θ_2 . Due to the dependencies in the derivation of these equations, (4.16) is also satisfied by these parameters. Therefore, any transmission line can be replaced by a range of equivalent SIC structures given values of Z_1 and Z_2 (i. e. M and K). This configuration is useful as many microwave circuits are made up from a number of TLs and the equivalent SIC structure is usually shorter in physical length than the original line.

Total electrical length of the SIC configuration is $\theta_T = 2\theta_1 + \theta_2$.

The ratio of lengths of a TL and the equivalent SIC structure is defined as $\gamma = \frac{\theta_T}{\theta}$. Gamma (γ) is less than unity and this is a measure of the miniaturisation.

4.4.1.1. Equivalent Structure of a Quarter-wavelength Transmission Line

The equivalent SIC structure to a quarter-wavelength transmission line is given by the electrical lengths θ_1, θ_2:

$$\theta_1 = tan^{-1}\sqrt{\frac{K^2 - M^2}{K^2M^2 - 1}} \quad (4.20)$$

$$\theta_2 = sin^{-1}\frac{K(M^2 - 1)}{M(K^2 - 1)} \quad (4.21)$$

Figure 4.22 illustrates the variation of γ with K and M. It can be seen that the overall length of the quarter-wave SIC structure is reduced as K is increased and for each value of K an optimal value of M exists. In practise M and K are limited by the characteristics

of the substrate and circuit fabrication capability. Also, as K is increased, the characteristic impedance of the middle section becomes relatively small (about 10 to 20 Ohms) requiring an extremely large width. Ultimately the width approaches the physical constraints of the circuit and may lead to a larger footprint than the original quarter-wave TL.

Some equivalent SIC structures of quarter-wavelength TLs used to construct the microstrip BM are verified by Agilent ADS software in the following sections.

4.4.1.2. Equivalent SIC of the Quarter-wavelength 50-Ω TL

The values of the equivalent SIC structure are set: M = 2.5 and K = 5. These values are chosen because they provide feasible line dimensions and useful miniaturisation.

Matlab software is used to evaluate equations (4.20) and (4.21) yielding $Z_1 = 25\ \Omega$, $\theta_1 = 19.16°$ for sections 1 and 3; and $Z_2 = 25\ \Omega, \theta_2 = 25.94°$ for section 2. These parameters have been verified using ADS. In Fig. 4.23, three TL sections are ideal TLs (TLIN) with the calculated characteristic impedance Z and electrical length E. This SIC structure is connected with two 50-Ω ports (Term 1 and Term 2).

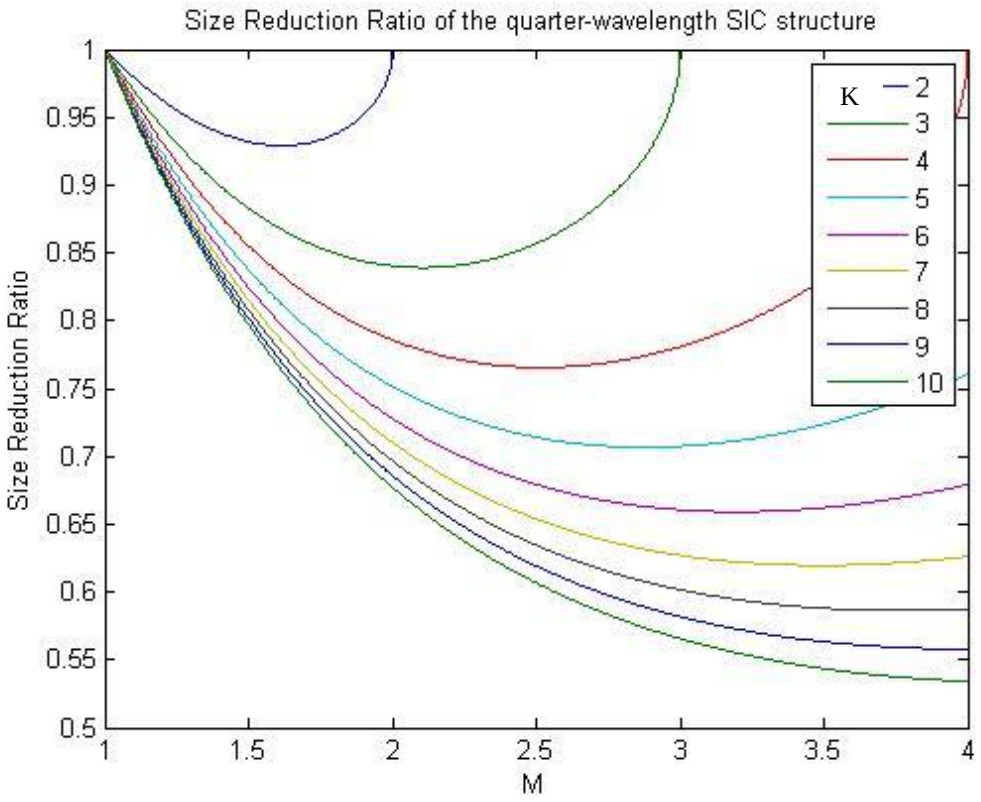

Figure 4.22. The size reduction ratio (γ) of the quarter-wavelength line SIC structure against *M* for different values of K

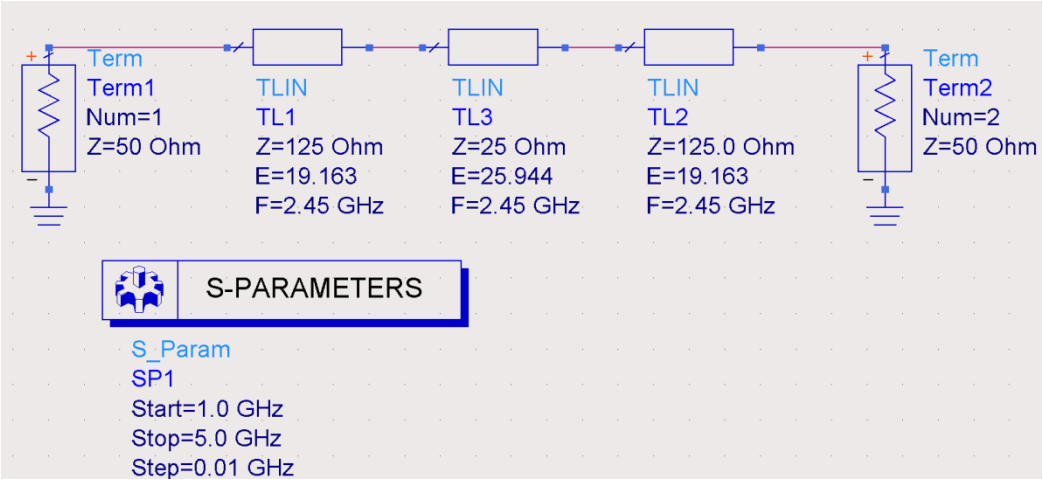

Figure 4.23. ADS verification of SIC structure 50-Ω TL

The simulated S-parameters of the SIC structure are shown in Fig 4.24 and 4.25.

Fig. 4.24 shows that there is almost no reflection loss ($S_{11} < -98\,dB$) and no transmission loss ($S_{21} \approx 0$) at 2.45 GHz. In Fig 4.25 it can be seen that the phase delay introduced by the structure is very close to $-90°$.

These results verify that the SIC structure is equivalent to a quarter wavelength of 50-Ω line.

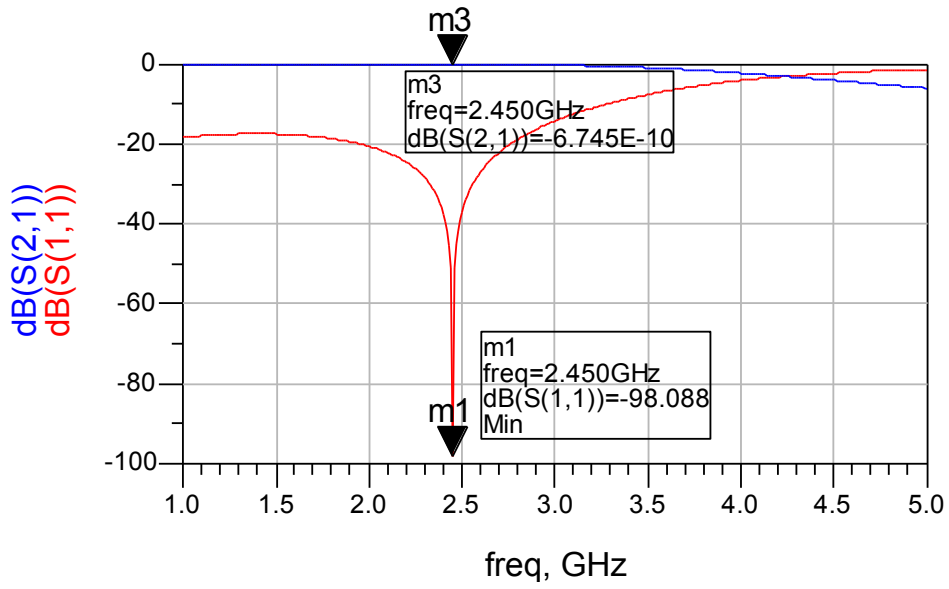

Figure 4.24. Simulated RL and Transmission Coefficients of the SIC structure for 50-Ω TL

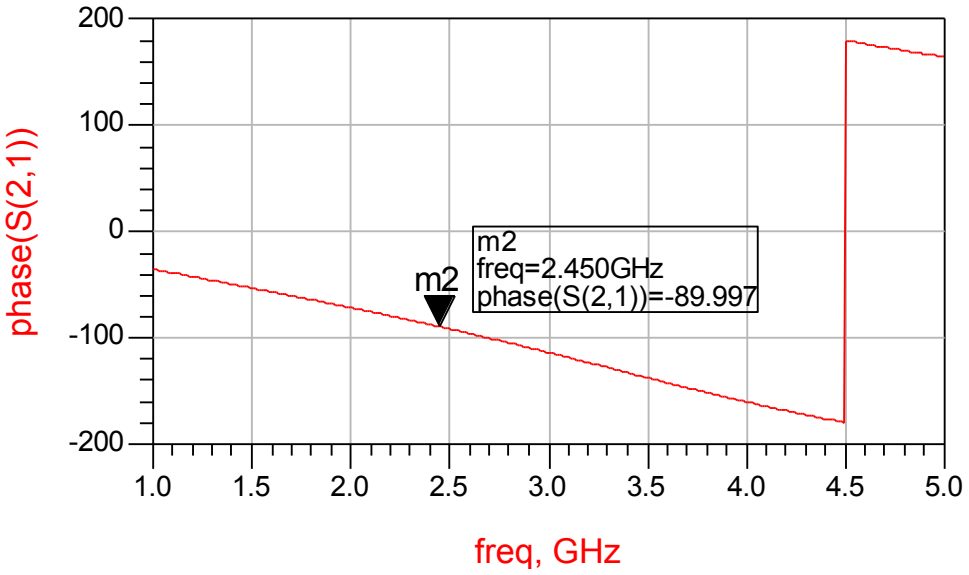

Figure 4.25. Simulated phase delay of the SIC structure for 50-Ω TL

The dimensions of SIC TLs are obtained from Agilent's ADS LineCalc tool. Sections 1 and 3 have a width of 0.39 mm and length of 3.88 mm while section 2 has a width of 8.76 mm and length of 4.71 mm.

The effect of the discontinuity at the transition between these sections is taken into account and verified by ADS. In Fig. 4.26, 3 TL sections of the SIC structure are microstrip lines (MLIN): TL1; TL2 and TL3. Placed between them, there are two microstrip steps (MSTEP).

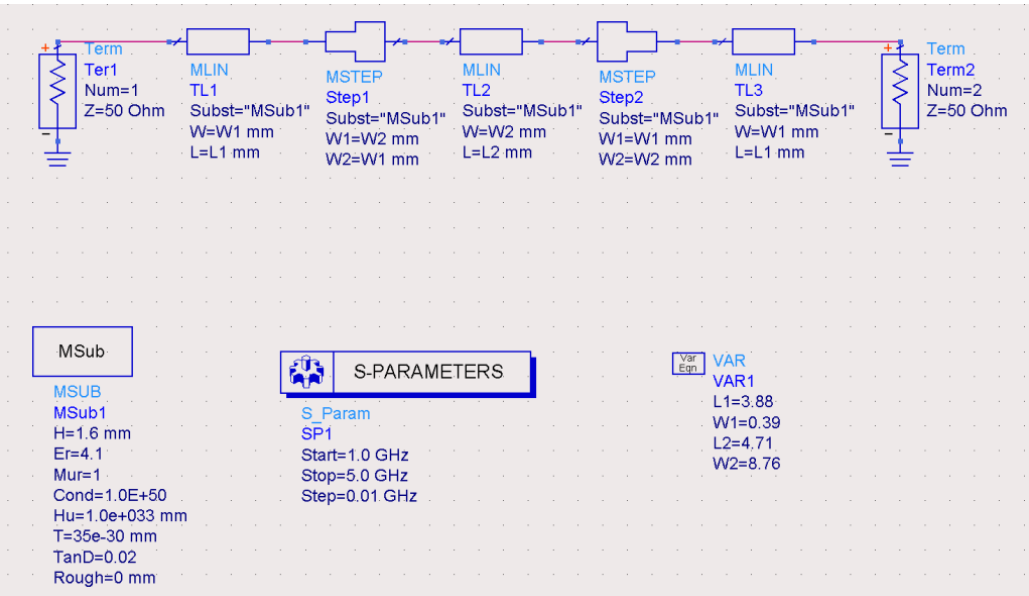

Figure 4.26. ADS model of the microstrip SIC structure for 50-Ω TL with discontinuity

The simulated results (Fig. 4.27) show the effect of the discontinuity at the transition to the performance of the SIC structure in practice. In order to achieve equivalent 50-Ω quarter-wavelength line at 2.45 GHz, the TL sections' widths are modified.

Moreover, the discontinuity of the SIC structures within the circuit elements, such as the hybrid coupler and the crossover, requires the equivalent structures to be lengthened by 5-10% [Balanis, 2005]. Alternatively, this can be achieved by modifying only the middle section's width to 7.09 mm. Performance of the modified structure is shown in Fig. 4.28.

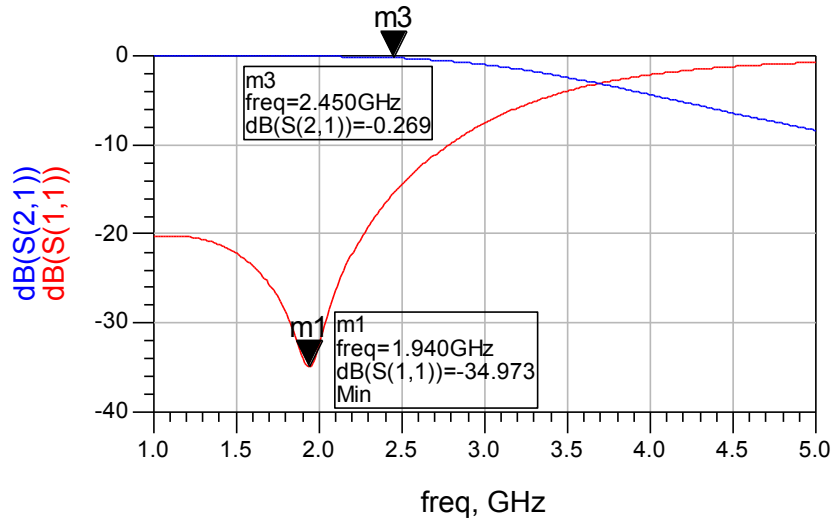

a)

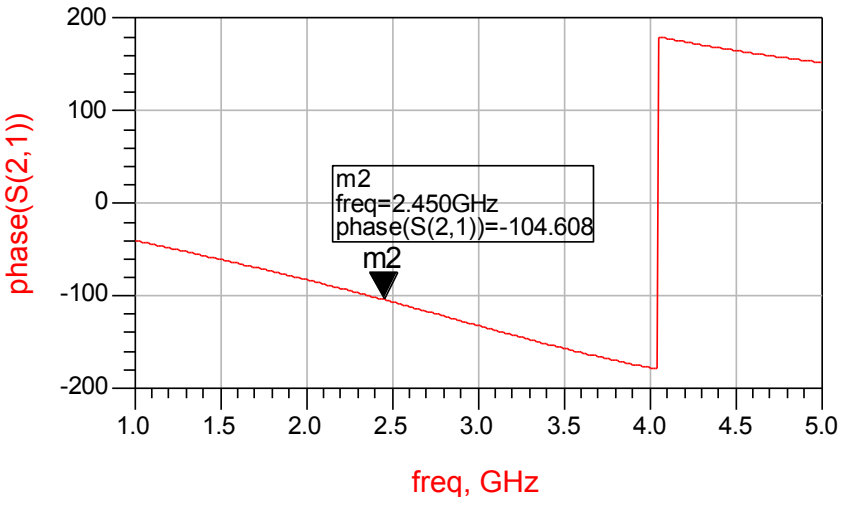

b)

Figure 4.27. ADS S-parameters of the calculated SIC structure for 50-Ω TL: a) Magnitude b) Phase

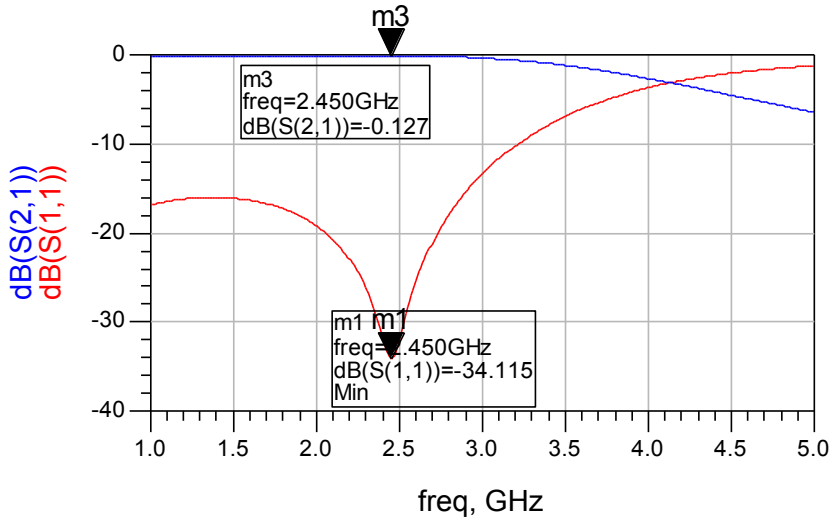

a)

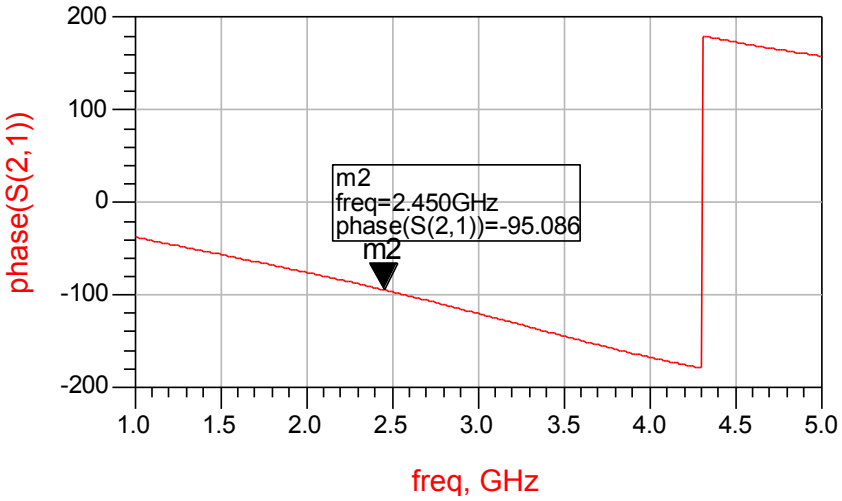

b)

Figure 4.28. ADS Simulated S-parameters of the modified SIC for 50-Ω TL: a) Magnitude; b) Phase

The equivalent structure of the 50-Ω quarter-wavelength TL is also simulated by HFSS. The obtained results are almost identical to the ADS simulation results. Fig. 4.29 shows the simulated performance of the modified structure, calculated using HFSS.

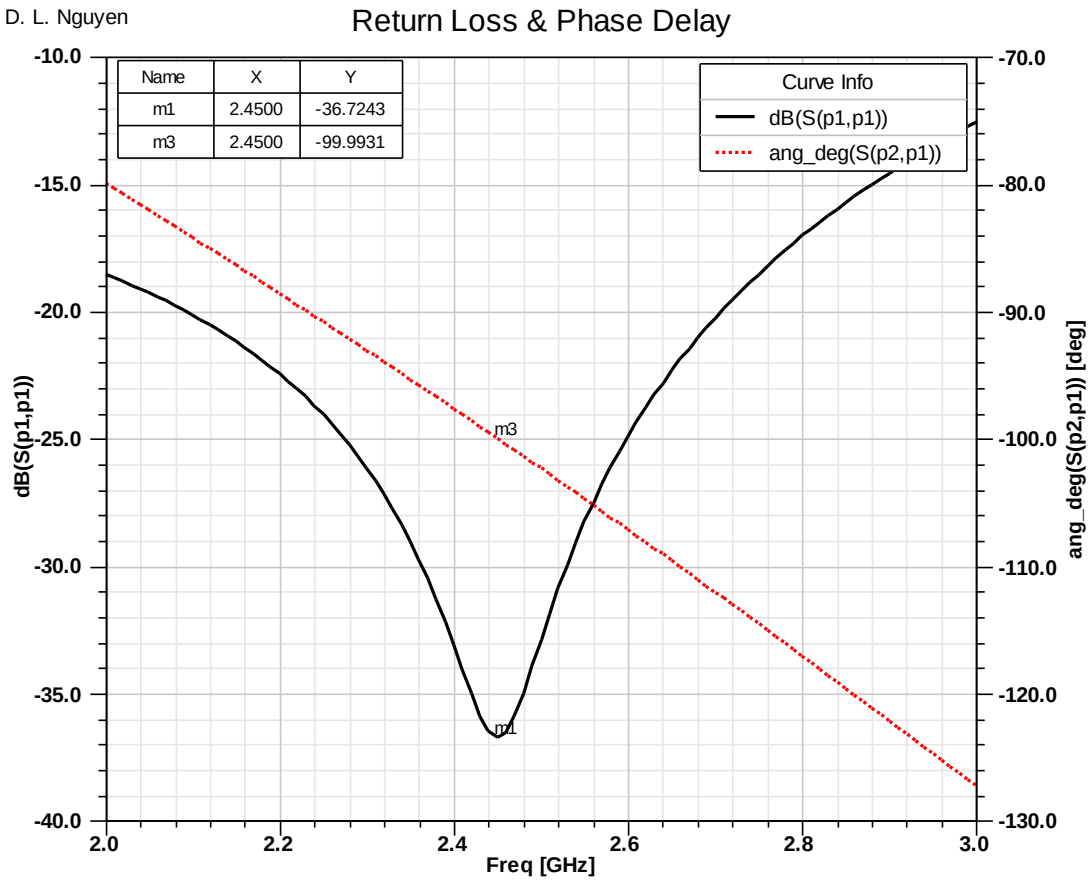

Figure 4.29. HFSS Simulated S-parameters of the modified SIC structure

4.4.1.3. Equivalent SIC for a Quarter-wavelength 35.35-Ω TL

The values of the SIC structure of the quarter-wavelength 35.35-Ω TL are chosen as: M = 3.5 and K = 5. The same procedures used in section 4.4.1.2 were performed to determine the characteristic impedance and electrical length of the end sections: $Z_1 = 123.72\ \Omega$ and $\theta_1 = 11.55°$ respectively. The required TL width and length are 0.41 mm and 2.34 mm. Section 2 has impedance and delay of $Z_2 = 24.745\ \Omega$ and $\theta_2 = 42.04°$ i.e. width and length 8.88 mm and 7.80 mm respectively. When the discontinuity is taken into account, the actual length for the circuit, including the coupler and the crossover, is 7.63 mm.

ADS simulations of the ideal SIC structure and its performance are shown in Fig. 4.30, 4.31 and 4.32.

A more practical model of the structure with discontinuities at the steps, has been simulated and results are shown in Fig. 4.33 and 4.34.

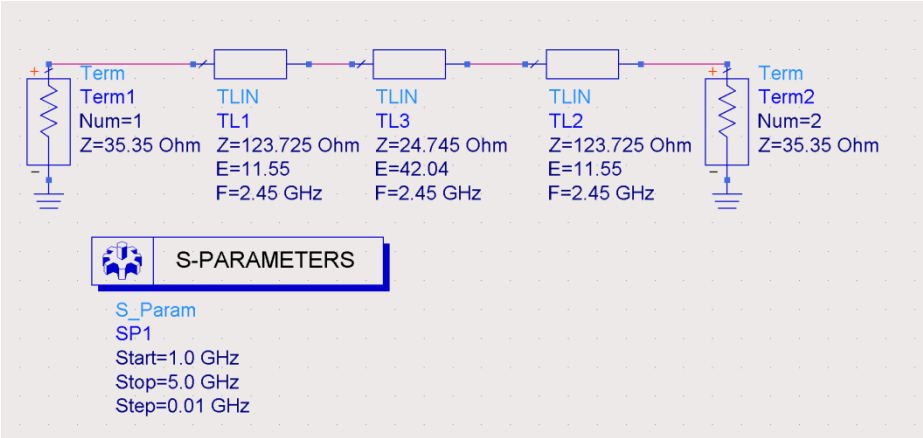

Figure 4.30. ADS verification of SIC structure 35.35-Ω TL

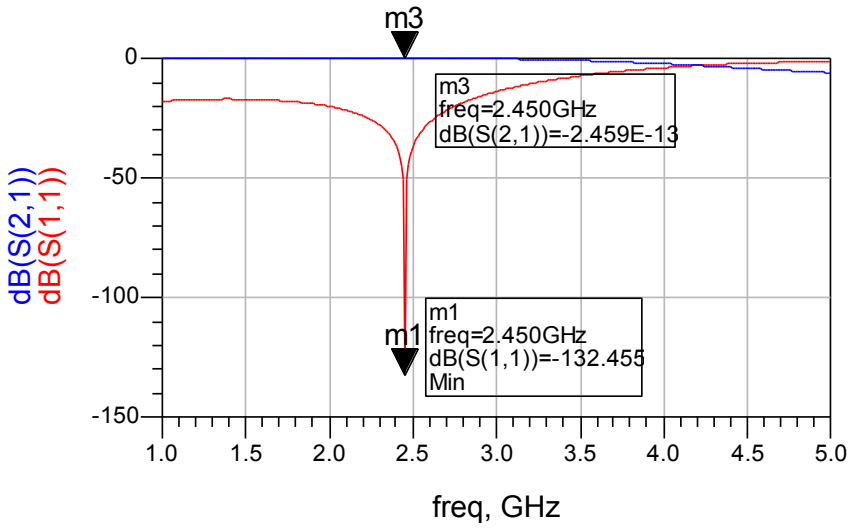

Figure 4.31. Simulated RL and Transmission Coefficient of the SIC structure for 35.35-Ω TL

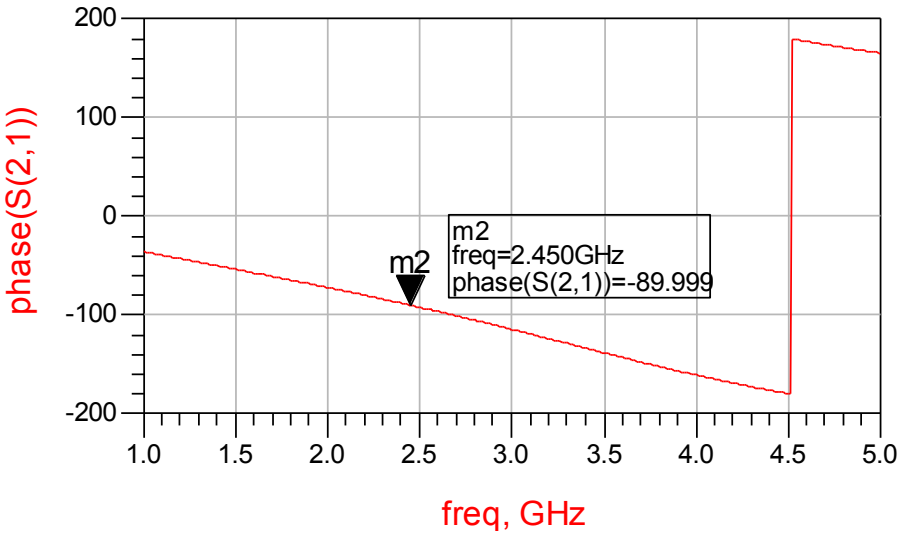

Figure 4.32. Simulated phase delay of the SIC structure for 35.35-Ω TL

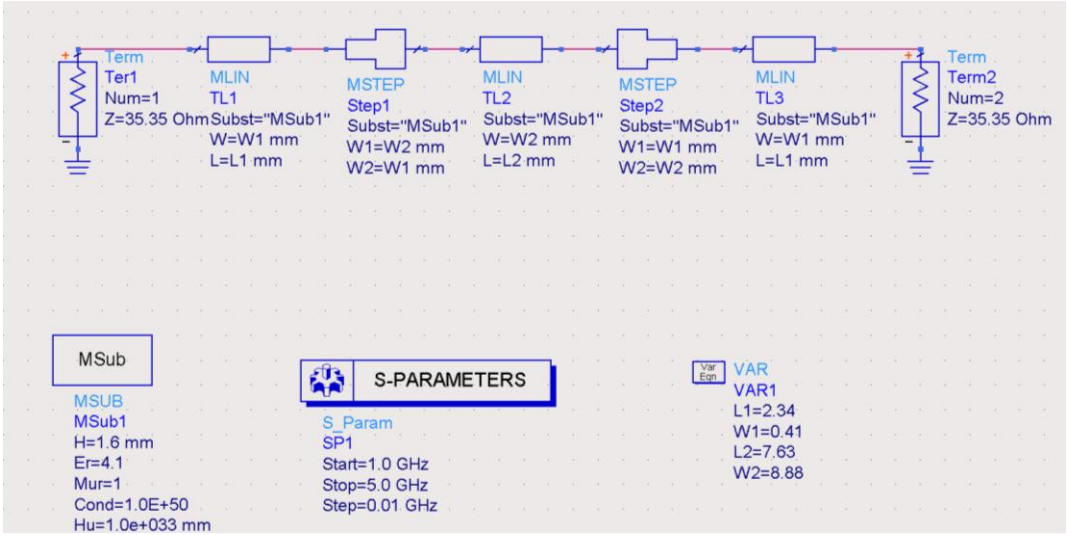

Figure 4.33. ADS model of the microstrip SIC structure for 35.35-Ω TL with discontinuity effect

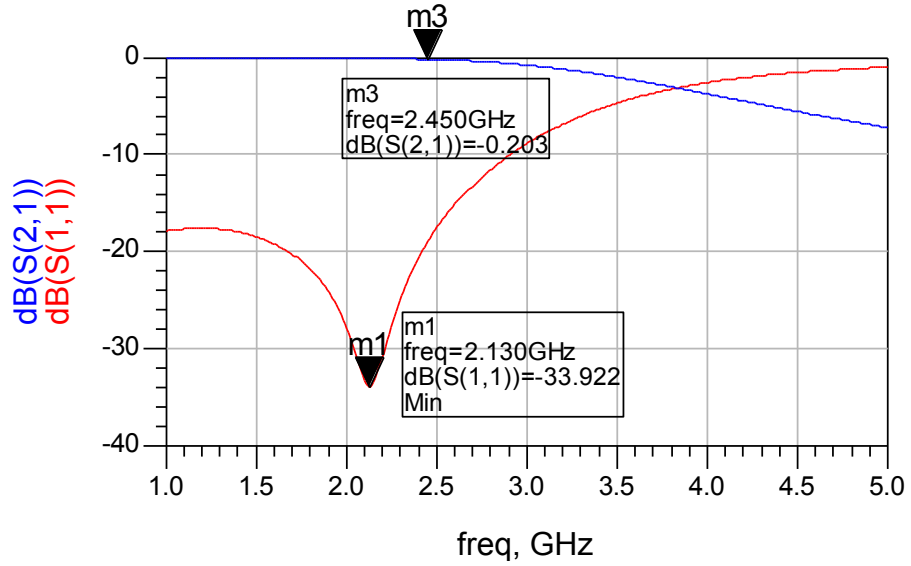

a)

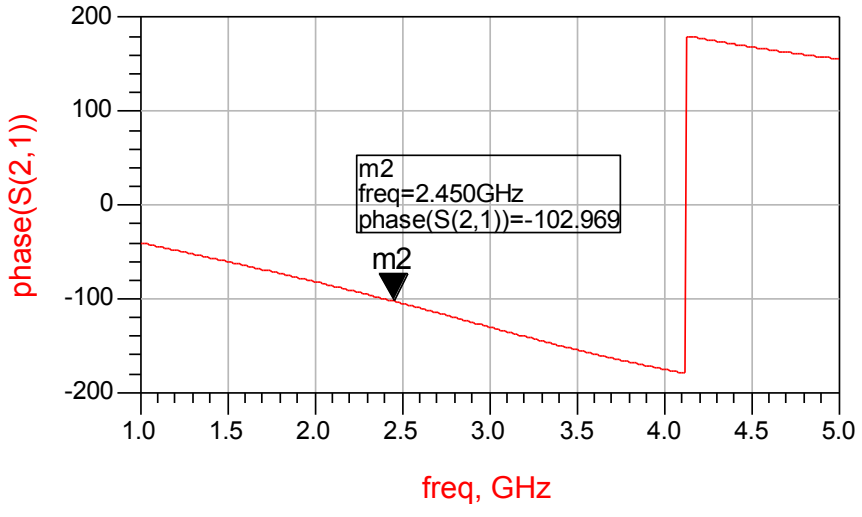

b)

Figure 4.34. ADS S-parameters of the calculated SIC for 35.35-Ω TL: a) Magnitude b) Phase

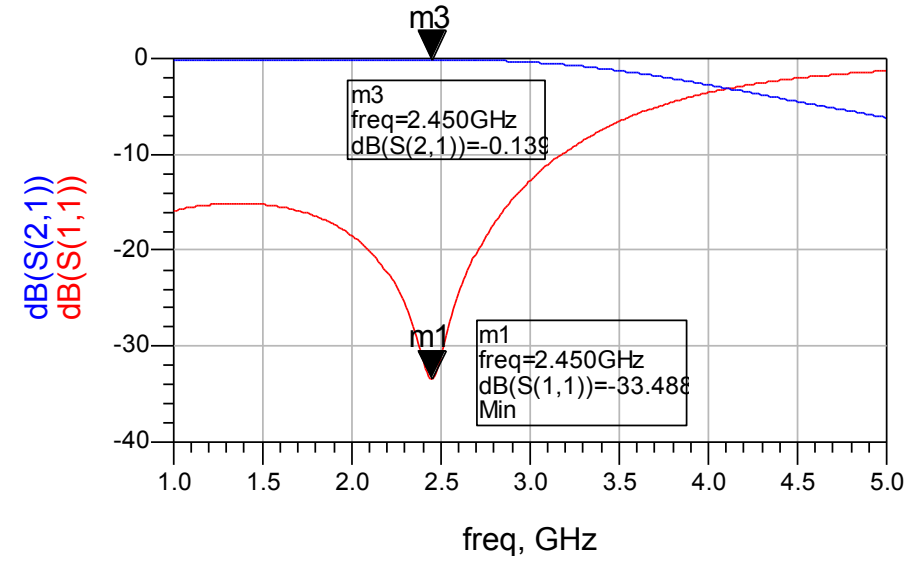

a)

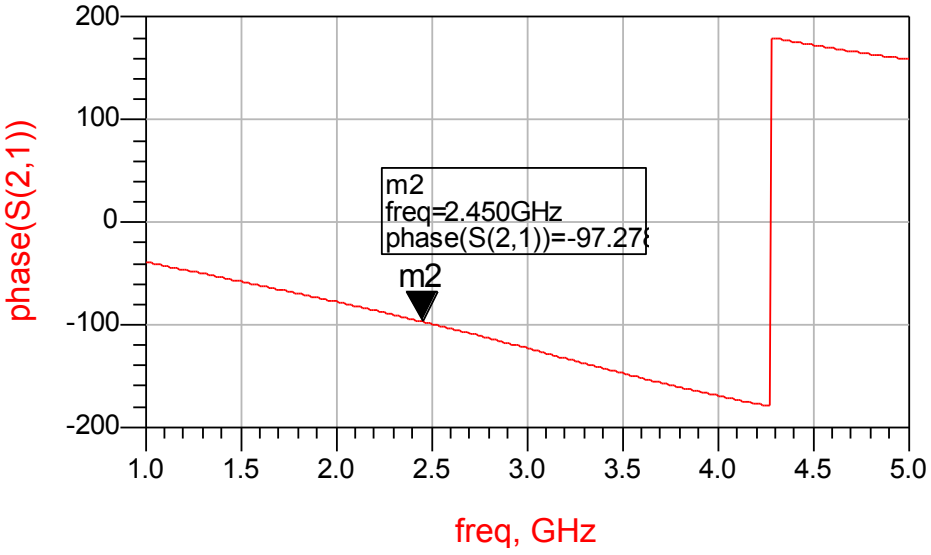

b)

Figure 4.35. ADS Simulated S-parameters of the modified SIC for 35.35-Ω TL: a) Magnitude b) Phase

The results show the discontinuity at the transition effects the structure performance. In order to achieve an equivalent 35.35-Ω quarter-wavelength TL, the widths of the sections require modification. After optimisation using HFSS, the phase delay of the SIC structure is about 5-10% more than phase delay of the quarter-wavelength (i.e. 90°). The widths of section 1 and 3 are kept at 0.41 mm and the section 2 width is 7.8 mm. The performance of the modified structure is shown in Fig. 4.35 and 4.36.

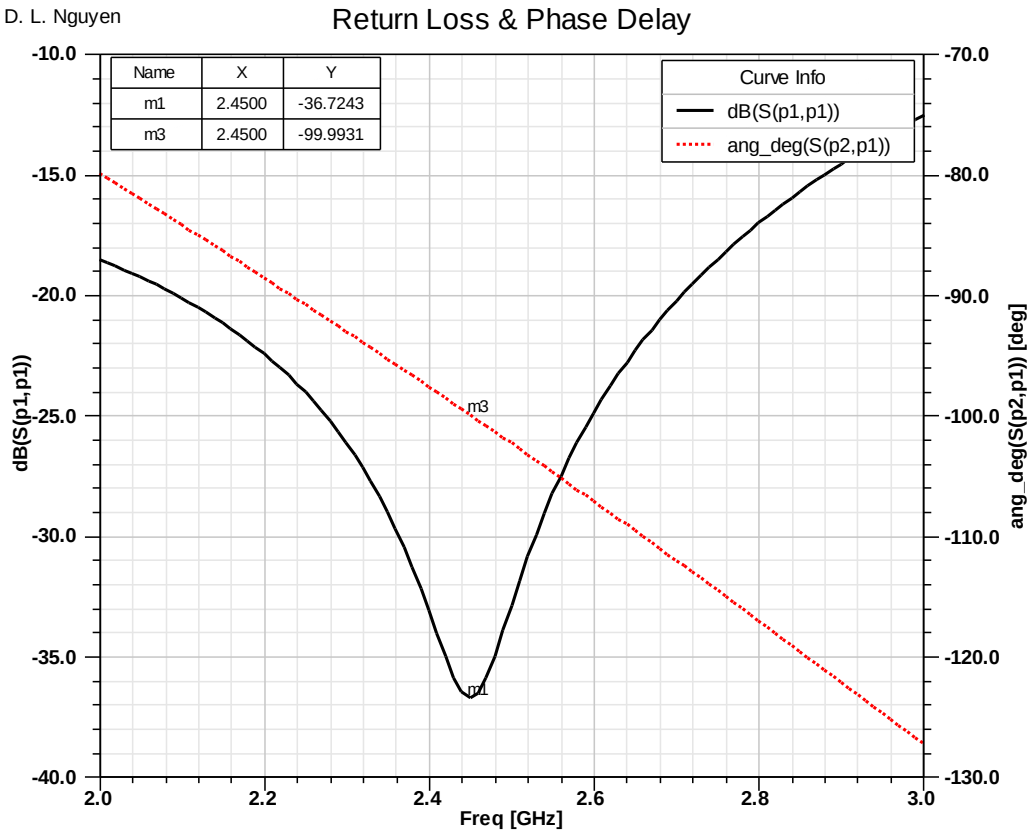

Figure 4.36. HFSS Simulated S-parameters of the modified SIC structure for 35.35-Ω TL

4.4.2. Compact SIC Quadrature Hybrid Coupler

In recent years, many techniques for reducing the size of the quadrature hybrid coupler have been devised, such as combinations of short high-impedance transmission lines, shunt lumped capacitors, [Hirota, 1990; Singh, 2001; Hettak, 2005], lumped elements [Liao, 2006; Hongerheiden, 1997], periodic open-ended stubs [Eccleston, 2003], discontinuous microstrip lines [Sun, 2005], T-shape equivalent configuration [Liao, 2005], high- low impedance resonators [Wang, 2007], high impedance lines [Mandal, 2008] and defected ground structure (DGS) [Sung, 2001; Dwari, 2006; Maddah-Ali, 2008]. Among them, techniques based on microstrip technology have the advantage of simple fabrication at low cost as they are fabricated on a single layer substrate without any additional lumped elements or wires.

The proposed SIC compact coupler also has these advantages. The circuit is easier than other designs and provides similar performance to conventional ones.

The conventional quadrature hybrid coupler (section 4.3.1) consists of 50-Ω and 35.35-Ω quarter-wavelength arms. These arms are designed and simulated in sections 4.4.1.2. and 4.4.1.3.

When combined into a hybrid coupler, the component arms overlap at the corners.

These results can be used as an initial design input into an iterative optimisation which adjusts the dimensions to match the desired performance while minimising the overall area of the coupler. After some numerical experimentation, it was found that the addition of small microstrip squares, 2 × 2 mm, to the middle section of the 35.35-Ω arm yielded close to optimal performance. The result of this process is illustrated in Fig. 4.37.

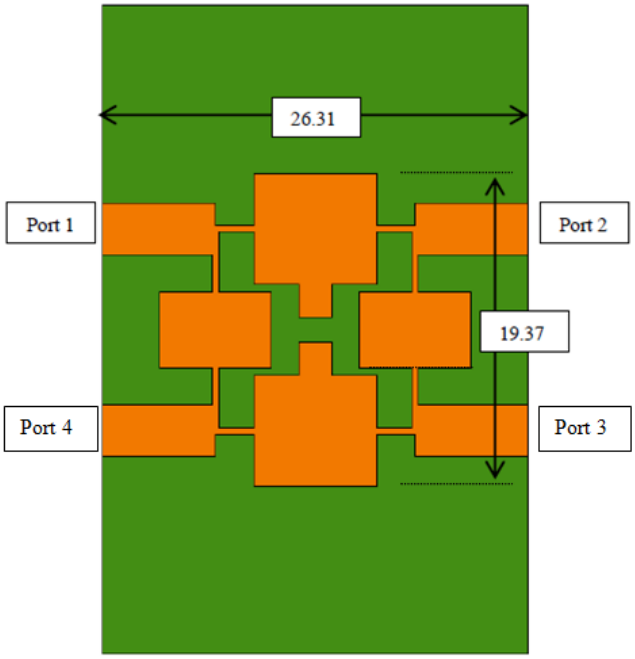

Figure 4.37. Layout of the compact SIC Coupler (Dimensions in mm)

The compact SIC coupler covers only 58.87% of the area of the conventional coupler i.e. a size reduction is 41.13%. Simulated coupler performance, obtained using HFSS, is shown in Fig. 4.38. The simulated S-parameters of the conventional and the SIC coupler are compared to the ideal one and summarised in Table 4.6. Performance of the compact coupler is similar to the conventional coupler. The RL and isolations are below -20 dB at the design frequency, and the power output at ports 2 and 3 differ by less than 1%, with a phase difference of approximately 88.6 degrees. As the transmitted power ($P_{transmitted}$) is related to the Return Loss (RL) in dB by:

$$P_{transmitted} = \left(1 - 10^{\mathrm{RL}/10}\right) \times 100\% \qquad (4.18)$$

Less than 0.1% of the input power is dissipated in the coupler.

Table 4.6. Simulated S-parameters of the standard coupler and the compact coupler

Frequency 2.45 GHz	S_{11} (dB)	S_{21} (dB)	S_{31} (dB)	S_{41} (dB)	$ang(S_{21}) - ang(S_{31})$
Theoretical	-∞	-3.0	-3.0	-∞	90°
Simulated standard coupler	-22.36	-3.55	-3.58	-33.65	88.63°
Simulated compact coupler	-30.28	-3.48	-3.52	-30.05	88.55°

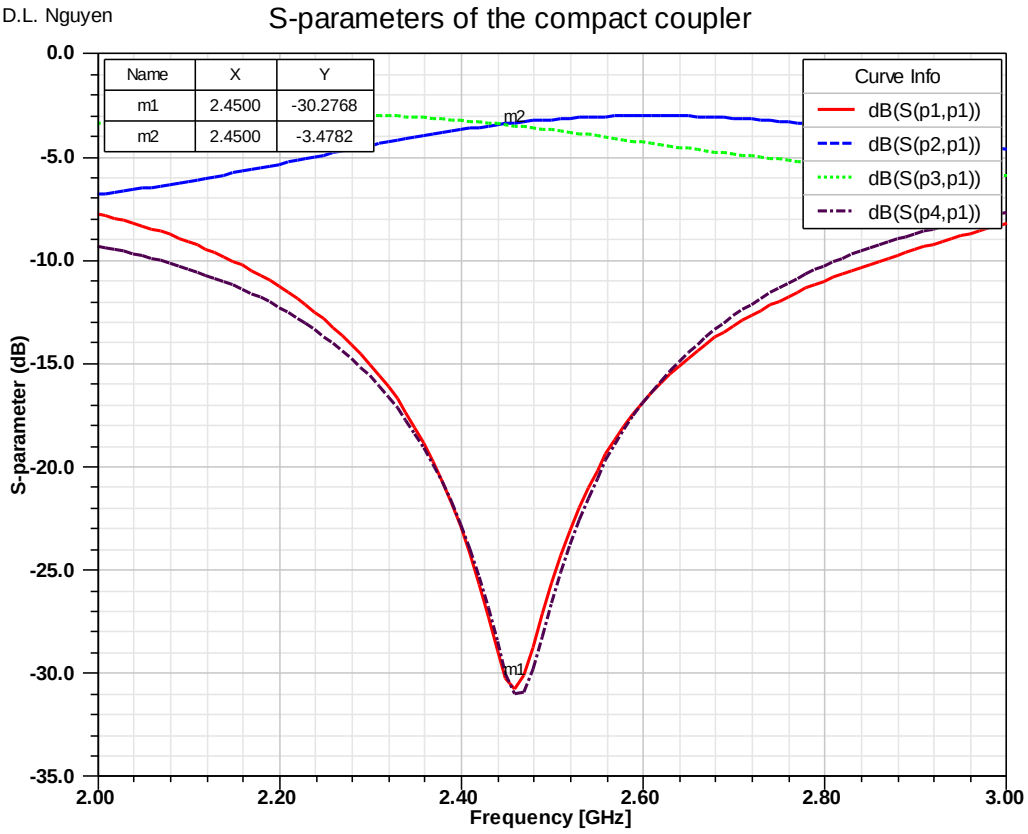

Figure 4.38. HFSS S-parameters of the compact coupler

4.4.3. Compact SIC Crossover

The compact SIC crossover is obtained by applying the equivalent SIC structure of the quarter-wavelength TL described in section 4.4.1.2 into the conventional crossover (see 4.3.2). Fig. 4.39 shows the model of the microstrip compact SIC crossover. This crossover was milled on the same board as the compact coupler.

The simulated performances of the compact crossover, Fig. 4.40, are similar to those of the conventional one. Simulated results show that at the design frequency of 2.45 GHz, 99.88% of input power is transmitted with a 0.85 dB substrate loss between ports 1 and 3. The area of this crossover is 37.49% less than a conventional crossover.

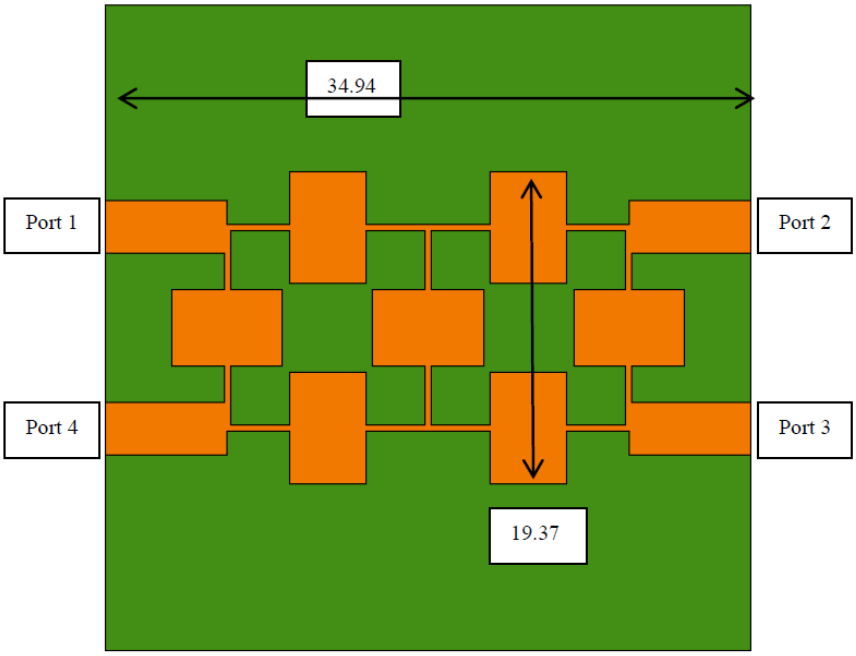

Figure 4.39. Layout of the Compact SIC crossover (Dimensions in mm)

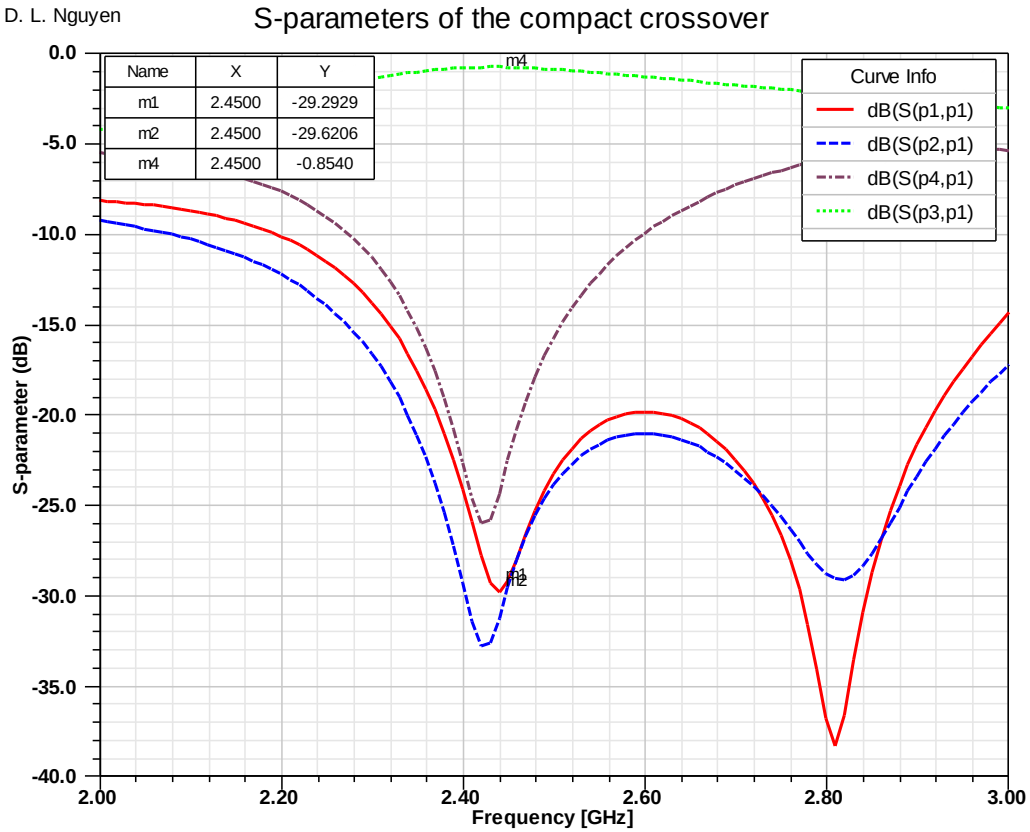

Figure 4.40. HFSS Simulated S-parameters of the compact crossover

4.4.4. Phase Shifter

The phase shifter chosen for the compact BM is a meandered TL phase shifter PS_1 (see Fig. 4.15.a in section 4.3.4.1).

The lengths s_1 and s_0 are 40 mm and 8 mm, respectively. The length of s_2 was modified to achieved the desired phase delay when fed in conjunction with the crossover. To achieve a 0° and a 45° phase delay, the lengths of are s_2 are 8.40 mm and 10.57 mm respectively.

4.4.5. Compact 4 × 4 SIC BM

The compact SIC 4 × 4 BM layout is shown in Fig. 4.41 with the dimensions of components as described in the sections above. The circuit size is 80 mm × 122.5 mm.

Simulated return losses and the isolation between port 1 and other ports have been obtained by HFSS and are illustrated in Fig. 4.42. The RL at all input ports ($S_{11}, S_{22}, S_{33}, S_{44}$) is lower than the -20 dB at 2.45 GHz, that is considered sufficient for most wireless applications. The transmission coefficients between input and output ports range from -7.70 dB to -9.02 dB showing that when one input is fed the power is almost equally separated into the four output ports.

When port 1 is fed, the phase progressions at output ports are $46.51°, 42.26°$ and $44.06°$ (Table 4.7). The simulated results show that the phase progression error is within $2.74°$ of the theoretical phase progression of $45°$. Table 4.7 also shows the phase progressions when port 2 is fed. When this BM is used to feed a switched-beam antenna, different path lengths through the Butler matrix from the input port to four output ports are inevitable. This may lead to the output amplitude imbalance and unequal phase progression.

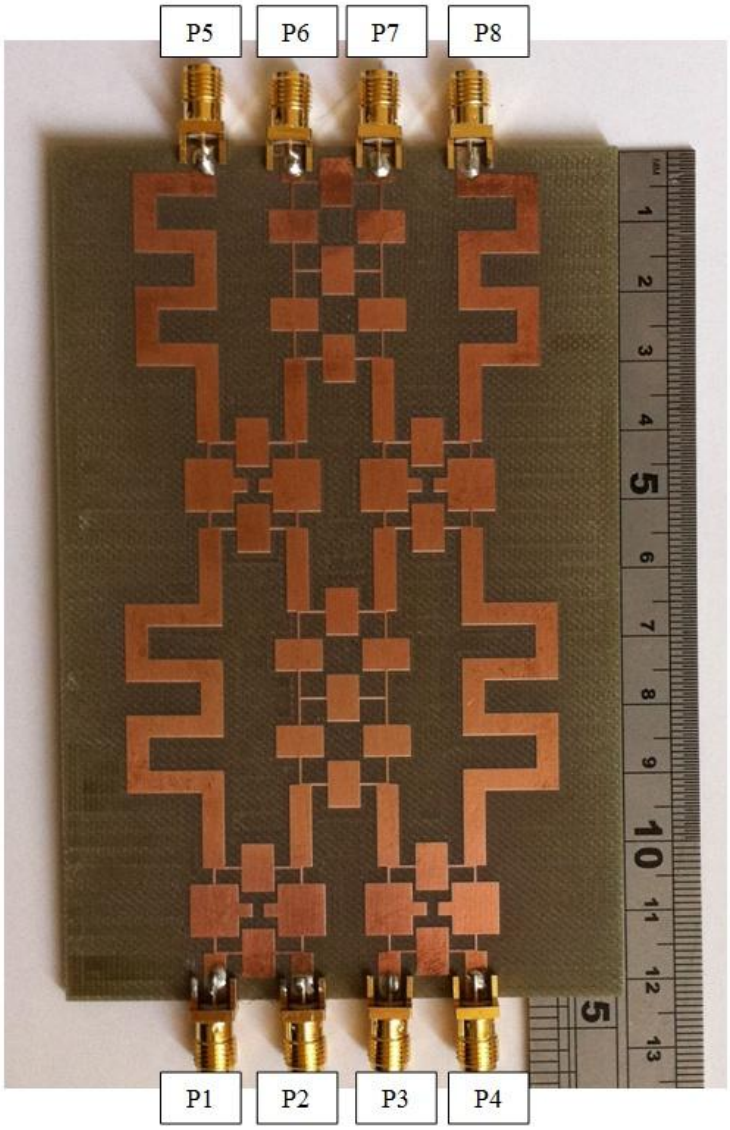

Figure 4.41. Layout of compact SIC 4 × 4 Butler Matrix

In order to test the performance of the circuits, an Agilent Network Analyzer E8358A was used with BM ports connected to 50-ohm terminators.

Measured and simulated performance agrees within expected errors. The measured and simulated return losses at ports 1 and 2 are shown in Fig 4.43. In the entire ISM band from 2.4 to 2.5 GHz, the return losses are greater than 15 dB. Detailed performance of the fabricated circuit at the design frequency 2.45 GHz is provided in Table 4.7.

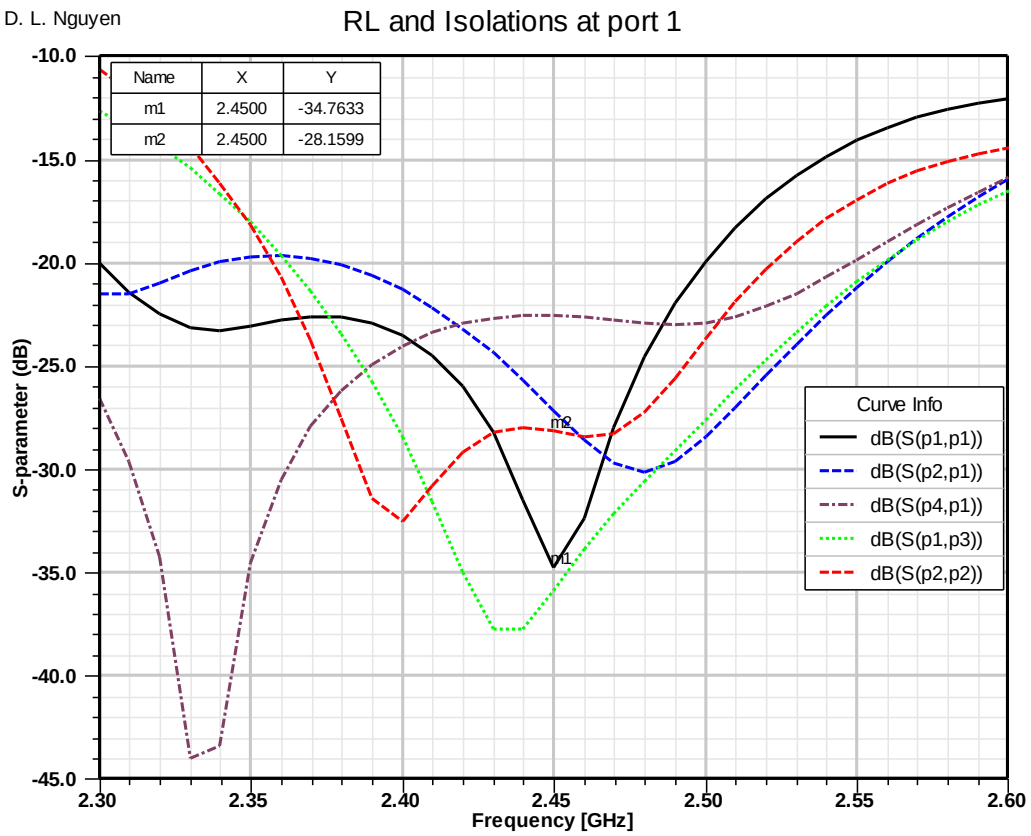

Figure 4.42.a) Simulated Return Losses at port 1;2 and Isolation between port 1 and other ports

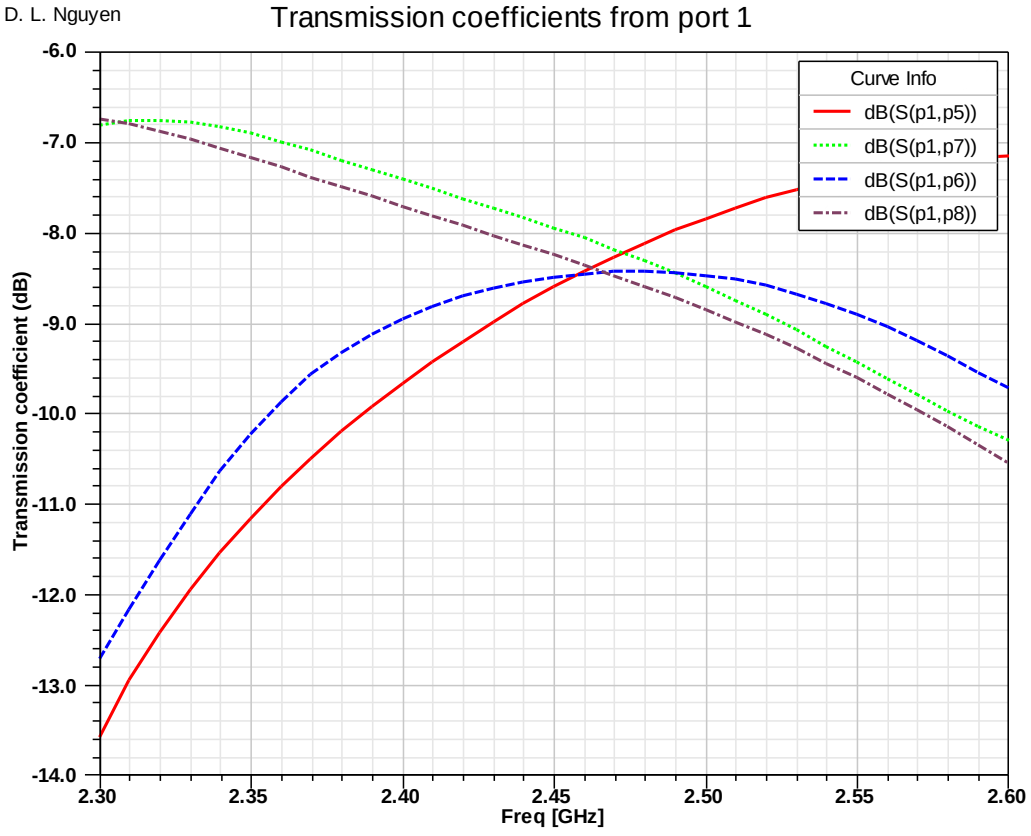

Figure 4.42.b) Simulated Transmission coefficients from port 1

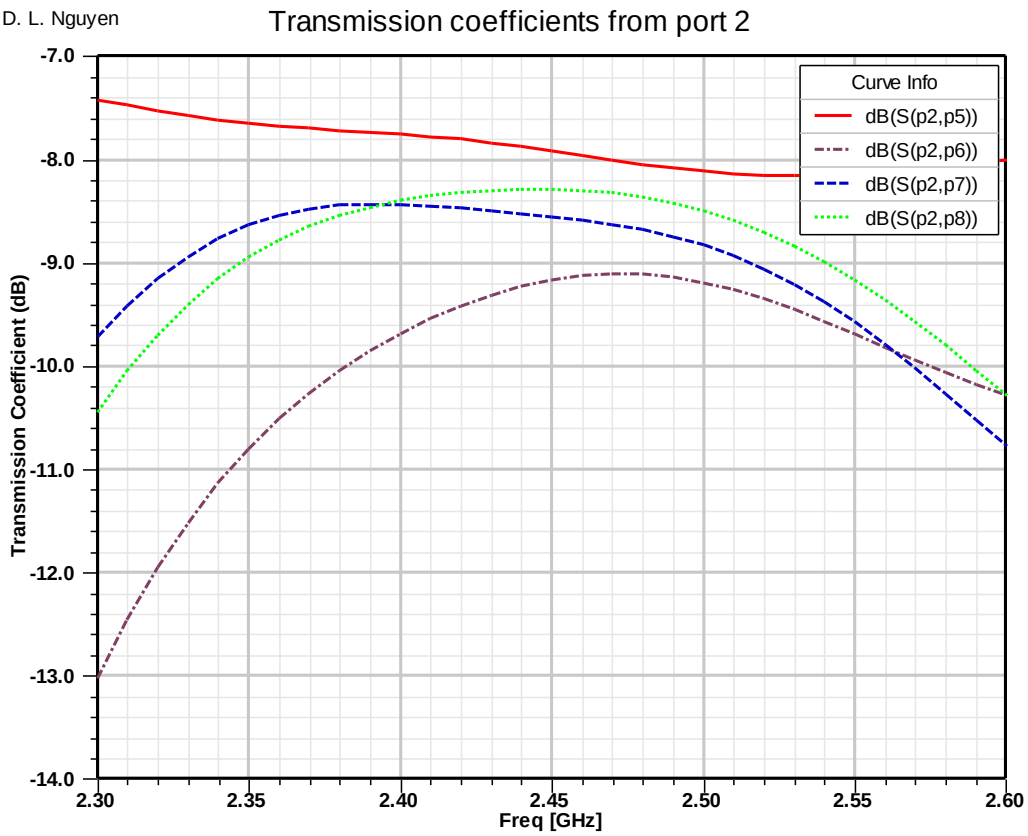

Figure 4.42.c) Simulated Transmission coefficients from port 2

Figure 4.42. Simulated S-parameters of the compact Butler Matrix

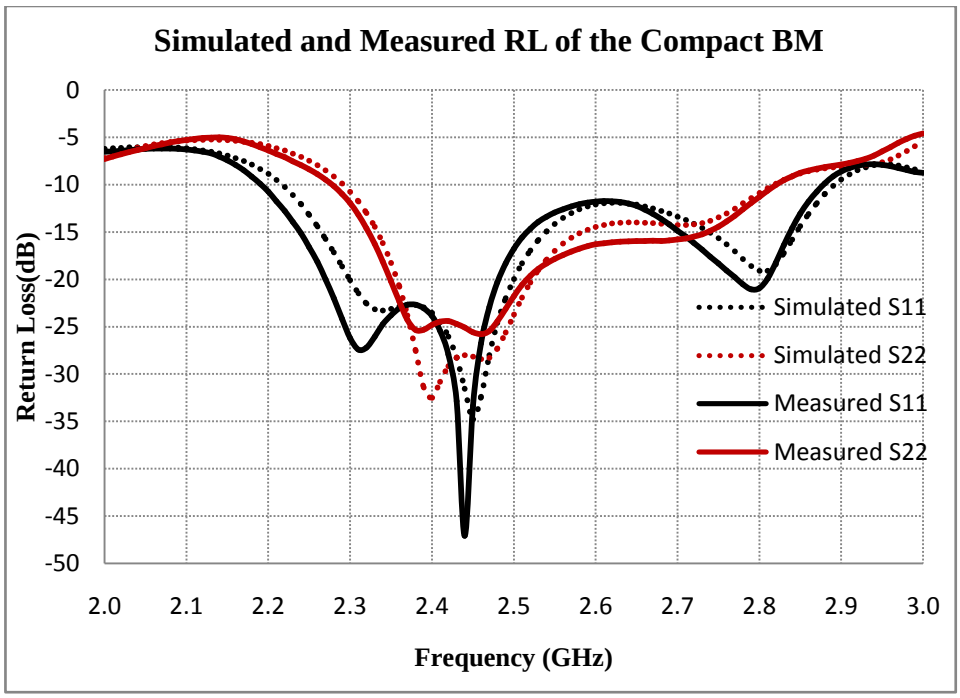

Figure 4.43. Simulated and measured Return Losses at port 1 and port 2

Table 4.7. Simulated and measured results of the compact BM

Frequency (2.45 GHz)	Ideal	Simulated	Measured
S_{11}	-∞	-34.73 dB	-33.36 dB
S_{21}	-∞	-27.18 dB	-
S_{31}	-∞	-35.87 dB	-40.44 dB
S_{41}	-∞	-22.61 dB	-20.22 dB
S_{22}	-∞	-28.16 dB	-25.58 dB
S_{51}	-6.00 dB	-8.61 dB	-8.65 dB
S_{61}	-6.00 dB	-8.50 dB	-9.03 dB
S_{71}	-6.00 dB	-7.96 dB	-8.56 dB
S_{81}	-6.00 dB	-8.25 dB	-8.95 dB
S_{52}	-6.00 dB	-9.02 dB	-8.34 dB
S_{62}	-6.00 dB	-8.93 dB	-9.93dB
S_{72}	-6.00 dB	-7.70 dB	-9.31 dB
S_{82}	-6.00 dB	-8.69 dB	-8.99 dB
$Ang(S_{61} - S_{51})$ degrees	45	46.51	44.85
$Ang(S_{71} - S_{61})$ degrees	45	42.26	46.80
$Ang(S_{81} - S_{71})$ degrees	45	44.06	45.31
$Ang(S_{62} - S_{52})$ degrees	-135	-129.37	-129.83
$Ang(S_{72} - S_{62})$ degrees	-135	-136.45	-136.38
$Ang(S_{82} - S_{72})$ degrees	-135	-136.63	-131.37

4.5. Switched Beam Array for Localisation

This section investigates a switched beam array based on square patch antennas driven by a 4 × 4 BM. The target application is a 2D localisation system for 2.45 GHz RFID. A single RFID reader uses a four-element array antenna to determine the Angle of Arrival (AoA) of signals from RFID tags. The ratio of received powers (PRs) measured at the four BM outputs is used to estimate the AoA. The proposed system is evaluated by simulation and results are compared to measurements performed on a real system.

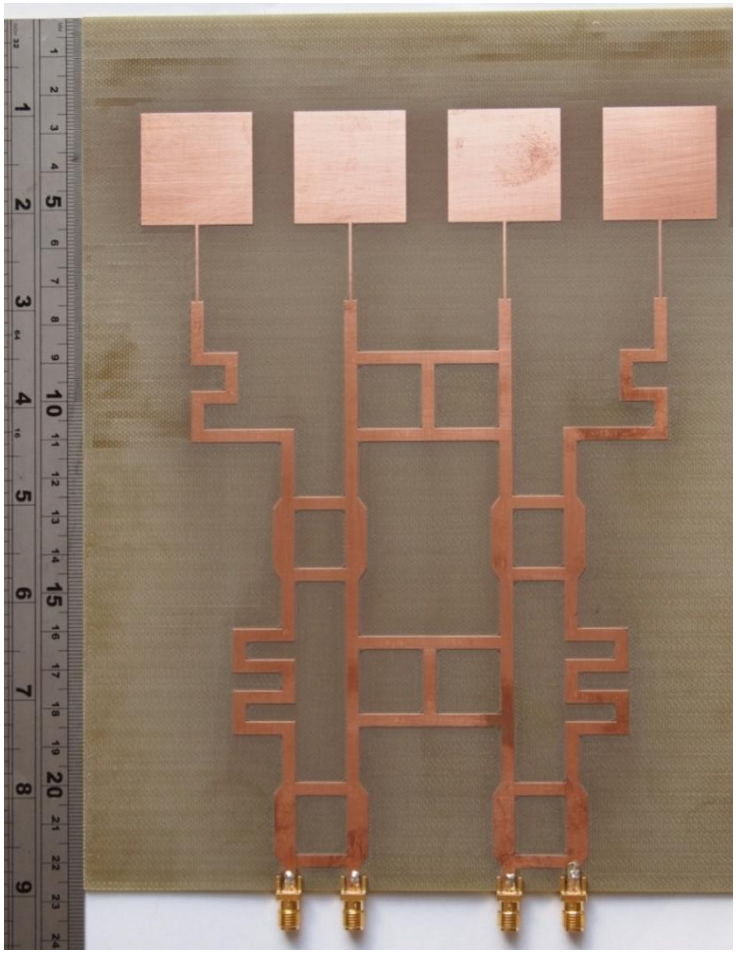

Figure 4.44. Switched beam array with 4 × 4 BM on FR4 board

The design of a 4 × 4 BM using TLs milled on standard FR4 substrate has been described in previous sections. This board is illustrated in Fig. 4.44. Due to the mirror symmetry of the circuit i.e. reversing the numbering of the inputs and outputs has no effect, the performance of the BM can be characterised by the response to inputs at ports 1 and 2.

Four square patches, studied in section 3.3, laid on the FR4 substrate are separated by distance $d = 40$ mm between centres. This array is fed by the BM described in section 4.3. The circuit size is 227 mm × 180 mm.

4.5.1. Simulated and Measured Return Losses, Isolations of the Switched-beam Antenna

The model of the switched beam array antenna (Antenna's dimensions can be found in section 3.3 and 4.3) was simulated using HFSS. The Return losses and isolations of the array were measured using the Network Analyzer. The simulated and measured data were plotted using Microsoft's Excel for comparison.

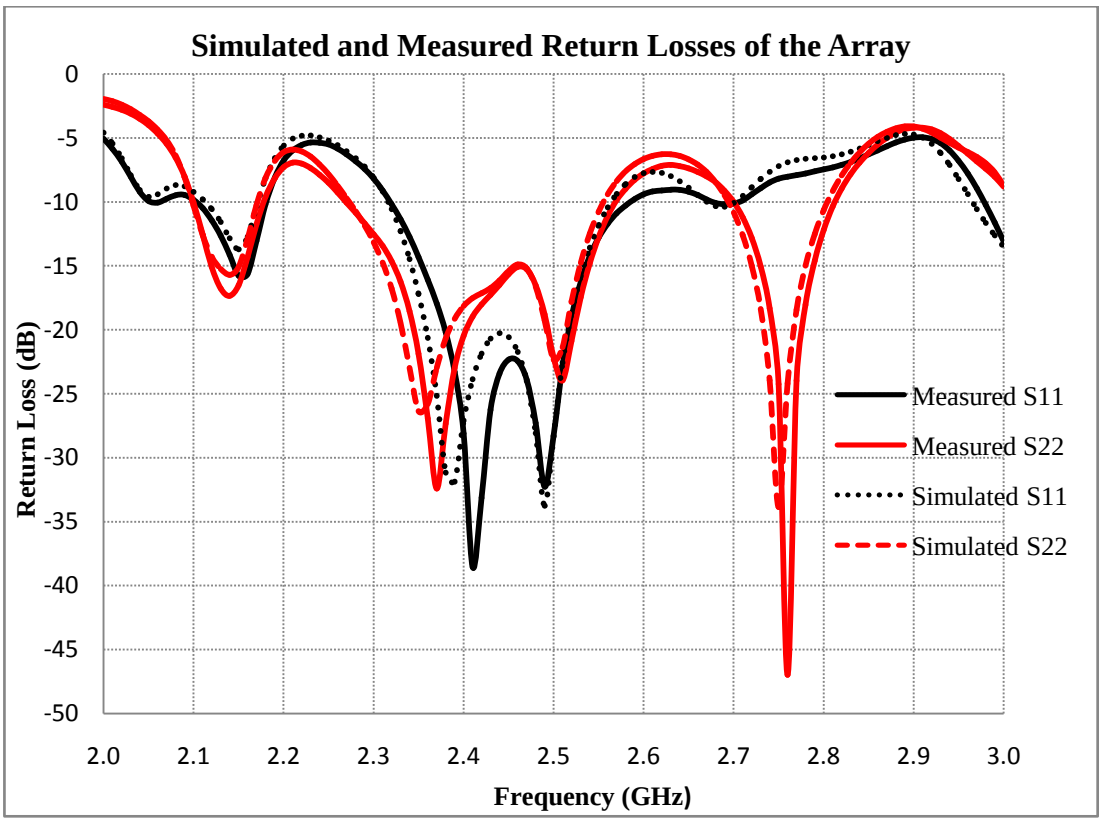

Figure 4.45. Simulated and Measured Return Losses of the Array Antenna

Fig. 4.45 shows the simulated and measured return losses at port 1 and port 2. They are greater than 15 dB thorough ISM band from 2.4 GHz to 2.5 GHz. Good isolation is achieved between the four ports (Fig. 4.46). The detailed S-parameters at 2.45 GHz are given in Table 4.8.

Table 4.8. Return Losses and Isolations of the Array Antenna

Frequency 2.45 GHz	Simulated (dB)	Measured (dB)
S_{11}	-20.58	-22.33
S_{21}	-33.29	-30.11
S_{31}	-24.40	-25.33
S_{41}	-15.24	-15.40
S_{22}	-15.38	-15.64
S_{32}	-14.56	-16.69

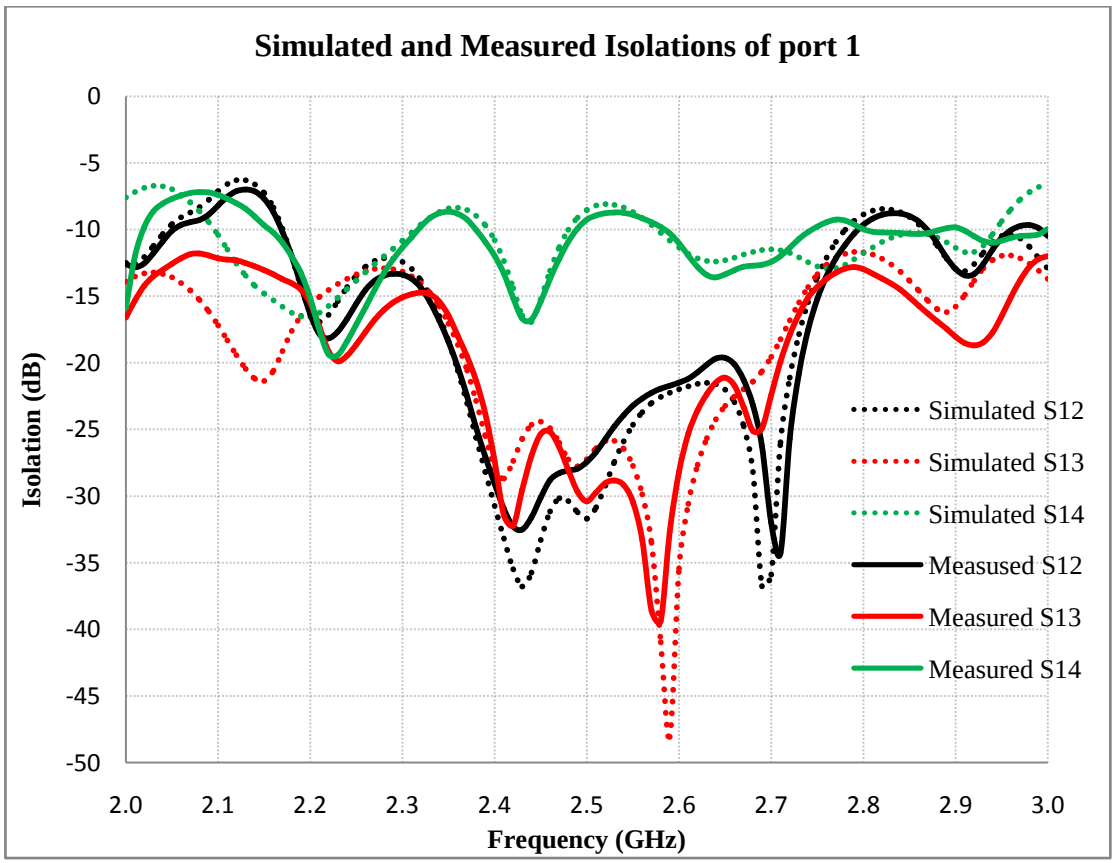

Figure 4.46. Simulated and Measured Isolations between port 1 and other ports

4.5.2. Simulated 3D Patterns

The switched beam property of the array can be seen with the simulated 3D patterns when one port is fed (Fig. 4.47). Top-left, top-right, bottom-left and bottom-right patterns are excited with port 1, port 2, port 3 and port 4, respectively. The symmetry of the patterns is clear. Therefore, verification is performed only on the antenna patterns resulting from inputs into ports 1 and 2.

In theory, the main beam position when only BM port 1 is excited is given by [Milligan, 2005]:

$$\theta = sin^{-1}\left(\frac{\lambda_0}{2Nd}\right) \qquad (4.19)$$

where d is the distance between adjacent, omni-directional, antenna elements.

With element separation $d = 40mm = 0.33\lambda_0$, the main beam points at an azimuth of $22.25°$. The simulation shows that when port 1 is fed, the main beam azimuth is 18°, with a gain of 10.22 dBi and the main beam switches to $-56°$ with a gain of 5.97 dBi when port 2 is fed. The differences between theory and practise are mainly due to the non-isotropy beam pattern of the individual patch antenna elements and mutual

inductance.

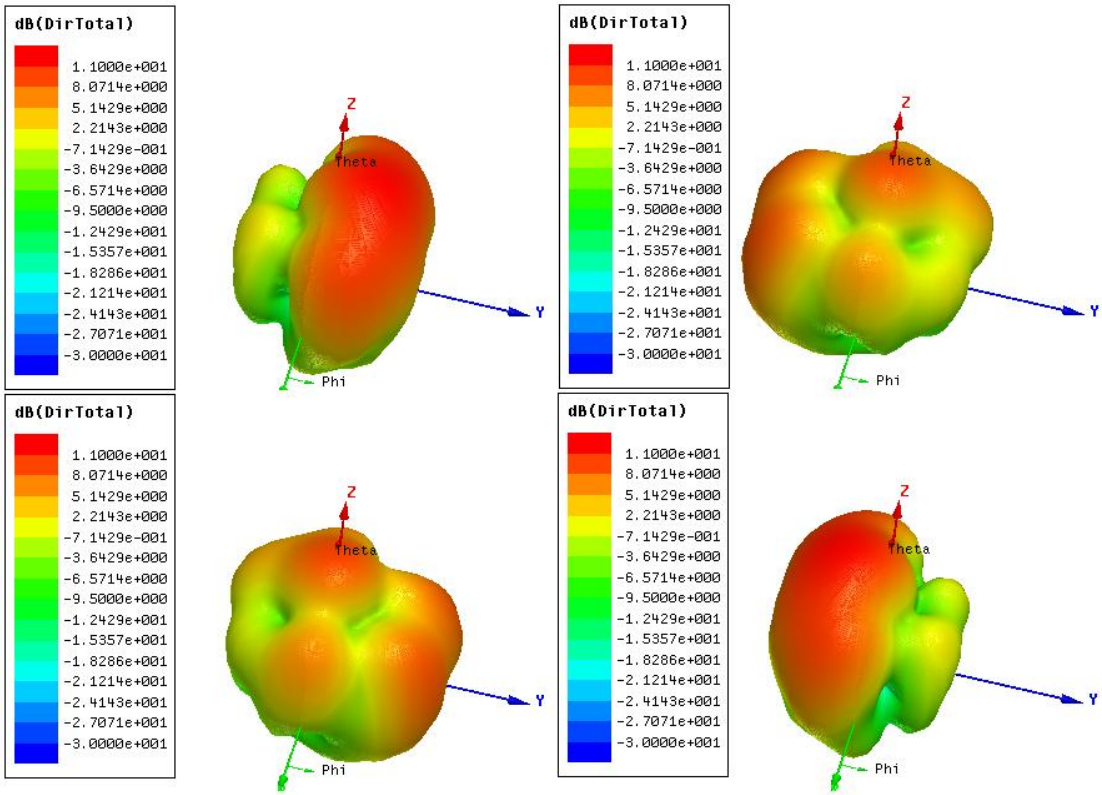

Figure 4.47. Simulated 3D patterns when one port is excited --

The antenna array is placed along y-axis, facing z-axis

(Top-left: port 1, top-right: port 2, bottom-left: port 3 and bottom right: port 4)

For the beams at a azimuth of $-19°$, the side lobe levels (SLL) are lower than –10dB. However, for the beam at $-53°$, the grating lobe appears at a broadside angle. This is due to the combination of array pattern with grating lobe (because $d > \frac{\lambda_g}{2}$, with λ_g is the wavelength on the substrate) and non-isotropic beam patterns of the antenna elements.

4.6. AoA Algorithm and Estimation Error

The Angle of Arrival (AoA) of the tag signal in YZ plane is estimated using relationships between the power levels received at the four BM ports (See Fig. 4.48). In practice, the reader antenna is often put on or near a wall so that an angle range from -90 to 90 degree is sufficient.

For verification, a system consist of a single patch (described in section 2.2) is used as a fixed source antenna and the array antenna is attached to a frame that can be rotated to

produce any azimuth angle to the source. The array antenna and the single source patch are separated by 4 metres. The distance is sufficient for far-field approximations to be used. Balanis [Balanis, 2005] defines the far filed to be when:

$$R \gg \frac{2D_{max}{}^2}{\lambda_0}$$

where D_{max} is the maximum dimension of the antenna.

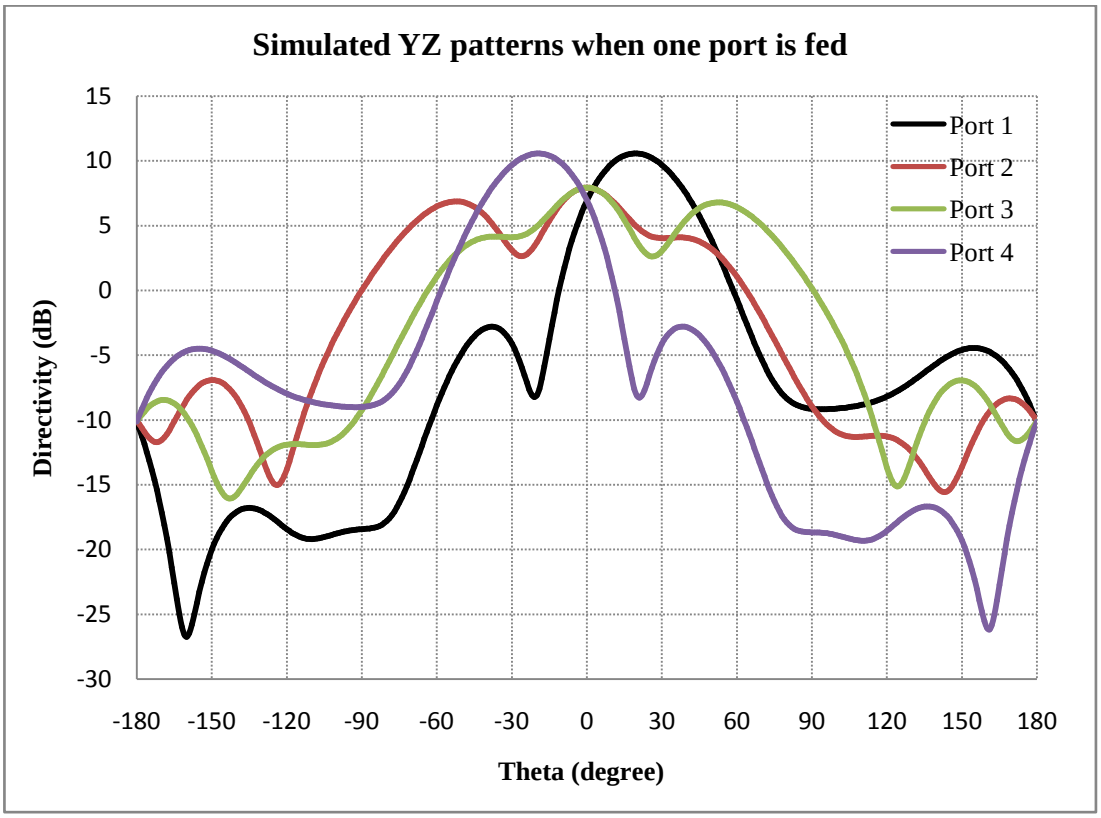

Figure 4.48. Simulated patterns on YZ plane when one port is fed

This range is also sufficiently large for the AoA from the source to all elements to be considered the same.

Table 4.9. Received power ratios between ports, in dB, with system range of 4 metres

AoA	0°	10°	20°	30°	40°	50°	60°	70°	80°	90°
PR_{14}	-1.23	2.76	5.70	5.62	3.52	0.73	-1.79	-3.29	-2.89	-0.30
PR_{12}	-0.14	8.57	17.89	13.17	10.01	8.15	7.59	8.32	9.49	9.40
PR_{23}	-0.09	0.25	1.20	0.93	-1.56	-3.70	-5.50	-7.21	-8.64	-9.21

Table 4.9 lists ratio of powers measured at pairs of BM output ports as a function of AoA, where PR_{ij} is received power ratio between port *i* and port *j*. For a source in the far field, these ratios are expected to be largely independent of range.

The measured power ratios are well approximated by the simulation results (Fig. 4.48). The slight differences between simulation and measurement are due to range limitations leading to slight difference between signal AoA for different array elements and the patch anisotropy.

Estimation of the Angle of Arrival (AoA) is posed as a minimisation. Ratios of received powers at the four outputs of the Butler Matrix have been determined by simulation for a range of AoAs to create a look-up table. An error functional is defined as the sum of the squared differences between the power ratios for an observed AoA and a test AoA. A minimisation is performed over test AoAs until a minimum of the error functional is found. Interpolation between values allows AoAs between simulated angles to be determined. Minimisation is performed using the Nelder Mead Simplex method [Nelder, 1965]. The method does not require knowledge of the gradients of the error functional but does rely upon a sufficiently accurate initial estimate of the AoA or it can diverge or converge to a local minima. An initial AoA estimate is determined by brute-force search of the coarsely sampled AoA solution space.

To determine the sensitivity of localisation to noise, AoA is estimated using BM port power ratios, in dB, perturbed by additive white Gaussian noise. The AoA estimation algorithm has been implemented in Matlab (Appendix 3). Fig. 4.48 illustrates the standard deviations of the AoA estimation errors of 200 samples at AoA from -90 degrees to 90 degree with power ratios perturbed by additive noise of standard deviation 0.5 dB. This yields an AoA estimate with a standard error less than 1.6° for most angles in the operational range and a standard error less than 0.6^{o} for AoA angles with 20^{o} of the perpendicular. Accuracy varies with angle due to the complicated relationships between AoA and port output powers.

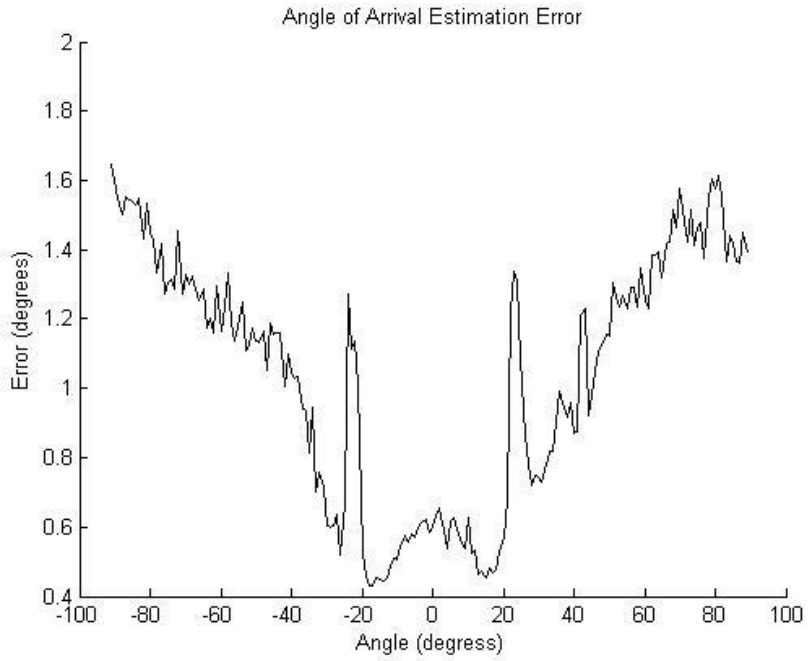

Figure 4.49. AoA Estimations Error

4.7. Summary

In this chapter, a new approach for 2.45 GHz RFID localisation is presented. The reader uses a switched beam antenna to determine the azimuth AoA of the tag. The reader antenna consists of a uniformly spaced linear array of four square patch antennas (the square patch is designed in chapter 3), and a feed network consisting of a 4 × 4 BM. The BM feed network is designed on a single FR4 board.

The reader antenna with feed network are compact in size (approximately 400 cm^2) and light weight, so that it can be used in most RFID applications.

The AoA of the tag in azimuth can be obtained from the received power ratios at outputs from a switched beam reader. The AoA information can combine with other techniques such as range estimation by phase delay to provide 2D tag location. 2D tag location can also be obtained by triangularisation by placing multiple switched-beam antennas. This approach has key benefits over most RFID systems using RSS because it is not affected by the orientation of the tag or the mismatched losses in the systems.

The compact design of BM introduced in this chapter suggests a compact reader design for future research.

CHAPTER 5. CONCLUSIONS AND FUTURE WORK

Initially, a summary of the research work reported in this thesis is provided. Recommendations for related future research are discussed in the second part of this chapter. To conclude, a summary of the original contributions to knowledge made by the research work presented in this thesis is given.

5.1. Thesis Conclusions

Radio Frequency Identification (RFID) systems have achieved pervasive use in tracking items during manufacture and through the supply chain.

The primary purpose of RFID systems is to identify the tagged objects. Tagged items are known to be within the read range of the reader but no other location information is derived from the communications. Adding localisation to existing RFID systems is a way of adding value to systems with enormous economic importance. This thesis introduced a new approach for localisation using UHF RFID systems working in ISM band of 2.45 GHz. The proposed system uses an enhanced reader capable of determining the location of a tag from the standard communications signal. The proposed system is an economical, versatile, and powerful solution for RFID localisation as it can apply to both passive and active systems, it does not require additional components and it overcomes the problem of unknown tag orientation. The unknown polarisation loss severely limits the accuracy of RFID localisation systems relying upon Received Signal Strength (RSS). The proposed microstrip antennas, fabricated on cheap FR4, are suitable to produce in a large number. The switched beam array antenna is remarkably compact and light (the antenna laid on a board area of approximate 400 cm^2 and weighted about 135 grams) so that it can be widely deployed in practice. In addition, the use of switched beam antenna with higher gain and narrower beam than a single element antenna also provides key advantages such as extended range and mitigation against multipath and interference.

Chapter 1 of this thesis summarised the contribution and outline of the work. Chapter 2 has provided a literature review of passive UHF RFID systems, particularly focusing on reader antenna constructed using microstrip technology. RFID localisation techniques and electromagnetic simulation software were also reviewed. Several designs of portable, circularly polarised microstrip antennas for the reader were developed in Chapter 3. The compact designs will have application in handheld RFID readers. All designs were simulated and optimised with the use of Ansoft HFSS software. The antennae and microwave circuits were fabricated and measured performance data agreed well with computer simulations. Proposed techniques for RFID localisation

utilising readers with switched beam antennas were introduced in chapter 4. The antenna and circuit components of the hardware solution have been fabricated and integrated into a working system. The measured results show only a 0.2 dB variation in PRs relative to simulation predictions. Chapter 4 also presented an algorithm to estimate AoA and a noise sensitivity analysis was performed.

5.2. Future Work

Although this research mainly focused on RFID reader antenna, it has highlighted a range of topics worthy of future investigation, related not only to RFID but also in microstrip antenna design. The following areas are recommended for future work:

1. *Microstrip Antenna optimisation algorithm*
   Through the research work presented in this thesis, it has been shown that commercial simulation software can be quite efficient and reliable when used to design compact microstrip antenna. However, for academic research purposes, it is also beneficial to have a more theoretical analysis of electromagnetic fields behaviour and an algorithm to design microstrip antenna of any shape to meet a variety of requirement constraints.
2. *Improvement of the proposed system*
   There are a number of methods to improve the performance of the proposed system including:
   - The proposed system performance can be improved by using a larger number of elements for the array antenna (e.g. 8 elements array). The $N \times N$ BM with N larger than 4 ($N = 8, 16, ..$) can be constructed from the design of 4×4 matrix of this project with an appropriate set of couplers, phase shifters and crossovers [Kaifas, 2006].
   - The work on compact circularly polarised (CP) patch antennas in chapter 3 and compact Butler Matrix in chapter 4, can be integrated to create a compact switched beam CP array. By using miniaturised patch antennas, the separation between elements can be reduced to smaller than half-wavelength of the waves on the substrate so that the switched beam array does not have grating lobes. The compact array also improves the localisation accuracy as the variation in AoA between antenna elements is reduced. This allows for more accurate localisation of items near the reader.
   - The proposed antenna can be improved by using smart antenna technology that provides continuous steerable pattern, but the system will be much more complex and expensive.
3. *Deployment of a localisation system in practice*

The proposed system needs to be tested to determine the effects of the surrounding environment to its performance and localisation analysis. In particular the effects of multipath need to be determined.

4. *3D localisation system based on switched beam array antenna*
   The proposed array antenna for the reader is linear. It only provides AoA information in the azimuth plane. In order to extract the AoA information in three dimensions, the reader antenna should be a planar array. The idea of feeding planar array by a network of BMs, introduced by Fakoukakis et. al. [Fakoukakis, 2005] could be used as a straightforward technique to steer the beam pattern in 3D space. In practise it is likely that most items will be within a small angular variation of the azimuth plain and the added complexity and expense is unlikely to be cost-effective.
5. *Cost analysis*
   The reader presented in this thesis is designed to be as simple as possible with low cost materials used to minimise the overall cost. However, it would be of great interest to be able to calculate and estimate the actual cost of these reader antennas, if they were manufactured commercially in larger quantities. It is common knowledge that the larger the quantity of the circuit manufactured, the lower the reader cost will be. Therefore, the first part of the cost analysis is to obtain relevant material and manufacturing cost information to predict how the manufacturing cost varies with respect to the quantity of antennas manufactured. The second part of the cost analysis will be to estimate the value of benefits attributable to RFID localisation. That calculation should take into account both costs and business benefits of having the system.

5.3. Thesis Contribution

The contributions to knowledge of the research work presented in this thesis have been discussed earlier in Chapter 1 (Section 1.2). They are summarised here as follows:

1. *Design of compact microstrip CP antennas for a RFID reader*
   Several designs of new, compact, slotted, CP, patch antenna with microstrip line feeding have been proposed, simulated and fabricated. The performance of these designs can be optimised to meet specific requirements as the size reduction is usually a trade off with the antenna's characteristics such as gain and matching difficulty. The measured results obtained confirm the antenna performance is sufficient for most RFID application and some wireless systems.
2. *Design compact microstrip BM using SIC*
   Miniaturisation is achieved by replacing BM components, including quadrature hybrid couplers and crossovers, with SIC equivalent structures. The SIC

structure is shown to be simple to design and provides effective size reduction. SICs are widely applicable and can reduce the length of any transmission line. In addition, the performance of the compact circuits is similar to the standard ones.

3. *Switched beam array antenna for RFID localisation*

   The switched beam array antenna fed by the 4 × 4 BM is demonstrated to be a simple but powerful solution to 2.45 GHz RFID localisation systems. The reader antenna, along with the feed network, fabricated on the single layer FR4 board, is light and compact so that can be easily implemented. The AoA of the tag in azimuth can be obtained from the received power ratios at outputs. This technique can provide the 2D location of the tags with two or more readers located at fixed positions by triangularisation. In addition, the AoA estimation based on the power ratios eliminates the localisation errors caused by power losses that effect all four BM outputs equally e.g. polarisation loss due to tag orientation and system losses in cables and connections.

5.4. Summary

The accomplishments of this PhD project are summarised in this chapter. In a sentence, the original contribution of this project is the detailed design of a RFID localisation system using a switched beam antenna array in the RFID reader. The simple structure and stable performance of the antenna and feed network makes them ideal for mass manufacture and deployment in industry.

In addition, several novel methods have been developed for the miniaturisation of RF circuits and antennas. These methods are suitable for future investigation and have already yielded RF components with commercial applications.

APPENDIX 1. Specifications LPKF ProtoMat S62

Minimum track width	4 mils (0.1 mm)
Minimum isolation width	4 mils (0.1 mm)
Minimum drill hole diameter	6 mils (0.15 mm)
Working area (Z/ Y/ Z)	229 mm × 305 mm × 38 mm
Resolution	0.01 mil (0.25 µm)
Milling motor rpm	62000 rpm
Tool change	Automatic, 10 positions
Drilling speed	150 holes per minute
Travel speed (max)	150 mm per second
X/ Y positioning system	3- phase stepper motors
Z drive	Stepper motor
Dimensions (W/ H/ D)	650 mm × 510 mm × 800 mm
Weight	55 kg
Power supply	120/240 V, 50-60 Hz/ 200 VA
USB computer connection requirement	USB 1.1 port or better

APPENDIX 2. Specifications of Farnell Photo-Resist Copper Cladboard

Base Material	FR4 epoxy all woven glass laminate to BS4584 part 3
Thickness	1/16 inch (1.6 mm)
Copper foil cladding per square ft	1 oz (35 microns)
Water absorption	0.1%
Specific Gravity	1.85 - 1.9
Dielectric Constant at 1 MHz	5.0
Dissipation Factor at 1 MHz	0.020
Flex Strength Length Wise	$550N/mm^2$
Surface Resistance	$10^{11}\ \Omega$
Volume Resistivity	$10^{15}\ \Omega$
Foil pull off strength	140 N
Photoresist	Positive working
Sensitivity	Ultra Violet
Coating Thickness	7 microns÷ 0.7 micron
Exposure Time	2- 8 minutes (clear carrier film)

APPENDIX 3. Matlab Code

```
% AoA Estimation Error
global Angle  Powers  MeasuredPowers

load('Loi_BM_Data')
Powers(361,:) = [];

Angle = Powers(:,2);
NumAngle = length(Angle);
% delete columns
Powers(:,1:2) = [];


   Noise_STDev = 0.5;          % additive noise
   AoA_Error = zeros(NumAngle,1);

   NumTest = 1000;
   AoA_Error = zeros(270-90+1,NumTest);

   for j = 1:NumTest

      for iTestAngle = 90:270

         % measured BM output powers with WSSWGN additive noise
         MeasuredPowers = Powers(iTestAngle,5:7) + Noise_STDev*randn(1,3);

         if false
            x0 =  Angle(iTestAngle) ;                % first gues AoA.
         else
            Test_AoA_Error = zeros(NumAngle,1);
            for iTest = 1:NumAngle
               Test_AoA_Error(iTest) = sum( (MeasuredPowers - Powers(iTest,5:7)).^2 );
            end
            [C,I] = min( Test_AoA_Error );
            x0 =  Angle(I) ;                % first gues AoA.
         end
         [AoA] = fminsearch( @Error_BM_OP_PowerRatio3 , x0  );

         end
```

```
    end


    % work out standard deviation of errors

    AoA_STD_Error = std(AoA_Error');


    figure(4)
    hold on
    plot(Angle(90:270),AoA_STD_Error , 'k')

    xlabel( 'Angle (degrees)' )
    ylabel( 'Error (degrees)' )
    title('Angle of Arrival Estimation Error')

end

% Error_BM_OP_PowerRatio3

function [Error] = Error_BM_OP_PowerRatio3(X)

global Angle  Powers  MeasuredPowers

PR1_X = interp1(Angle, Powers(:,5) , X);
PR2_X = interp1(Angle, Powers(:,6) , X);
PR3_X = interp1(Angle, Powers(:,7) , X);

Error = sum( (MeasuredPowers - [ PR1_X PR2_X PR3_X]).^2 );
```

REFERENCES

Abedin, M. J. and **Mohan, A. S.,** (2009), *Use of smart antennas for the localization of RFID reader*, Proc. of the Asia Pacific Microwave Conference, pp. 1036–1039, Singapore, 2009.

ADS software, Agilent website, [Online] Available: http://www.home.agilent.com/agilent/product.jspx?cc=GB&lc=eng&ckey=1297113&nid=-34346.0.00&id=1297113 [Accessed 13/09/2011].

Alejos, A. V. et. al., (2010), *Sensor Area Network for Active RTLS in RFID tracking applications at 2.4 GHz*, Progress In Electromagnetics Research, Vol. 110, pp. 43-58. [Online] Available: http://www.jpier.org/PIER/pier110/03.10100204.pdf [Accessed 26/09/2011].

Angerer, C., Langwieser, R. and **Rupp, M.**, (2010), *Direction of Arrival Estimation by Phased Arrays in RFID*, Proceedings of the third international EURASIP Workshop on RFID Technology, September 2010.

Arumugam, D., Ambravaneswaran, V., Modi, A., and **Engels, D.**, (2007), *2D localization using SAW-based RFID systems: a single antenna approach*, International Journal of Radio Frequency Identification Technology and Applications, Vol. 1, No. 4, 2007.

Balanis, C., (2005), *Antenna theory: Analysis and Design*, 3rd edition, Wiley & Sons Inc.

Balanis, C., (2008), *Modern antenna handbook*, Jon Wiley and Sons.

Bechteler, T., and **Yenigun, H.**, (2003), *2-D localization and identification based on SAWID-tags at 2.5 GHz*, IEEE Trans. Microwave Theory and Techniques, Vol. 51, No. 5, 2003.

Bekkali, A., Sanson, H., and **Matsumoto, M.**, (2007), *RFID indoor positioning based on probabilistic RFID map and kalman filtering*, In Proc. of WiMOB, 2007.

Bhatia, A., Mehta, B., and **Gupta, R.** (2009) *Different localization techniques for real time location sensing using passive RFID*. [Online] Available at: http://filedb.experts-exchange.com/incoming/2009/02.../RFID-DTOA.pdf

Bouet, M. and **Pujolle, G.,** (2008), *A range-free 3-D localization method for RFID tags based on virtual landmarks*, In Proc. of PIMRC, 2008.

Butler, J. and **Lowe, R.**, (1961), *Beam forming matrix simplifies design of electronically scanned antennas*, IEEE Transactions on Applied Superconductivity, vol. 9, pp. 170–173, Apr 1961.

Chin, K. W. and **Klair, D.**, (2010), Book chapter: *Aloha-based protocols*, in *RFID systems: Research trends and challenges*, Edited by Bolic, M. et. al., John Wiley & Sons Ltd.

Chen, W. S., Wu, C. K. and **Wong, K. L.,** (1998a), *Single-feed square-ring microstrip antenna with truncated corners for compact circular polarization operation*, Electronics Letters., Vol. 34, No. 11, pp. 1045-1047, May 1998.

Chen, W.-S., **Wu, C.-K.** and **Wong, K. L.**, (1998b), "*Compact circularly polarized microstrip antenna with bent slots*", Electronics Letters, Vol. 34, June 1998.

Chen, W. S. and **Chen, H. D.,** (1998c), *Single-feed circularly polarized square-ring microstrip antennas with a slit*, in IEEE Antennas and Propagation Society International Symposium, Vol. 3, pp. 1360- 1363, June 1998.

Chen, W.-S., **Wu, C.-K.** and **Wong, K. L.**, (2001), "*Novel compact circularly polarized square microstrip antenna*" IEEE Transactions on Antennas and Propagation, Vol. 49, No. 3, 340- 342, March 2001.

Cisco, Book chapter: *Location tracking approach, in Wi-Fi Location-Based Services 4.1 Design Guide*, [Online] Available at: [Accessed 21/12/2011] http://www.cisco.com/en/US/docs/solutions/Enterprise/Mobility/wifich2.pdf

Deschamp, G. A., (1953), *Microstrip microwave antennas*, in Proceedings of the Antenna Applications Symposium, September 1953.

Dobkin, D., (2008), "*RF in RFID: Passive RFID in practice*", Elseriver Inc.

Dwari, S. and **Sanyal, S.**, (2006), "*Size reduction and harmonic suppression of microstrip branch-line coupler using defected ground structure*", Microwave and Optical Technology Letters, Vol. 48, Issue 10, July 2006.

Eccleston, K. W. and **Ong, S. M.**, (2003), "*Compact planar microstripline branchline and rat-race couplers*", IEEE Transaction on Microwave Theory and Techniques, Vol. 51, No. 10, pp. 2119–2125, October 2003.

ERC Recommendation 70-03, *Relating to the use of short range devices (SRD)*, [Online] Available: http://www.erodocdb.dk/docs/doc98/official/pdf/rec7003e.pdf [Accessed 26/09/2011].

EU commission, *Harmonisation of the radio spectrum for radio frequency identification (RFID) devices operating in the ultra high frequency (UHF) band*. [Online] [Accessed 10/07/2011].
http://eur-lex.europa.eu/LexUriServ/LexUriServ.do?uri=OJ:L:2006:329:0064:0066:EN:PDF

Fakoukakis, F. E., Diamantis, S. G., Orfanides, A. P. and **Kyriacou, G. A.,** (2005), *Development of an Adaptive and a Switched Beam Smart Antenna System for Wireless Communications*, Progress in Electromagnetics Research Symposium, Hangzhou, China, August 2005.

Fan, Z. G. et. al. (2007) *Signal descriptions and formulations for long range UHF RFID readers*, Progress in Electromagnetics Research (PIER) 71, 2007.

Finkenzeller, K. (2003), *RFID handbook: Fundamentals and applications in contactless Smart cards and identification*, 2nd edition, John Wiley& Sons Ltd.

Finkenzeller, K. (2010), *RFID handbook: Fundamentals and applications in contactless Smart cards and identification and near field communication*, 3rd edition, John Wiley& Sons Ltd.

Garg, R. et al, (2001), *Microstrip antenna design handbook*, Artech house Inc.

Griffin, J. D., and **Durgin, G. D.** (2007), *Reduced fading for RFID tags with multiple antennas*, Antenna and Propagation Society International Symposium 2007 IEEE, 9-15 June, pp. 1201- 1204.

Gross, F. B., (2005), *Smart Antennas for Wireless Communications with MATLAB*, McGraw-Hill companies.

Han, S., Lim, H. and **Lee, J.,** (2007), *An efficient localization scheme for a differential-driving moblie robot based RFID system*, IEEE Transactions on Industrial Electronics, Vol. 54, No. 6, pp. 3362–3369, December 2007.

Haneisi, M. and **Suzuki, Y.**, (1989), Book chapter: *Circular polarisation and Bandwidth,* in *Handbook of microstrip antenna*, Edited by James, J. R. and Hall, P. S., IEE Electromagnetic Series 28, Peter Peregrinus Ltd.

Heidari, M. and **Pahlavan, K.**, (2008), Book chapter: *Performance evaluation of Wifi RFID localization technologies*, in *RFID Technology and application*, edited by Miles, S. B. et. al., Cambridge University Press.

Hekimian-Williams, C. et. al., (2010), *Accurate localization of RFID tags using phase difference,* IEEE International Conference on RFID, April 2010.

Hettak, K., Morin, G. A. and **Stubbs, M. G.**, (2005), *Compact MMIC CPW and asymmetric CPS branch-line couplers and Wilkinson dividers using shunt and series stub loading*, IEEE Transaction on Microwave Theory and Techniques, Vol. 53, pp. 1624-1635, May 2005.

HFSS, Ansys website, [Online] Available: http://www.ansoft.com/products/hf/hfss/ [Accessed 13/09/2011].

Hirota, T., Minakaw, A. and **Muraguchi, M.**, (1990), *Reduced-size branch-line and rat-race hybrids for uniplanar MMIC's*, IEEE Transaction on Microwave Theory and Techniques, Vol. MTT-38, No. 3, pp. 270–275, March 1990.

Hongerheiden, J., Ciminera, M. and **Jue, G.** (1997), *Improved planar spiral transformer theory applied to a miniature lumped element quadrature hybrid*, IEEE Transaction on Microwave Theory and Techniques, Vol. 45, No. 4, pp. 543–545, April 1997.

Huang, **J.**, (1984), *Circularly Polarized Conical Patterns from Circular Microstrip Antennas*, *IEEE Trans. Antennas Propagation*, Vol. AP-32, No. 9, September 1984.

Huang, **J.**, (2008), Book chapter: *Microstrip antennas: Analysis, design and application*, in *Modern Antenna Handbook*, Edited by Balanis, C. A., John Wiley & Son Inc.

Huang, X., Janaswamy, R. and **Ganz, A.,** (2006), *Scout: Outdoor localization using active RFID technology,* In Proc. of BROADNETS, 2006.

IDTechEx, (2011), *RFID Forecasts, Players and Opportunities 2011-2021*.

Jin, G., Lu, X. and **Park, M.,** (2006), *An indoor localization mechanism using active RFID tag*, In Proc. of the IEEE International Conference on Sensor Networks, Ubiquitous, and Trustworthy Computing, June 2006.

Kaifas, T. N. and **Sahalos, J. N.**, (2006), *On the design of a single layer wideband Butler Matrix for Switched-Beam UMTS System Applications*, IEEE Antenna & Propagation Magazine, Vol. 48, Issue 6, pp. 193-204.

Karmakar, N. C., Roy, S. M., and **Ikram, M. S.**, (2008), *Development of a low cost compact low profile Phase Array Antenna for RFID Applications*, in book of Smart Sensors and Sensing Technology, Springer- Verlag Berlin Heidelberg.

Kharrat, I. et al., (2011), *Customized RSSI Method for Passive UHF RFID Localization System*, Journal of Telecommunications, Vol. 10, Issue 2.

Kim, S. C., Park, H., Lee, D. and **Choi, J.,** (2006), *A novel design of an UHF RFID reader antenna for PDA*, Proceedings of Asia-Pacific Microwave Conference, Yokohoma, pp. 1471–1473, Japan 2006.

Kim, M. and **Chong, N. Y.,** (2009), *Direction sensing RFID reader for mobile robot navigation,* IEEE Transactions on Automation Science and Engineering, Vol. 6, No.1, pp. 44–54, January 2009.

Lahiri, S., (2006), *RFID sourcebook*, 1st edition, IBM press.

Landt, J., (2005), *The history of RFID*, IEEE Potentials, Vol. 24, Issue 4, pp. 8-11, October-November 2005.

Liao, S. S. and **Sun, P.T.**, (2005), *A novel compact-size branch line coupler*, IEEE Transaction on Microwave Theory & Techniques, Vol. 15, pp. 588-590, September 2005.

Liao, S. S., and **Peng, J. T.**, (2006), *Compact planar microstrip branch-line coupler using the quasi-lumped elements approach with nonsymmetrical and symmetrical T-shaped structure*, IEEE Transactions on Microwave Theory and Techniques, Vol. 54, Issue 9, 3508–3514, September 2006.

LPKF, ProtoMat S62, [Online] Available: [Accessed 28/08/2011]
http://www.lpkfusa.com/RapidPCB/CircuitboardPlotters/s62.htm

Ma, T. G., Wang, C. W., Hua, R. C. and **Yang, C. F.**, (2008), *Phased Array Antenna for UHF RFID applications Using Artificial Transmission Lines*, International Workshop on Antenna Technology: Small Antennas and Novel Metamaterials, pp. 454-457, March 2008.

Maddah-Ali, M., Oskouei, H. D. and **Forooraghi, K.**, (2008), *A compact branch-line coupler using Defected ground structures*, Microwave and optical technology letters, Vol. 50, No. 2, pp. 386-389, February 2008.

Mailloux, R. J., (2005), *Phased array antenna handbook*, 2nd edition, Artech House Inc.

Mandal, M. K., Velidi, V. K., Bhattacharya, A. and **Sanyal, S.**, (2008), *Miniaturized quadrature hybrid coupler using high impedance lines*, Microwave and optical technology letters, Vol. 50, No. 5, pp. 1135-1137, May 2008.

Milligan, T. A., (2005), *Modern antenna design*, 2nd edition, John Wiley and Sons.

Muhammad, N. A. et al., (2010), *Beam Forming Networks Using Reduced Size Butler Matrix*, Wireless Personal Communications, Published online: 30 October 2010, Springer Netherlands.

Nasimuddin, Zhi, Z. N. and **Qing, X.**, (2010), *Asymmetric-Circular Shaped Slotted Microstrip Antennas for Circular Polarization and RFID Applications*, IEEE Transactions on Antennas and Propagation, Vol. 58, No. 12, pp. 3821-3828, December 2010.

Nasimuddin, **Chen, Z. N.** and **Qing, X.**, (2011), Book chapter: *Circularly Polarized Slotted/Slit-Microstrip Patch Antennas* in *Microstrip Antennas*, Edited by Nasimuddin, Published by Intech, Croatia.

Nelder, J. A. and **Mead, R.**, (1965), A *simplex method for function minimization*, Computer Journal, Vol.7, No. 4, pp. 308–313, 1965.

Neron, J. S. and Delisle, G. Y., (2005), Microstrip EHF Butler Matrix Design and Realization, ETRI Journal, Vol. 27, No. 6, pp. 788-797, December 2005.

Ni, L., Liu, Y., Lau, Y., and **Patil, A.**, (2004), *LANDMARC: indoor location sensing using active RFID*, ACM Wireless Networks, Vol. 10, No. 6, 2004.

Nikitin, P. V., and **Rao, K. S. V.,** (2006). *Theory and measurement of backscattering from RFID tags*, IEEE Antennas and Propagation Magazine, Volume: 48, Issue: 6, Dec. [Online] Available: [Accessed 10/07/2011] http://www.ee.washington.edu/faculty/nikitin_pavel/papers/APmag_2006.pdf

Nikitin, P.V. and **Rao, K. S. V.** (2008), *Antennas and Propagation in UHF RFID Systems*, IEEE RFID 2008 Conference, Las Vegas, April 16-17 [Online] Available: http://ee.washington.edu/people/faculty/nikitin_pavel/papers/RFID_2008.pdf [Accessed 19/01/09].

Nikitin, P.V., Martinez, R., Ramamurthy, S., Leland, H., Spiess, G. and **Rao, K.V.S.**, *Phase Based Spatial Identification of UHF RFID Tags*, IEEE International Conference on RFID, April 2010.

Oktem, R., Aydin, E., and **Cagiltay, N.**, (2008), *An RFID based location finding and tracking with guidance*, in Proc. Int. Conf. Wireless Communications, Networking and Mobile Computing (WiCOM), October 2008.

Omron (2006)**,** *Omron develops World's First Antenna Technology that Boosts UHF RFID Tag Read Performance*, Omron Press Realease [Online] Available: http://www.omron.com/media/press/2006/03/n_270306.html [Accessed 10/07/2011].

Pozar, D., (2005), *Microwave engineering*, 3rd edition, John Wiley and Sons.

RFID-Radar, RFID-Radar website, [Online] Available: http://www.rfid-radar.com [Accessed 10/07/2011].

Roy, S. M. and **Karmakar, N. C.**, (2010), Book chapter: *Introduction to RFID systems*, in Handbook of Smart Antennas for RFID systems, Edited by Karmakar, N. C., John Wiley & Sons.

Sharma, P. C. and Gupta, K. C., (1983), *Analysis and optimized design of single feed circularly polarized microstrip antennas*, IEEE Transactions on Antennas and Propagation, vol. 29, pp. 949–955, 1983.

Singh, R. B. and **Weller T. M.**, (2001), *Miniaturized 20 GHz CPW quadrature coupler using capacitive loading*, Microwave and Optical Technology Letters, vol. 30, no. 1, pp. 3–5, July 2001.

Stockman, H. (1948), *Communication by means of reflected power*, Proceedings of the IRE, Vol. 36, Issue 10, October 1948.

Sun, K. O., Ho, S. J., Yen, C. C. and **Weide, D. V. D.**, (2005), *A Compact Branch-Line Coupler Using Discontinuous Microstrip Lines*, IEEE Microwave and wireless component letters, Vol. 15, No. 8, August 2005.

Sung, Y.J. Ahn, C.S. Kim, Y.-S., (2001), *Size reduction and harmonic suppression of rat-race hybrid coupler using defected ground structure*, IEEE Microwave and Wireless Components Letters, Vol. 14, Issue 1, pp. 7-9, January 2001.

Tseng, J. D., Ko, R. J. and **Wang W. D.**, (2007), *Switched Beam Antenna Array for UHF Band RFID System*, IEEE International Workshop on Anti-counterfeiting, Security, Identification, pp. 92- 95, April 2007.

Tseng, C. H., Chen, C. J. and **Chu, T. H.**, (2008), *A Low-Cost 60-GHz Switched-Beam Patch Antenna Array With Butler Matrix Network*, IEEE Antennas and Wireless Propagation Letters, Vol. 7, pp. 432-435, 2008.

Wang, C., Wu, H. and **Tzeng, N.-F.,** (2007), *RFID-based 3-D positioning schemes*, In Proc. of INFOCOM, pp. 1235–1243.

Wang, J., Wang, B. J., Guo, Y. X., Ong, L.C. and **Xiao, S.**, (2007), *A Compact Slow-Wave Microstrip Branch-Line Coupler With High Performance*, IEEE Microwave and Wireless Components Letters, Vol. 17, Issue 7, pp. 501- 503, July 2007.

Wi-Fi RFID, Aeroscout website, [Online] Available: http://www.aeroscout.com/content/wi-fi-rfid [Accessed 10/07/2011].

Wong, K. L. et al, (2000), *Inset microstripline-fed circularly polarized microstrip antennas*, IEEE Transactions on Antennas and Propagation, Vol. 4, no. 8, pp. 1253-1254, August 2000.

Wong. K. L., (2002), *Compact and Broadband Microstrip Antennas*, Johns Wiley & Sons.

Zhang, Y., Amin, M.G., and **Kaushik, S.**, (2007), *Localization and tracking of passive RFID tags based on direction estimation*, International Journal Antennas and Propagation, December 2007.

Zhao, Y., Liu, Y. and **Ni, L. M.,** (2007)*VIRE: Active RFID-based localization using virtual reference elimination*, In Proc. of ICPP, 2007.

Zhou, J. and **Shi, J.**, (2008), *RFID localization algorithms and applications - A review, Journal of Intelligent manufacturing*, Vol. 20, No. 6, pp. 695- 707.